PORE-SCALE ANALYSIS OF SOLUBILIZATION AND MOBILIZATION OF TRAPPED NAPL BLOBS IN POROUS MEDIA

A Dissertation

by

SUN HEE YOON

Submitted to the Office of Graduate Studies of
Texas A&M University
in partial fulfillment of the requirements for the degree of

DOCTOR OF PHILOSOPHY

August 2007

Major Subject: Civil Engineering

PORE-SCALE ANALYSIS OF SOLUBLIZATION AND MOBILIZATION OF TRAPPED NAPL BLOBS IN POROUS MEDIA

A Dissertation

by

SUN HEE YOON

Submitted to the Office of Graduate Studies of
Texas A&M University
in partial fulfillment of the requirements for the degree of

DOCTOR OF PHILOSOPHY

Approved by:

Chair of Committee,	Yavuz Corapcioglu
Committee Members,	Hongbin Zhan
	Hamn-Ching Chen
	Kung-Hui Chu
Head of Department,	David V. Rosowsky

August 2007

Major Subject: Civil Engineering

ABSTRACT

Pore-scale Analysis of Solubilization and Mobilization of Trapped

NAPL Blobs in Porous Media. (August 2007)

Sun Hee Yoon, B.S., Keimyung University, South Korea:

M.S., Keimyung University, South Korea

Chair of Advisory Committee: Dr. Yavuz Corapcioglu

NAPL (non-aqueous phase liquid) blob mobilization and solubilization models were developed to predict residual NAPL fate and describe flow dynamics of various displacing phases (water and surfactant foam). The models were achieved by pore-scale mass and force balances and were focused on the understanding of the physico-chemical interactions between NAPL blobs and the displacing phases. The pore-level mass balance indicated changes in NAPL saturation instead of mass reduction occurring with blob solubilization. The force balance was used to explain the complex flow configurations among NAPL blobs and the displacing phases. Some factors such as the wettability and the spreading/entering coefficients were useful in determining flow configurations. From the models developed in this study, dimensional analysis was performed to identify NAPL blob motion during water or surfactant foam flooding. In non-dimensionalized forms, a Trapping number employed as an indicator of blob displacement performance was modified to quantify the onset of blob mobilization. Its

value for water flooding was nearly 2-3 orders of magnitude greater than that of surfactant foam flooding. Next, to investigate the blob flow regime in porous media, a blob velocity was computed. Regardless of the displacing phases, a blob's velocity increased with increasing blob sizes after commencement of blob motion, and the velocity of DNAPL (dense non-aqueous phase liquid) blobs was greater than that of LNAPL (light non-aqueous phase liquid) blobs.

From this investigation, it is expected that the pore-scale solubilization and mobilization models would provide better understanding leading to a predictive capability for the flow behavior of NAPL blobs removed by various displacing phases in a porous medium. Additionally, the models based on newly approached concepts and modified governing equations would be useful in conceptualization, as well as the model prediction of other immiscible or miscible fluids flowing through a porous medium. Further, the models developed in our study would be a useful contribution to the study of small-scale contaminants or substances such as particle and bacterial transport in porous media.

DEDICATION

This dissertation is dedicated to God, my parents, my baby,

and specifically, to my husband, Dong Suk Han,

with all my love.

ACKNOWLEDGEMENTS

I gratefully acknowledge my advisor, Dr. M. Yavuz Corapcioglu, for his guidance, persistence and inspiration throughout the years. I am especially thankful for his advice and support in making this dissertation possible from creating this research topic to finishing this final document. I would like to specifically acknowledge one of my committee members, Dr. Timothy A. Kramer, who passed away just last year. He openly shared his knowledge with me and inspired me to work in this research area. I would also like to thank the assistance of my committee members: Dr. Hongbin Zhan, Dr. Hamm-Ching Chen, and Dr. Kung-Hui Chu for their support of this research. I am also thankful to Dr. Chanam Lee for her help during the latter stages of the research.

I especially would like to thank to my family members. My husband, Dong Suk Han who is a Ph.D student in the same department as I, has instilled in me a sense of motivation and encouragement and provided his complete support for my graduate study. I am also thankful to my father-in-law, Chulsun Han, my mother-in-law, Seook Kim, my father, Boungchil Yoon, and my mother, Insuk Do, for their constant patience and support throughout the course of my work toward the doctoral degree. Thanks to my younger brother, Jinho Yoon, and my sister, Seonghae Yoon, who taught me how to "cheer up".

Finally, I wish to acknowledge a great many friends and colleges who made my study enjoyable: Seonghwa Hwang, Jinkun Song, Jiseok Han, Min An, Miae Ha, Itza Mendoza, Jinwook Kim, Bangmi Jeong, and Chunwoo Lee.

TABLE OF CONTENTS

CHAPTER Page

CHAPTER Page

LIST OF TABLES

TABLE Page

LIST OF FIGURES

FIGURE Page

FIGURE Page

CHAPTER I

INTRODUCTION

1. 1 Problem Statement

Since the mid-1920's, non-aqueous phase liquids (NAPLs) have been considered to be one of the major concerns in the contaminated groundwater and soil (Simpkin et al. 1999). The NAPLs have been found in oil reservoir rocks or aquifers contaminated with various components i.e., a pure chemical (PCE, TCE, and dodecane) or a mixture of several organic compounds (gasoline). When they enter the subsurface environments, they initially flow as a continuous phase. Most of the flowing NAPLs are trapped by soil capillarity and then leave behind an immobile phase called residual NAPLs (Babchin and Nasr 2006). Generally, 20 ~ 50 % of the residual NAPL is retained within porous media in the form of NAPL blobs (i.e., singlet, doublet, and complex blobs) which are dependent on pore geometry (Figure 1.1) (Payatakes 1982; Mayer and Miller 1993a; Hilfer and Øren 1992; Chu 1997). The NAPL blobs also contain over 50 % of singlet and doublets, which are in a pore and extend to the adjacent two pores, respectively. However, their saturations are less than 15 % (Conrad et al. 1992; Mayer and Miller 1993a). Complex or larger blobs expanding over more than two adjacent pores are less common, however they are present in nearly 50 % of residual NAPL saturations (Conrad et al. 1992; Mayer and Miller 1993b).

The style and format of this thesis follows that of *Journal of Environmental Engineering*.

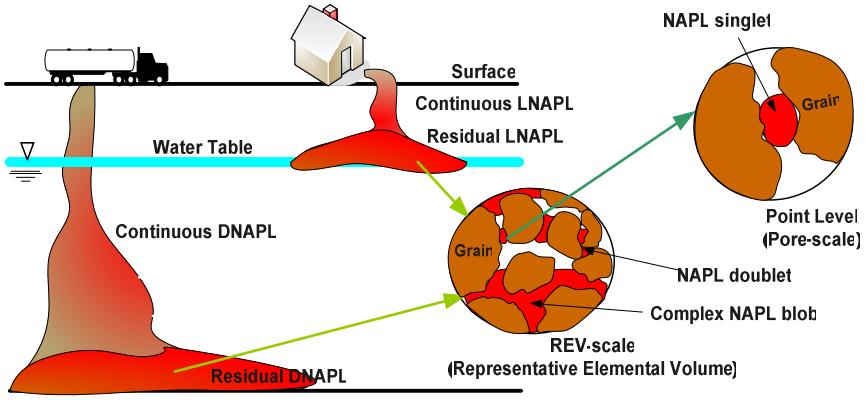

Figure 1.1 General schematic diagram for generating NAPL blobs.

Even though a trivial amount of the NAPL blobs is present in subsurface environments, they may become a long-term source of contamination in the area due to their low aqueous solubility or miscibility, volatility, and low mobility in water (Power et al. 1994; Dawson 1997; Chu 1997; Chevalier 2003). Furthermore, it is more difficult to remove discontinuous or discrete NAPL blobs than to remove continuous flowing NAPLs (Fu and Imhoff 2002). Therefore, complete removal of the NAPL blobs is necessary to the overall clean-up and restoration of subsurface environments contaminated with NAPLs.

Until now, various in-situ remediation techniques such as air sparging, soil vapor extraction (SVE), surfactant/co-solvent flushing, and pump and treat methods along with surfactant solution have been introduced to remove NAPL blobs (Lee et al. 2000; Duffield and Ramamurty 2003). Their operations, however, are limited in removing the phase under low permeability and hydrogeological heterogeneity (Kim et al. 2004). For example, in the case of surfactant/co-solvent solution flushing, the technique drives migration of the NAPL blobs downward, widening a contaminated region. Injections of

CO_2, steam or other gases are not greatly expected to remove NAPL blobs due to their short residence time in contact with the NAPL, undesirable air flow pattern, low gas density, and low gas viscosity (Kovscek and Radke 1996; Kim et al. 2004). Therefore, an alternative technique such as surfactant-enhanced air sparging has been recommended, in order to overcome such limitations. Currently, it is also called as surfactant foam flooding, or surfactant-alternating-gas flooding (SAGF). The technique was pioneered first by petroleum engineers for enhanced oil recovery (EOR). (Chu 1997; Jeong 1999; Jeong and Corapcioglu 2003; Wang and Mulligan 2004; Kim et al. 2004). It is effective in enhancing NAPL solubility and dislodging NAPL blobs by reducing surface tension (Jeong 2005).

In situ surfactant foam generation is performed by simultaneously or alternatively injecting air and surfactant solution beneath the water table to remediate the subsurface environments contaminated by NAPL blobs (Wang and Mulligan 2004). The application of this technique mitigates heterogeneous effects, increases the reactive surface areas between NAPL blobs and surfactant foam, and improves the sweep efficiency of NAPL blobs. It is also cost-effective due to the possibility of the reuse of the surfactant solution (Schramm and Novosad 1990; Wang 1997; Kam and Rossen 2003; Wang and Mulligan 2004; Jeong 2005). Surfactant foam operation allows control of the air (gas) phase mobility to avoid bypassing the source zone containing the trapped NAPLs through preferential flow paths (Kovscek et al. 1995). In the operation process of in-situ surfactant foam, however, mechanisms governing foam and NAPL blobs traveling through pore spaces are not well understood since their migrations are

relatively complex in porous media (Dalland et al. 1994; Sagar and Castainer 1997; Singh et al. 1997; Rossen et al. 1999; Yan et al. 2006). Another less understood feature is the complex interactions between NAPL blobs and other fluids (foam and aqueous solution) during the surfactant foam operation (Olbricht 1996; Chu 1997). Due to lack of such information and uncertain analysis of the operation, the use of the surfactant foam technique is restricted in the regulatory application to the field scale. During application of surfactant foam flooding, unclear relationships among three immiscible phases (bubble, surfactant solution, and NAPL) could result in the possibility of remaining surfactant residuals, even though surfactant concentration would be greatly reduced by the use of food grade surfactants. Therefore, injection of surfactant foam into a field site would pose many environmental engineering challenges.

However, surfactant foam flooding is still considered to be a more effective way of removing NAPL blobs than the other techniques discussed above. Several studies conducted in a laboratory have shown that NAPL blobs flow in a manner that is reactive to surfactant foam flow, and vice versa. They have evaluated the flow behaviors of foam and NAPL blobs through phenomenal and qualitative analysis (Llave et al. 1990). However, their studies have not been successfully applied evaluating the roles of surfactant foam displacing NAPL blobs and thus was limited to identifying the complex interactions between them. Therefore, the quantitative relationships between foam and NAPL blobs flow are needed to complete the explanation rather than the qualitative or descriptive relationships. Nevertheless, quantification of NAPL blobs flow removed by surfactant foam flowing through porous media is challenging since the NAPL blobs

migration is a complex manner at the pore-level. Additionally, the fluid conformation is difficult to identify because NAPL blobs is not analyzed on the scale of individual pores (Olbricht 1996). Hence, development of a mathematical model for predicting the NAPL blobs flow behaviors at pore-scale is necessary.

In this study, the fate of NAPL blobs removed by surfactant foam will be determined from a mathematical model. Blobs are primarily removed in the solubilization (dissolution) and the mobilization (displacement) processes, as discussed above. However, compared to dissolution, the mobilization mechanism has not yet been systematically investigated. To describe blobs displaced by surfactant foam in porous media more clearly, pore-scale mechanisms, including pore-scale analysis of forces acting on discontinuous blobs are studied. Jeong et al. (1999) suggested three displacement mechanisms between TCE blobs and surfactant foam in a micromodel: (1) direct displacement, (2) indirect displacement and (3) break-up or snap-off of TCE blobs. Similarly, Torza and Mason (1970), Øren et al. (1992), and Grattoni et al. (1997) observed the mechanism between two phases (air and oil) or among three phases (air, oil, and water), based on spreading coefficients: (1) double drainage displacement and (2) direct displacement. Each mechanism was identified in terms of threshold capillary pressures between phases (Øren and Pinczewski 1994; Øren et al. 1994).

In our work, understanding surfactant foam flow pattern in a pore or from a pore to an adjacent pore will contribute to the assessment of pore-scale phenomena of surfactant foam and NAPL blob. In previous studies, surfactant foam flow patterns at pore-scale are characterized as two types: a discrete foam bubble/surfactant solution and

a foam bubble-train (or bubble-thread) containing more than one of two bubbles divided by individual lamellae or liquid film (Rossen 1988; Chu 1997; Jeong 2000; 2003; Yan et al. 2006). Furthermore, the two types of the surfactant foam differently react with NAPL blobs trapped in pore constrictions.

The study will provide a better understanding of the prediction of NAPL flow behaviors during surfactant foam flooding and will be useful in conceptual and mathematical models predicting the fate and transport of NAPL blobs and surfactant foams in porous media.

1.2 Theoretical Background

1.2.1 Two Main Removal Mechanisms for Displacement of NAPL blobs; Solubilization and Mobilization

First, solubilization of trapped NAPL blobs may be defined as the concept of NAPL dissolution. As noted earlier, NAPL blobs are a long-term threat to humans due to their low solubility and high toxicity, and NAPL concentrations typically exceed the safe drinking water standard, even though the amount of NAPL blobs are low (Kennedy and Lennox 1997). Therefore, understanding blob solubilization is important in improving the removal efficiency of NAPL blobs. However, dissolved NAPL blobs would enlarge the NAPL source zone. Therefore, to predict the behaviors of NAPL blobs solubilized in porous media, a mathematical model that is capable of explaining pore-scale dissolution is required.

Generally, as the NAPL solubility increases, the dissolution rate increases as well. The dissolution rate is also affected by equilibrium condition as well as pore geometry. The rate-limited dissolution coefficient and aqueous solution concentration determine blob solubilization (Pennell et al. 1993, 1994; Imhoff et al. 1994; Brown and Pope 1994; Mayer et al. 1999; Schaerlaekens et al. 2000; Schaerlaekens and Feyen 2004). A quantitative study of solubilization is sometimes accomplished by dimensional analysis, which is commonly expressed in terms of non-dimensional numbers such as a Peclet, a modified Sherwood or Sherwood, a Schmit, and a Reynolds number (Miller et al. 1990; Powers et al. 1991; Kennedy and Lennox 1997; Zhou et al. 2000; Dillard and Blunt 2000; Sahloul et al. 2002). A typical dimensional term used to describe solubilization is in the form of $Sh' = a + b\,\mathrm{Re}^*$ (where* would be a Schmit number, normalized grain size, and NAPL volume fraction). However, the dimensional analysis is limited in explaining NAPL blobs flowing through soil pores. In recent years, pore-scale dissolution models evaluating the blob solubilization quantitatively are of interest (Kennedy and Lennox 1997). To date, models correlated to the dissolution rate coefficient have been developed to simulate the dissolution process of NAPL blobs trapped at pore-scale (Zhou et al. 2000).

Second, mobilization of NAPL blobs is assessed by the balancing the forces acting on a blob. It is based on the characteristics of the NAPL, the properties of displacing phases (herein, water and surfactant foam) and soil pore size distribution. Recently, blob mobilization was evaluated by considering empirical relationships (i.e., viscous coupling, relative permeability, and saturation) between NAPL blobs and the

displacing phases (Wang 1997; Vassenden and Holt 1998; Lenhard et al. 2002). The critical condition of blob mobilization is commonly determined by using a Trapping number N_T, which is obtained from the sum of the Capillary number N_{Ca} and the Bond number N_{Bo}. Previously, several other dimensionless numbers were also used to study NAPL mobilization (Table 1.1).

Table 1.1 Summary of the dimensionless numbers used for NAPL mobilization.

	N_{Ca}	N_{Bo}	$N_{Ca} + N_{Bo}$	N_T
Larson et al. (1981)	$\frac{k\Delta p}{L\sigma}$			
Morrow and Songkran (1981)	$\frac{\mu_w q_w}{\sigma\cos\theta}$	$\frac{\Delta\rho g k}{n\sigma\cos\theta}$	$N_{Ca} + 0.001412 N_{Bo(R^2)}$	
Lenormand and Zarcone (1988)	$\frac{\mu_w Q_w}{A\sigma}$		*Critical Capillary number $N_{Cac} = \frac{2kk_r}{R_o L}$	
Pennell et al. (1993)	$\frac{kk_{rw}\nabla P}{\sigma_{ow} L} = \frac{\mu_w q_w}{\sigma_{ow}}$	$\frac{\Delta\rho g k k_{rw}}{\sigma_{ow}}$	$\lvert N_{Bo} + N_{Ca}\rvert$	
Mayer and Miller (1993)	$\frac{\mu_w q_w}{\sigma}$	$\frac{\lvert\Delta\rho\rvert g R_n^2}{\sigma}$		
Powers et al. (1994)	$\frac{\mu_w q_w}{\sigma}$	$\frac{\Delta\rho g R^2}{\sigma}$		
Hall et al. (1997)	$\frac{\mu_w q_w}{\sigma\cos\theta}$	$\frac{\lvert\Delta\rho\rvert g k k_{rw}}{\sigma_{ow}}$	$\sqrt{\left(N_{Ca}^2 + N_{Bo}^2 - 2N_{Ca}N_{Bo}\sin\alpha\right)}$ * Bank number $N_{Ba} = \frac{NCa - (\sin\alpha)N_{Bo}}{(\cos\alpha)N_{Bo}}$	
Dawson and Roberts (1997)	$\frac{\mu_w q_w}{\sigma\cos\theta}$	$\frac{\Delta\rho g k}{n\sigma\cos\theta}$		
Pennell et al. (1996); Saripalli et al. (1997); Hall et al. (1997); Padgett and Hayden. (1999); Childs et al. (2004);Schaerlaekens et al. (2005)	$\frac{\mu_w q_w}{\sigma\cos\theta}$	$\frac{\Delta\rho g k k_{rw}}{\sigma\cos\theta}$	$\lvert N_{Bo} + N_{Ca}\rvert$ (vertical) $\sqrt{\left(N_{Ca}^2 + N_{Bo}^2 + 2N_{Ca}N_{Bo}\sin\alpha\right)}$ (horizontal)	$\frac{2\beta k k_{rw}}{\Delta l r_n}$ $(\beta = 1 - \frac{r_n}{r_p})$

Table 1.1 (Continued)

	N_{Ca}	N_{Bo}	$N_{Ca} + N_{Bo}$	N_T
Chevalier and Fonte (2000)	$\frac{\mu_w q_w}{\sigma \cos\theta}$ $N_{Bo(k)} = 0.00317 B N_{Bo(R^2)}$	$\frac{\Delta\rho g k}{\sigma\cos\theta}$ $\frac{\Delta\rho g R^2}{\sigma\cos\theta}$		
Pope et al. (2000)	$\frac{\left\lvert \bar{\bar{k}} \cdot \bar{\nabla}\Phi \right\rvert}{\sigma}$	$\frac{kg\Delta\rho}{\sigma}$	$\frac{\left\lvert \bar{\bar{k}} \cdot \left(\bar{\nabla}\Phi + g\Delta\rho\bar{\nabla}D\right) \right\rvert}{\sigma}$	
Boving and Brusseau (2000)	$\frac{k\rho g \Delta H}{\sigma} = \frac{\mu q}{\sigma}$	$\frac{k\Delta\rho g}{\sigma}$	$\sqrt{\left(N_{Ca}{}^2 + N_{Bo}{}^2\right)}$ (horizontal)	
Fu and Imhoff (2002)	$\frac{\mu_w q_w}{\sigma\cos\theta}$	$\frac{\Delta\rho g k k_{rw}}{\sigma\cos\theta}$	$\sqrt{\left(N_{Ca}{}^2 + N_{Bo}{}^2 + 2N_{Ca}N_{Bo}\sin\alpha\right)}$ (horizontal) *Trapping number for pools $N_T^P = \frac{\mu_w \bar{\bar{k}} \bar{k}_{rw} \bar{q}_w \cdot \bar{\ell}}{(P_c^{B*} - P_c^A)} - \frac{\Delta\rho g \nabla z \cdot \bar{\ell}}{(P_c^{B*} - P_c^A)}$	
Duffield et al. (2003)	$\frac{\mu_w q_w}{\sigma}$	$\frac{\Delta\rho g k k_{rw}}{\sigma}$	$\left\lvert N_{Bo} + N_{Ca} \right\rvert$ (vertical)	
Jeong et al. (2005)	$\frac{\mu_w q_w}{\sigma\cos\theta}$, $\frac{\mu_w u_w}{n\sigma\cos\theta}$, $\frac{\mu_{app} u_w}{n\sigma\cos\theta}$	$\frac{\Delta\rho g k k_{rw}}{\sigma\cos\theta}$	$\sqrt{\left(N_{Ca}{}^2 + N_{Bo}{}^2 + 2N_{Ca}N_{Bo}\sin\alpha\right)}$ (horizontal)	
Lovoll et al. (2005)	$\frac{\mu_w q_w R^2}{\sigma k}$ $\frac{\Delta P l \bar{r}}{2\sigma L}$	$\frac{\Delta\rho g R^2}{\sigma}$ $\frac{\Delta\rho g l \bar{r}}{2\sigma}$		
Gioia and Urciuolo (2006)	$\frac{\mu_w q_w}{\sigma}$	$\frac{\Delta\rho g k k_{rw}}{\sigma}\mathbf{k}$	$N_{Bo} \pm N_{Ca}$	

* ΔH is the hydraulic gradient, q_w [$L^3L^{-2}T^{-1}$] is the Darcy's velocity of the aqueous phase. Q_w [L^3T^{-1}] is the volumetric flow rate and A [L^2] is the cross-sectional area of the media, Herein, the Bank number is not completely discussed. $N_{Ba} = \frac{\text{Total force in the flow direction}}{\text{Total force to perpendicular to the flow direction}}$, R [L] is a representative pore dimension, k [L^2] is the intrinsic permeability and k_r is the relative permeability for the displacing phase , R_o [L] is the blob length and L [L] is the characteristic length related to the pore geometry and the shape of the menisci at the interface between two phases. Further information about the factors above is provided by each study.

1.2.2 Dimensional Analysis of NAPL Blob Displacement

Dimensional analysis is commonly used to characterize the flow and transport conditions of phases in a multiphase system. In such analysis, dimensionless numbers can describe and quantify the magnitude of forces governing multiphase flow. In our work, three primary dimensionless numbers are used to describe blob mobilization or displacement.

First, the Capillary number, N_{Ca}, is defined as the ratio of viscous to capillary retention forces (Powers et al. 1994; Al-Gharbi and Blunt 2005). Morrow and Chatzis (1982) and Payatakes (1982) explained that residual NAPLs were broken into smaller blob types such as a singlet or doublet at $N_{Ca} > 10^{-3}$, and a singlet was displaced at the same range of N_{Ca}. According to their studies, N_{Ca} can characterize blob size and determine blob mobilization as well. Zhong et al. (2001) also observed similar results in micromodel experiments. They found that trapped NAPLs were split into smaller blobs and that a larger number of small blobs were produced during surfactant flushing than during water flooding at $N_{Ca} < 10^{-3}$ (Zhong et al. 2001). Mayer and Miller (1993) observed that NAPL saturation began to decrease at the range of $N_{Ca} > 10^{-2}$ however, it became constant at $N_{Ca} < 10^{-2}$. They concluded that N_{Ca} could be used to the magnitude of residual saturation at $N_{Ca} > 10^{-2}$. On the other hand, Gioia et al. (2003) observed oil displacement at $10^{-6} \sim 10^{-5}$ of N_{Ca} during water flooding. Lenormand and Zarcone (1988) and Gioia and Urciuolo (2006) also found that the non-wetting phase (oil) displacement began at $10^{-6} \sim 10^{-5}$ of N_{Ca} and at around 2×10^{-4} of N_{Ca}, respectively.

Complete oil recovery from an oil reservoir was obtained at 10^{-3} ~ 10^{-2} of N_{Ca} (Lenormand and Zarcone 1988; Zhong et al. 2001; Jeong and Corapcioglu 2003). For NAPLs displaced by water, Powers et al. (1992) observed that residual NAPL displacement occurs at 1.5×10^{-7} of N_{Ca}, at low water velocity (0.1 cm/h) and also at 7.3×10^{-6} of N_{Ca} for high water velocity (6 cm/h). However, in other experimental works, trapped NAPL volume begins to decrease at 2×10^{-5} of N_{Ca} during water flooding (Ng et al. 1978; Powers et al. 1994). As stated above, N_{Ca} is dependent on the morphology of porous media. Hilfer and Øren (1996) showed that N_{Ca} was 10^{-4}, 3×10^{-6}, and 2×10^{-7} for unconsolidated sand, sand-stone, and limestone, respectively. Dawson and Roberts (1997) found that the value of N_{Ca} was different under vertical or horizontal flow.

Second, the Bond number, N_{Bo}, is the ratio of buoyant to capillary retention forces (Powers et al. 1994; Al-Gharbi and Blunt 2005). This number is considered in spite of the horizontal flow direction (Pennell et al. 1996; Boving and Brusseau 2000; Childs et al. 2004; Schaerlaekens et al. 2005). In previous papers, the buoyant force used in N_{Bo} was usually expressed with permeability. However, some researchers employed droplet/blob radius or solid grain radius instead of permeability, as shown in Table 1.1. Dawson and Roberts (1997) established N_{Bo} in terms of porosity. Gioia et al. (2003) observed that trapped oil is partially mobilized at 10^{-3} ~ 10^{-2} of N_{Bo} and completely dislodged over 10^{-2} of N_{Bo}. However, the critical value of NAPL blob mobility could be increased by increasing the difference of density between NAPLs and the displacing

phases. Additionally, blob mobility is enhanced when grain or blob sizes increase (Gioia et al. 2003). It also increases as the interfacial tension between NAPLs and the displacing phases decreases (Gioia et al. 2003). Gioia and Urciuolo (2006) attempted to describe N_{Bo} in terms of a vector and found oil mobilization at approximately 10^{-3} of N_{Bo}.

As discussed above, NAPL blob or oil mobilization could be evaluated by N_{Bo} or N_{Ca}. Nevertheless, to estimate the magnitude of blob mobilization, Pennell et al. (1996) employed a Trapping number N_T (see Table 1.1). Sometimes, N_T was also evaluated by the sum of N_{Bo} and N_{Ca} (see Table 1.1). Until now, N_T has been used to evaluate a displacement performance. Duffield et al. (2003) demonstrated that during surfactant solution flushing, residual LNAPL and DNAPL mobilization occurred at $4.5 \times 10^{-5} \sim 4.7 \times 10^{-5}$ and $2 \times 10^{-5} \sim 5 \times 10^{-5}$ of N_T for homogeneous sands, respectively. Gioia et al. (2003) discovered that during water flooding, oil was mobilized upward at $N_T > 0$, as the N_T was used. Morrow and Songkran (1979) found that residual NAPL saturation decreased from 14 % to nearly 0 % with an increasing N_T.

A Trapping number may be affected by NAPL phase continuity, shape, pore geometry or permeability. For example, Fu and Imhoff (2002) observed that the mobilization of a PCE pool could occur at a lower N_T, unlike PCE ganglia observed by Pennell et al. (1996). As noted above, the value of N_T evaluating blob displacement

would vary due to different characteristics of a porous medium or pore geometry (i.e., pore size distribution, grain size or packing arrays) or NAPL forms.

1.2.3 Effects of Parameters on NAPL Blob Motion

NAPL blobs are increasingly displaced through water-wetting soil pores when NAPL viscosity, density and the interfacial tension between displacing phases (water or surfactant foam)-NAPL decrease (Slattery 1979). Specifically, during the injection of surfactant foam, NAPL blobs are more effectively mobilized due to lower apparent viscosity, lower surface tension of surfactant foam and higher surfactant concentration (Kim et al. 2004). In addition, foam bubble size and lamellae film thickness would also affect blob mobilization.

In looking at pore geometry, as the aspect ratio of pores increases, the blob motion flows faster, where the aspect ratio is defined as the ratio of pore body to pore throat. Chatzis et al. (1983) showed that a higher aspect ratio increased the mobilization of small blobs. The ratio may also affect pore-level mechanism describing blob or foam flow in porous media. The mechanism is commonly categorized into snap-off and coalescence mechanisms (Chatzis et al. 1983). In a snap-off (breakup) mechanism, NAPL blobs or foam bubbles are split into smaller sizes as they pass through pore constrictions. Thus, individual singlet/doublet blobs or foam bubbles are mostly generated in the breakup process (Chatzis et al. 1983). The coalescence (by-passing) mechanism may be defined as a reverse action of the snap-off mechanism where the most complex blobs or bubbles would be produced (Chatzis et al. 1983). Therefore, understanding the two mechanisms is important in identifying the motion of blobs and

bubbles in soil and aquifers. Because of the action of foam bubbles specifically, studies on these mechanisms encourage the use of surfactant foams (Gauglitz et al. 1988). The mechanisms were also affected by the velocity of displacing fluids such as water or surfactant foam. Herein, the relationships between the two pore-level mechanisms and the velocity of the displacing phase were still unclear.

1.2.4 Phenomenological Theory for Surfactant Foam-NAPL Blob Interaction

In this study, the flow of surfactant foam is assumed to be a bubbly flow (discrete foam bubble) or a slug flow (bubble-train) through water-wet porous media in which the flow patterns are governed by the surface tension gradient (Rezkallah 1996). However, the two flow patterns react differently with NAPL blobs trapped within soil pores. A discrete foam bubble flows as a single fluid whereas a bubble-train is considered as two fluids. A bubble-train contains lamellae connecting two neighboring bubbles. In the bubble-train, lamellae and bubbles flow separately as a continuous phase and as discontinuous phase, respectively (Hanssen and Dalland 1990). Therefore, a foam bubble-train would control gas mobility. Chen et al. (2002) observed that a bubble-train, by and large, is filled with two or three connecting bubbles, and a few bubble-trains consist of more than ten bubbles.

In the system of a bubble-train without NAPL, a foam film, called lamellae, contains only surfactant (surface-active agent) and its location is between two air bubbles. However, as a bubble-train comes in contact with NAPL blobs, the lamella would be penetrated by the components of the NAPL blobs. After this, the lamella becomes a pseudoemulsion film, which is located at the interface of the NAPL emulsion

and an air bubble (Hessen and Dalland 1990; Bergeron et al. 1993). Pseudoemulsion film tends to break apart faster than foam film due to weak molecular interactions among NAPL-surfactant solution-air bubble (Hessen and Dalland 1990). Therefore, understanding of films would be significant in explaining the relationship between NAPL blobs and foam in porous media.

1.3 Research Objectives

The objectives of this research are to understand two removal mechanisms (mobilization and solubilization) of trapped NAPL blobs and to analyze the relations between the blobs and the displacing phases (water and surfactant foam) in water-wet porous media. To achieve theses ends, previous models predicting NAPL blobs and foam bubble flow will be improved with new concepts and theoretical approaches. The specific objectives will be accomplished by employing the following steps:

(1) Analyzing the NAPL blob flow at pore-scale and determining the effect of the parameters on blob dissolution and mobilization in removing NAPL blobs. For predicting blob flow in porous media, mathematical models are developed on the basis of force balance and mass balance governing a NAPL blob. Characteristics of NAPL blob (i.e., size and shape) and properties of soil geometry (i.e., grain mean diameter and pore size distribution) are also studied to develop the models.

(2) Carrying out dimensional analysis to evaluate when and at what rate a NAPL blob would flow. In this study, the previous Trapping number is modified to be

an indicator for blob removal performance. It is compared with existing experimental data in previous literature.

(3) Developing mathematical models to understand blob mobilization or displacement and to quantify the critical conditions of blob flow during surfactant foam operation. However, as discussed above, surfactant foam flows as a discrete foam bubble or a bubble-train in porous media and the two different flow types react differently with NAPL blobs. Thus, a model is developed to analyze the effects of the individual foam bubbles and surfactant solution on blob mobilization.

First, pore-level flow arrangements and configurations of three immiscible phases (foam bubble, surfactant solution and NAPL blobs) are identified; foam bubble as a gas (non-wetting) phase, surfactant solution as a liquid (wetting) phase, and NAPL as an oil (intermediate) phase. Their flow configurations are well understood by the study of spreading coefficients.

Next, forces acting on NAPL blobs displaced by discrete foam bubbles flowing through a porous medium are balanced. The force balance extended by pore-level configurations quantifies the removal amount of NAPL blobs. Then, non-dimensionalization of the force balance determines how much the NAPL blobs would be displaced by discrete foam bubbles. Another study is performed to determine discrete foam bubble and blob velocities. A variety of factors (i.e., relative permeability, porosity, bubble or blob sizes) affecting the bubble and blob velocities are investigated as well as apparent viscosities of discrete foam bubbles and surfactant solution flowing through pore constrictions.

(4) Investigating complex interactions between foam bubble-train and NAPL blobs using conceptual and mathematical models. As discussed above, a foam bubble-train consists of two fluids (surfactant solution and air bubbles). Thus, its flow is somewhat difficult to understand. In this study, forces acting on a foam bubble-train are investigated and the bubble-train flow is predicted. Furthermore, various parameters (i.e., apparent foam viscosity, lamellae number, foam quality, and bubble-train volume) affecting the bubble-train motion are examined. The velocity of the bubble-train calculated in this work is compared to experimental data presented in previous studies. A NAPL blob displaced by bubble-train moves through a porous medium by interactive forces acting on both the bubble-train and a blob. Like the bubble-train velocity, the velocity of a NAPL blob is quantified and solved analytically. The critical condition of NAPL blob motion during a foam bubble-train flow is determined by dimensional analysis. From this study, the onset of NAPL blob mobilization in porous media is quantified and predicted in porous media.

CHAPTER II

ANALYSIS OF NAPL BLOBS ENTRAPPED WITHIN A WATER-WET POROUS MEDIUM

2.1. Overview of Theoretical Approach

As mentioned in Chapter I, residual NAPLs lodged in water-saturated soil pores remain as a discrete NAPL type (blobs) under normal groundwater flow regimes. However, the NAPL blobs may be traveling through soil pores as the driving forces (a buoyant and/or a viscous forces) are dominating over the retention forces (a capillary and/or a drag forces) acting on NAPL blobs (Pennell et al. 1996; Dawson and Roberts 1997). A buoyant force is generally dependent on the density difference between a NAPL and a displacing phase (water). A viscous force is proportional to the viscosity, the velocity, and the permeability of a displacing phase. In the case of a capillary force, it strongly depends on the pore throat size and the interfacial tension between NAPL and water. However, the forces are limited in characterizing and elucidating the relative motions between NAPL blobs and water flowing through soil pores because they have focused on NAPL blobs.

This chapter introduces conceptual theories related to flow behavior of NAPL blobs mobilized by water flooding and develops a mathematical model to describe relative motions between the two immiscible phases (NAPL blobs and water). The theoretical approaches are based on relative velocity, cross-mobility, relative permeability, and flow regimes of the two phases traveling through pores (Oren and

Brutsaert 2005). Herein, development of a mathematical model is based on a variety of forces acting on a NAPL blob occluded by water. Therefore, a balance of the forces can explain the static motion of NAPL blobs as well as relative motion between the blobs and water from the moment when the blobs begin to dislodge from pore constrictions. After this, the force balance is rearranged to yield dimensionless groups being capable of quantifying the onset of NAPL blob mobilization. This chapter, additionally, identifies the critical conditions for the blob mobilization and determines the displacement efficiency of water flooding.

2.2. Kinetic Model of Pore-scale Solubilization

During water flooding, trapped NAPL blobs would dissolve to reach the equilibrium condition through solubilization or they would break into smaller blobs in the snap-off mechanism by a high aspect ratio (ratio of pore body to pore throat) of a porous medium. There is a difference for the physical mechanisms between solubilization and the snap-off. Through a solubilization or dissolution process, total blob volume and NAPL concentration would change but with the snap-off mechanism, they are constant. Thus, during solubilization, a study of the total dissolved NAPL blobs volume is significantly important in order to assess blob displacement or removal since the blobs are diminished in size. This would induce blob mobilization during solubilization as well and was observed by Willson et al. (1999).

A change in total volume of blobs dissolved is obtained using a mass conservation equation describing pore-scale solubilization. In other words, it is

calculated by using residual NAPL saturation since the residual saturation can generally define the ratio of NAPL volume to pore space volume (Powers et al. 1992).

2.2.1 Mass Transfer Characteristics

NAPL blob dissolution should be analyzed by using a kinetic model of pore-scale solubilization. Generally, a dissolution process can be described by contaminant transport equations. However, equations describing trapped NAPL dissolution would be inappropriate due to an uncertain scale scheme (Kennedy and Lennox 1997).

In this study, NAPL blobs dissolved in a water-wet porous medium are assumed to follow a first-order rate law governing the inter-phase mass transfer (Miller et al. 1990; Powers et al. 1991). Total mass flux for the dissolved blobs is conjugated to a linear driving force model (Kennedy and Lennox 1997). It is a product of a concentration driving force and a lumped mass transfer coefficient, as shown in Equation (2.1). One such a model for mass transfer between NAPL and water can be expressed by a mass balance equation for the NAPL blobs (Powers et al. 1991),

$$\rho_o n \frac{\partial S_o}{\partial t} = -K\left(C_{eq} - C\right) = -k_m a_o \Delta C \tag{2.1}$$

where ρ_o is the NAPL density [M L^{-3}]; n is the porosity; S_o is the NAPL saturation; The lumped mass transfer K [L^3 L^{-3} T^{-1}] between phases is obtained by multiplying the mass transfer coefficient k_m [L^3 L^{-2} T^{-1}] by the specific interfacial area a_o [L^2 L^{-3}] (interfacial area per unit volume of porous medium) between the phases. K and k_m are plotted in Figure 2.1 (a) and (b), respectively. In this paper L, M, and T denote length, mass and time dimensions respectively.

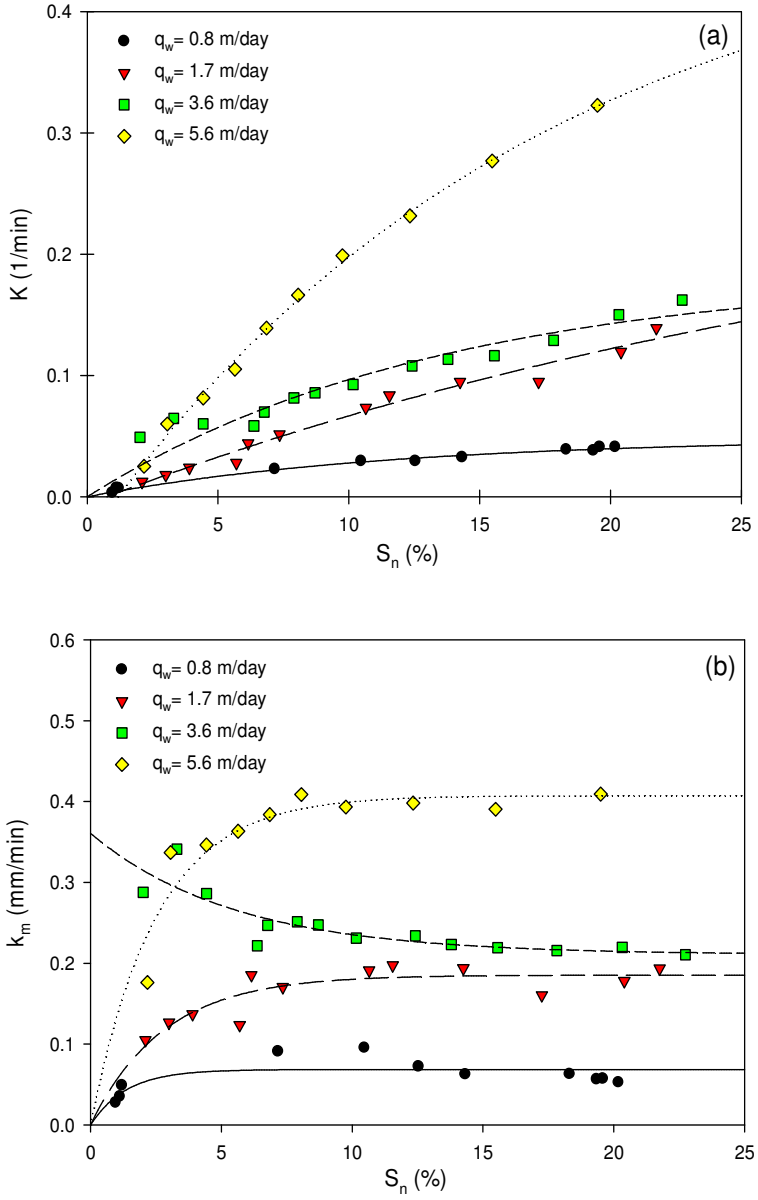

Figure 2.1 Variation of (a) lumped mass transfer rate coefficient K and (b) mass transfer coefficient k_m in TCE (as a typical DNAPL type) saturation S_n for q_w = 0.8, 1.7, 3.6, and 5.6 m/day. All lines in (a) and (b) represent second-degree polynomial fits to data and exponential rise fits to data, respectively.

ΔC is expressed in terms of the difference between the NAPL solubility limit in the water phase C_{eq} [M L^{-3}] and the NAPL concentration in the aqueous phase C [M L^{-3}].

An expression for NAPL concentration C is obtained by deriving an equation proposed by Chowdhury (1996).

$$C = \frac{\rho_o}{L q_w} \frac{\partial A_o}{\partial t} \tag{2.2}$$

where L [L] is the dimension of a target area perpendicular to the flow direction and its value is 7.86 mm in the experience of Chowdhury (1996). A_o [L^2] is the area of NAPL blobs within a target area, as shown in Figure 2.2 (a). q_w is the specific discharge or Darcy's velocity at 0.8, 1.7, 3.6, and 5.6 m/day. From the data obtained from a micromodel experiment conducted by Chowdhury (1996), TCE density is 1.47 g/cm^3, its solubility in water is 1235 mg/l. Additionally, C / C_{eq} has 0.35 of its initial value and decreases as a function of time, as plotted in Figure 2.2 (b). More detail for the parameters used in Equations (2.1) and (2.2) is provided by Chowdhury (1996).

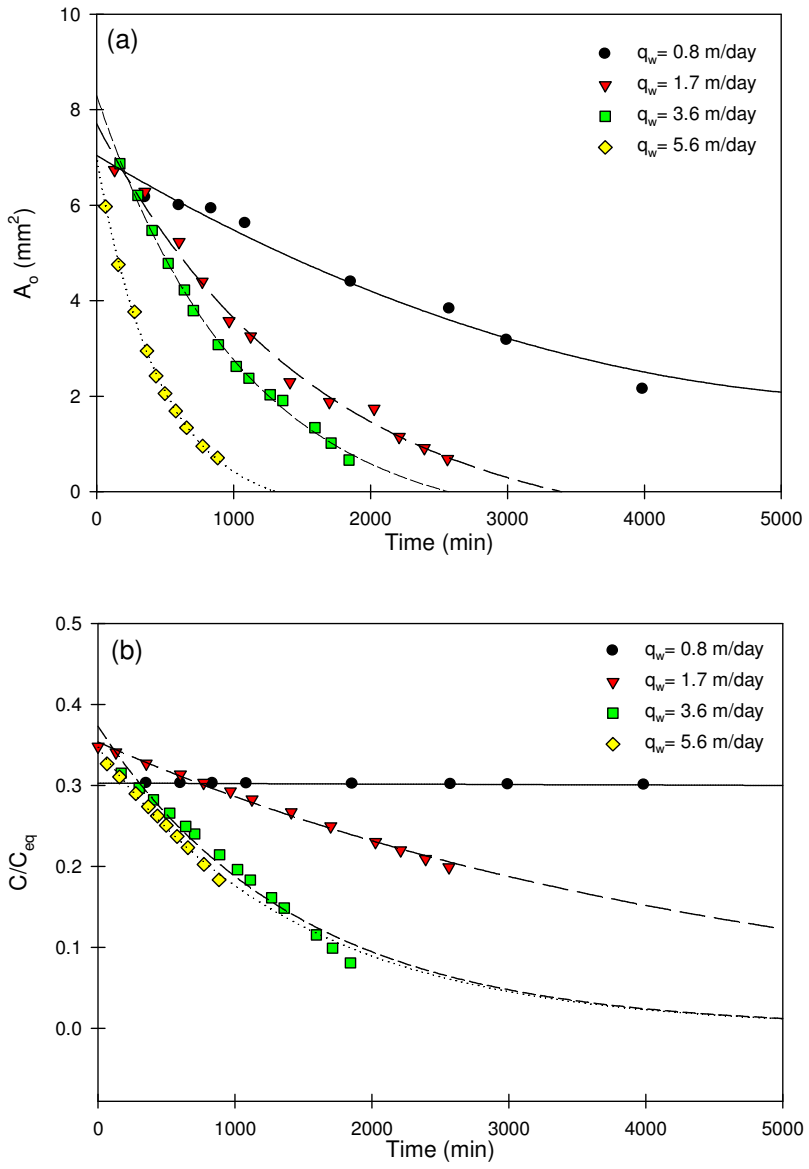

Figure 2.2 Decrease of (a) total TCE area A_o and (b) the ratio of TCE concentration to TCE solubility C/C_{eq} over time for specific discharges of 0.8, 1.7, 3.6, and 5.6 m/day. All lines in (a) and (b) represent second-degree polynomial fits to data except for the solid line in (b).

2.2.2. Dissolving NAPL Blob Volume

With total volume of dissolving NAPL blobs instead of NAPL saturation as expressed in Equation (2.1), the lumped mass transfer rate coefficient is obtained as,

$$K = -\frac{dV_{t,o}}{dt}\frac{1}{V_t}\frac{\rho_o}{\left(C_{eq} - C\right)} \tag{2.3}$$

By integrating Equation (2.3), a change in the total volume of the dissolving NAPL blobs $V_{t,o}$ would be determined by,

$$V_{t,o} = V_{t,oi} - K\frac{\Delta C}{\rho_o}V_T(t - t_i) \tag{2.4}$$

where $V_{t,oi}$ [L^3] and $V_{t,o}$ [L^3] are the initial volume of blobs and the change in the volume of blobs at an initial time t_o [T] before dissolution and a certain blob residence time t [T] after dissolution, respectively. In Equation (2.4), during water flooding, the change in the total volume of NAPL blobs is calculated (see Figure 2.3 (a)). With the same manner, the equation for determining NAPL saturation is given by integrating Equation (2.1),

$$S_o = S_{oi} - K\frac{\Delta C}{\rho_o}\frac{1}{n}(t - t_i) \tag{2.5}$$

where S_{oi} and S_o denote the NAPL saturation and the change in the NAPL saturation at t_o and t, respectively. By comparing Equations (2.4) and (2.5), a relationship of NAPL saturation to volume of dissolving NAPL blobs is expressed as,

$$S_o = \frac{V_{t,o}}{V_p}, \qquad (\text{if } 0 \le S_o \le 1) \tag{2.6}$$

Figure 2.3 shows the total volume of dissolving TCE blob which was obtained from Equations (2.4) to (2.6), respectively. Where NAPL saturation, S_o, is obtained by a micromodel experimental work (Chowdhury 1996). As shown in Figure 2.3, the total volume of the dissolving TCE blobs which was obtained by a kinetic model is in agreement with that obtained by Equation (2.6). The result also shows that the dissolved TCE blob volume decreases over time.

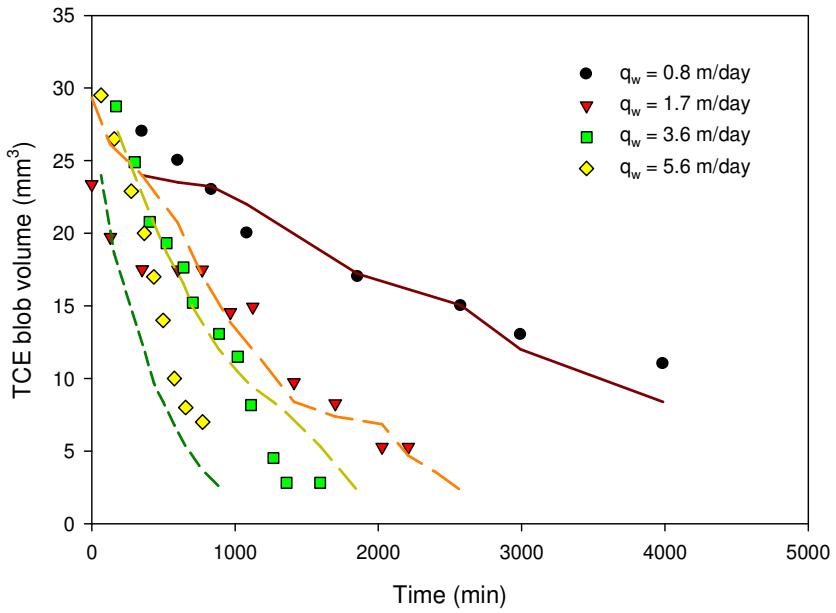

Figure 2.3 Representation of dissolving TCE blob volume obtained by a kinetic model for solubilization (symbols) and by a relationship between TCE saturation and the TCE blob volume (lines).

2.3 Governing Equations Describing Blob Mobilization

As discussed above, the volume of NAPL blobs decreases during solubilization and the process would lead to a mobilization process since the blobs would be small enough to pass through pore constrictions. In this section, forces acting on entrapped or dissolved NAPL blobs in a water-wet pore are investigated.

2.3.1. Buoyant Force

A buoyant force is a resulting fluid force which a NAPL blob body exerts on the water phase. As water is moving upward, the NAPL blobs would be co-currently or counter-currently flowing in the direction of the water flow. A force on the vertical surface of a blob body would be expressed as,

$$F_B = \Delta\rho_{ow} g \sin\alpha V_o \tag{2.7}$$

where $\Delta\rho_{ow} (= \rho_w - \rho_o)$ is the density difference between NAPL ρ_o [M L^{-3}] and water phase ρ_w [M L^{-3}]; V_o [L^3] represents a blob (singlet) of NAPL blobs $V_{t,o}$ [L^3] distributed in an area; and α is the surface inclination angle (Elsherbini and Jacobi 2006). As water is moving upward, DNAPL (Dense Non-aqueous Phase Liquid) tends to flow downward whereas LNAPL (Low Non-aqueous Phase Liquid) flows upward since DNAPL and LNAPL densities are greater and less than 1 g/cm^3 of water density, respectively. From this analysis, it is supposed that the direction of a buoyant force is greatly dependent on the density difference between a displaced (NAPL) and a displacing (water) phases. The force is, additionally, proportional to the change in an equivalent NAPL blob volume V_o. More detail is explained in section 2.4.

2.3.2. Capillary Retention Force

Capillary retention force comes from a concept of a capillary pressure caused by pressure gradient across the NAPL and water interface. A capillary pressure gradient, ∇P_c, is from the pressure difference between a non-wetting (NAPL) and a wetting (water) phase. It would be defined by the Laplace equation (Dullien 1979).

$$\nabla P_C = \nabla P_{nw} - \nabla P_w \tag{2.8}$$

where ∇P_{nw} and ∇P_w denote the pressure gradient of a non-wetting phase and that of a wetting phase, respectively. In Equation (2.8), a capillary pressure, P_C, is related to mean curvature and interfacial tension between the two immiscible phases and it would be expressed as (Corey 1994),

$$P_C = 2\sigma_{ow}\left(\frac{1}{R}\right)\cos\theta_{ow} \tag{2.9}$$

$$P_C = \sigma_{ow}\left(\frac{1}{R_f} + \frac{1}{R_r}\right) \tag{2.10}$$

where σ_{ow} [M T^{-2}] and θ_{ow} are the interfacial tension and the contact angle between NAPL-water, respectively; R [L] is the pore radius; and R_f [L] and R_r [L] denote the front and rear radii of curvature at the NAPL-water interface. Equation (2.10) indicates that migration of NAPL blobs is affected by pore geometry more clearly than in Equation (2.9).

For simplification, Equation (2.9) is multiplied by V_o, an expression for the capillary retention force acting on a NAPL blobs is obtained as,

$$F_C = \nabla P_C V_o = 2\sigma_{ow}\left(\frac{1}{R}\right)\frac{1}{L}\cos\theta_{ow} V_o \tag{2.11}$$

If we assume that a NAPL blob is entrapped at a pore throat and affected by pore throat size R_n, then Eq (2.11) would be rewritten as, (Wang et al. 2004; Corapcioglu et al. 2004)

$$F_C = 2\pi R_n \sigma_{ow}\cos\theta_{ow} \tag{2.12}$$

Herein, Equation (2.12) is employed to describe a trapping force acting on a NAPL blob at pore-scale.

2.3.3. Push Force

During water flooding, we expect viscous effects acting on a blob traveling from one pore to another adjacent pore. To investigate the viscous effects, a push force as a newly developed force is proposed instead of a viscous force. An expression for the push force would be given by a volumetric force proposed by Brustsaert and El-Kadi (1984) as,

$$F = -\mu_w (nS_w)\left\{\frac{1}{kk_{rw}}\left(\frac{1}{nS_w}q_w - q_s\right) + \frac{1}{k_{wo}}\left(\frac{1}{nS_w}q_w - \frac{1}{n(S_o)}q_o\right)\right\}V_o \tag{2.13}$$

where μ_w is the water viscosity [M L^{-1} T^{-1}]; k [L^2] and k_{rw} are the absolute permeability and the relative permeability of the water phase; The cross permeability k_{wo} [L^2] would be expressed in terms of various factors (i.e., drag coefficient, characteristic length or the viscosity ratio). To examine the crossflow effects on two immiscible fluids, k_{wo} would give an assessment of the relative contributions of forces acting on flowing fluids (Cinar et al. 2006); q_w [L3 L^{-2} T^{-1}] and q_o [L3 L^{-2} T^{-1}] denote

the specific discharges of the water phase and averaging NAPL blobs. Equation (2.13) explains that two continuous phases (NAPL and water) traveling through soil pores may cause a momentum exchange.

When trapped NAPL blobs are displaced by the relative motion between the NAPL blobs and water phase, it results in a push force which refers a force exerted on NAPL blobs mobilized by the water phase. The force results from a pressure gradient along a NAPL blob body. From Equation (2.13), an expression for a push force could be rewritten by assuming that the relationship between the velocity of water q_w and that of the soil phase q_s is negligible.

$$F_P = \frac{\mu_w}{k_{wo}}\left(q_w - \frac{S_w}{1-S_w} q_o \right) V_o \tag{2.14}$$

The second terms within the brackets on the right-hand side (RHS) of Equation (2.14) represents an additional force because a momentum transfer between discrete blobs and the water phase occurs. Equation (2.14) shows that a push force is dependent on water velocity and its viscosity. Unlike the previous viscous force inducing blob mobilization, the push force describes flow behavior of NAPL blobs displaced by water as well as the relative motion between NAPL blobs and the water phase.

2.3.4. Drag Force

As discussed in Section 2.2.3, a push force was a newly proposed term used to describe both the flow of NAPL blobs passing through pores and the relative motion between two immiscible fluids after the moment of NAPL mobilization. A drag force exerted along pore sidewalls obstructs a NAPL blob displaced by water. As water pushes

trapped NAPL blobs, the blobs are reluctant to move due to the drag force. The force places pressure and shear forces on the NAPL blob surface and its direction is opposite to the flow direction of the blob body. The drag force on discrete blobs depends on the blob's velocity (Tung and Dhir 1988). An expression for the drag force would be obtained as,

$$F_D = \frac{\mu_o q_o}{k k_{ro}} V_o \tag{2.15}$$

where μ_o [M L^{-1} T^{-1}] and k_{ro} are the viscosity and the relative permeability of the NAPL, respectively. In Equation (2.15), the drag force is dependent on the viscosity and the volume of a NAPL blob.

2.4. Force-law Model for Pore-scale Blob Mobilization

Until recently, the study of multiphase flowing through a porous medium has been challenged because of a lack of understanding of their flow on the scale of individual pores (Olbricht 1996). For NAPL blob displacement at pore-level, specifically, pore-scale phenomena needs to be investigated because NAPL blobs trapped within soil pores are ranged from one to thousands of pore sizes (Reddi and Wu 1996).

2.4.1 Balance of Forces

From Equations (2.16) and (2.17) describing head losses (∇h_o and ∇h_w) of two immiscible fluids introduced by Brutsaert and El-Kadi (2005), a push and a drag force acting on a NAPL blob would be obtained, assuming that the velocity of soil phase is negligible.

$$-\nabla h_o = \frac{\mu_o q_o}{k k_{ro} \gamma_o} + \frac{\mu_o}{k_{wo} \gamma_o}\left(q_o - \frac{1-S_w}{S_w} q_w \right) \tag{2.16}$$

$$-\nabla h_w = \frac{\mu_w q_w}{k k_{rw} \gamma_w} + \frac{\mu_w}{k_{ow} \gamma_w}\left(q_w - \frac{S_w}{1-S_w} q_o \right) \tag{2.17}$$

Expressions for the head losses would be replaced by density and pressure gradients acting on each phase, water and NAPL

$$\nabla h_w \gamma_w = \nabla P_{\mathrm{w}} + \rho_w g \sin\alpha \nabla z \tag{2.18}$$

$$\nabla h_o \gamma_o = \nabla P_o + \rho_o g \sin\alpha \nabla z \tag{2.19}$$

Substituting Equations (2.16) and (2.17) into (2.18) and (2.19), respectively and then subtracting Equations (2.18) and (2.19), a force balance is formed as,

$$\begin{aligned} &\left(\nabla P_{\mathrm{w}} + \rho_w g \sin\alpha \nabla z\right) - \left(\nabla P_o + \rho_o g \sin\alpha \nabla z\right) \\ &= \frac{\mu_w q_w}{k k_{rw}} + \frac{\mu_w}{k_{wo}}\left(q_w - \frac{S_w}{1-S_w} q_o \right) - \left[\frac{\mu_o q_o}{k k_{ro}} - \frac{\mu_o}{k_{ow}}\left(q_o - \frac{1-S_w}{S_w} q_w \right) \right] \end{aligned} \tag{2.20}$$

In the LHS of Equation (2.20), two capillary pressure gradients for the NAPL ∇P_o and the water ∇P_{w} would be expressed in terms of a capillary pressure gradient ∇P_C as expressed in Equation (2.8).

By inserting Equation (2.8) into Eq (2.20), each volumetric force acting on NAPL blobs (F_B^v, F_P^v, F_D^v, and F_C^v) would be represented as

$$F_B^v = \Delta\rho_{ow} g \sin\alpha \tag{2.21}$$

$$F_C^v = \nabla P_c \tag{2.22}$$

$$F_P^v = \frac{\mu_w q_w}{k k_{rw}} + \frac{\mu_w}{k_{wo}}\left(q_w - \frac{S_w}{1-S_w} q_o \right) \tag{2.23}$$

$$F_D^v = \frac{\mu_o q_o}{k k_{ro}} - \frac{\mu_o}{k_{wo}}\left(q_o - \frac{1-S_w}{S_w} q_w \right) \tag{2.24}$$

The volumetric forces above are limited in explaining the flow of discrete NAPL blobs and the water phase at pore-scale because the forces are induced by Darcy's law, which is based on the Representative Element Volume (REV)-scale. Equations (2.23) and (2.24) describe a momentum and a drag force acting on a continuous NAPL flow. However, the two equations are not adaptable for explaining a discrete NAPL blob. Thus, for a momentum and a drag force acting on a NAPL blob, Equations (2.23) and (2.24) are used instead of Equations (2.14) and (2.15). For a capillary retention force, Equation (2.22) is replaced by Equation (2.12). Additionally, in the above equations, instead of two Darcy's velocities of q_w and q_o, u_w and u_o are used for expressing pore-scale blob mobilization and they denote pore or effective velocities for the water phase and a discrete blob, respectively. The two pore velocities are obtained by,

$$u_i = \frac{q_i}{n} \tag{2.25}$$

where the subscript i is o or w for a discrete blob or water, respectively.

Secondly, in Equations (2.21) to (2.24), each volumetric force is limited to unit bulk volume or total volume of a porous medium, V_T, in order to describe a blob flow. For pore-level investigation, V_T is assumed to be equal to a blob volume, V_o. Then, multiplying each volumetric force by a blob volume, V_o, forces are obtained and are balanced as,

$$\sum F = \left(F_B^v + F_P^v - F_D^v - F_C^v \right) V_o = F_B + F_p - F_D - F_C \tag{2.26}$$

Equation (2.26) consists of four forces: buoyant (F_B), push (F_P), drag (F_D), and capillary retention forces (F_C). In Equation (2.26), the buoyant and the push forces act as driving forces to displace a NAPL blob trapped at a pore throat. The drag and the capillary retention forces are holding forces that hinder a NAPL blob's flow from a pore-throat.

Figure 2.4 depicts a NAPL blob trapped within a spherical pore of a constricted tube, which is chosen as an ideal model of a porous medium. By employing the constricted tube, pore-level models describing NAPL blobs would be well developed. In reality, a blob may be greater than a pore body and extend through pore constrictions. As a blob surrounded by a water film is at rest, it would be displaced through a pore to another an adjacent pore due to the pressure difference between the NAPL blob and the water, assuming that there is not any force.

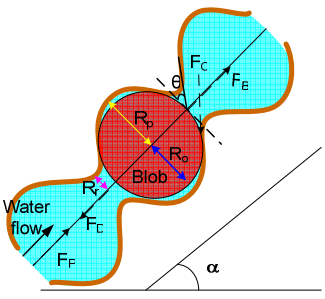

Figure 2.4. Definition sketch of forces acting on a discrete NAPL blob; a spherical blob flowing as a sinusoidal shape in a constricted tube.

By a force-law model, as the sum of push and buoyant forces is greater than that of capillary and drag forces, blob mobilization is expected. The force balance expressed in Equation (2.26) would be rewritten by the four forces in Equations (2.7), (2.12), (2.14), and (2.15)

$$\sum \mathrm{F}=\Delta\rho_{ow} g sin\alpha V_o + A_1\left[\frac{\mu_w}{k_{wo}}\left(u_w - \frac{S_w}{1-S_w}u_o\right)\right]V_o - A_2\left(\frac{\mu_o u_o}{kk_{ro}}\right)V_o - 2\pi R_n \sigma_{\mathrm{ow}}\cos\theta_{ow} \quad (2.27)$$

where A_1 and A_2 are the correction factor and they are assumed to be about 1.0. For unifying Equation (2.27), A_1 is as a function of saturation and porosity. Both A_1 and A_2 are a function of a discrete blob volume and unit bulk volume or total volume of a porous medium, V_T. However, under the assumption that V_T is equal to blob volume, V_o, both A_1 and A_2 would be 1 and the assumption would be plausible. In the equation above, it shows that a NAPL blob mobility is affected by an unbounded fluid (water) having its viscosity μ_w and velocity q_w.

2.4.2 Comparison of Various Formulations for NAPL Blob-Water Flow

We discuss various formulations describing two immiscible fluids flowing through a porous medium, based on Equation (2.27). In the equations, change in NAPL and water saturations are considered and the relative motion between NAPL blobs and the water phase is dealt with a cross-permeability during blob mobilization. However, Equation (2.27) is simply and efficiently expressed under the four different conditions discussed below.

(1) In the form of $\sum F_1$, saturation and relative permeability of residual NAPL are changed during mobilization. The form is similar to theories discussed by previous researchers (Trantham and Durnford 1998).

$$\sum F_1 = \Delta\rho_{ow} g sin\alpha V_o + A_1 \left[\frac{\mu_w}{k_{wo}} \left(u_w - \frac{S_w}{1-S_w} u_o \right) \right] V_o - A_2 \left(\frac{\mu_o u_o}{k k_{ro}} \right) V_o - 2\pi R_n \sigma_{ow} \cos\theta_{ow} \quad (2.28)$$

(2) In the form of $\sum F_2$, an expression for relative motion shown in Equation (2.28) is negligible in Equation (2.29) because they are relatively small compared to other values of terms shown in Equation (2.28). Thus, this term is not considered when calculating blob velocity (Morrow and Songkran 1981; Dawson and Roberts 1997; Boving and Brusseau 2000; Pope et al. 2000).

$$\sum F_2 = \Delta\rho_{ow} g sin\alpha V_o + A_1 \frac{\mu_w u_w}{k_{wo}} V_o - A_2 \frac{\mu_o u_o}{k k_{ro}} V_o - 2\pi R_n \sigma_{ow} \cos\theta_{ow} \quad (2.29)$$

(3) In the form of $\sum F_3$, a drag force acting on a blob is ignored. This

assumption is similar to studies proposed by Pennell et al. (1996), Padgett and Hayden (1999), Childs et al. (2004), and Schaerlaekens et al. (2005).

$$\sum \mathrm{F}_3 = \Delta\rho_{ow} g sin\alpha V_o + A_1 \frac{\mu_w}{k_{wo}} \left(u_w - \frac{S_w}{1-S_w} u_o \right) V_o - 2\pi R_n \sigma_{\mathrm{ow}} \cos\theta_{ow} \qquad (2.30)$$

(4) In the form of $\sum \mathrm{F}_4$, it focuses on blob motion, thus a drag force acting on a blob is considered instead of the pushing force of water. Therefore, a blob velocity may be similar to water velocity. The analogous expression is used in the studies of Corapcioglu et al. (2004).

$$\sum \mathrm{F}_4 = \Delta\rho_{ow} g sin\alpha V_o - A_2 \frac{\mu_o u_o}{k k_{ro}} V_o - 2\pi R_n \sigma_{\mathrm{ow}} \cos\theta_{ow} \qquad (2.31)$$

Expressions for blob velocity obtained by the assumptions above are symbolized as u_{o1}, u_{o2}, u_{o3}, and u_{o4} (Table 2.1). We compare the four equations above with study proposed by Olbricht (1996), as shown in Table 2.1 (Bear 1972).

Table 2.1 Various expressions for balances of forces affecting blob velocity.

	Force balances	Blob velocities	Assumptions
$\sum F_1$	$F_B+F_P=F_C+F_D$	$u_{o1}=\frac{u_w}{\left(A_1\frac{S_w}{1-S_w}+A_2\frac{\mu_o}{\mu_w}\frac{kk_{rw}}{kk_{ro}}\right)}+\frac{\Delta\rho_{ow}g\sin\alpha}{\left(A_1\frac{\mu_w}{kk_{rw}}\frac{S_w}{1-S_w}+A_2\frac{\mu_o}{kk_{ro}}\right)}-\frac{2\pi R_n\sigma_{ow}\cos\theta_{ow}}{\left(A_1\frac{\mu_w}{kk_{rw}}\frac{S_w}{1-S_w}+A_2\frac{\mu_o}{kk_{ro}}\right)}$	
$\sum F_2$	$F_B+F_P=F_C+F_D$	$u_{o2}=\frac{u_w}{\frac{A_2}{A_1}\frac{\mu_o}{\mu_w}\frac{k_{rw}}{k_{ro}}}+\frac{\Delta\rho_{ow}g\sin\alpha}{\frac{A_2\mu_o}{kk_{ro}}}-\frac{2\pi R_n\sigma_{ow}\cos\theta_{ow}}{\frac{A_2\mu_o}{kk_{ro}}V_o}$	No relative motion
$\sum F_3$	$F_B+F_P=F_C$	$u_{o3}=\frac{u_w}{\left(\frac{S_w}{1-S_w}\right)}+\frac{\Delta\rho_{ow}g\sin\alpha}{\frac{A_1\mu_w}{kk_{ro}}\left(\frac{S_w}{1-S_w}\right)}-\frac{2\pi R_n\sigma_{ow}\cos\theta_{ow}}{\frac{A_1\mu_w}{kk_{ro}}\left(\frac{S_w}{1-S_w}\right)V_o}$	No drag force
$\sum F_4$	$F_B=F_C+F_D$	$u_{o4}=\frac{\Delta\rho_{ow}g\sin\alpha}{\frac{A_2\mu_o}{kk_{ro}}}-\frac{2\pi R_n\sigma_{ow}\cos\theta_{ow}}{\frac{A_2\mu_o}{kk_{ro}}V_o}$	No push force and relative motion
$\sum F_5$ Olbricht (1996)	$F_P=F_D$	$u_{o5}=\left(2-\frac{4\times\frac{\mu_o}{\mu_w}}{3\frac{\mu_o}{\mu_w}+2}\left(\frac{R_o}{R_t}\right)+o\left(\frac{R_o}{R_t}\right)^3\right)q_w$ for $\frac{R_o}{R_t}<<1$	No buoyant and surface tension forces
$\sum F_6$ Buckely-Leverett (1942)		$u_{o6}=\left(1-\frac{1}{1+\frac{k_{rw}}{k_{ro}}\frac{\mu_o}{\mu_w}}\right)u_w\times\left(1+\frac{kk_{ro}\mu_w}{kk_{rw}\mu_o}\right)$	No gravity, capillarity, and liquid compressibility

In Table 2.1, we examine the effect of forces on a NAPL blob velocity in order to more clearly predict the flow behavior of NAPL blobs. To quantify blob velocities, properties of a porous medium are chosen from a micromodel experiment conducted by Chowdhury (1996) (Table 2.2). The micromodel is depicted in Figure 2.5. In the micromodel experiment, water flows vertically upward so that the surface inclination angle $\sin\alpha$ employed in Equation (2.7) is assumed to be 1.0. Contact angles between the water and TCE or dodecane Θ_{ow} used in Equation (2.12) are assumed to be 60°. Specific discharges or Darcy's velocities of water q_w are 0.8, 1.7, 3.6, and 5.6 m/day. Chemicals TCE and dodecane are chosen as typical DNAPL and LNAPL types, respectively. The physicochemical properties of TCE and dodecane are obtained by Chowdhury (1996) and Jeong and Corapcioglu (2003). For comparison, the correction factors A_1 and A_2 used in the four formulations above are assumed to be 1.0.

Table 2.2 Micromodel experimental data.

Micromodel		Fluids			
Micromodel length	60 mm		Density (g/cm^3)	Viscosity (cp)	Interfacial tension of water-NAPL (dyne/cm)
Micromodel width	40 mm				
Pore depth	0.1 mm				
Mean solid grain size	1.5 mm	Water	1	1	
Porosity	0.50	TCE	1.47	0.57	33.34
Total pore volume	120 mm^3	Dodecane	0.75	1.75	51.9
Total volume	240 mm^3				

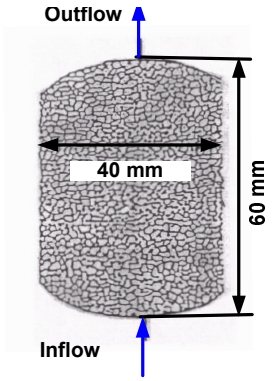

Figure 2.5 Schematic diagram of a micromodel employed by Chowdhury (1996).

Figure 2.6 shows that a discrete blob trapped within a water-wet pore is still captured by a pore under the conditions and data discussed above because u_{o1}, u_{o2}, u_{o3}, and u_{o4} have negative values, regardless of NAPL types. On the other hand, u_{o5} and u_{o6} are 0.0037 ~ 0.054 and 0.0018 ~ 0.00011 cm/sec for TCE, respectively (Figure 2.6(a)). For a dodecane blob, u_{o5} and u_{o6} are 0.0032 ~ 0.052 and 0.0018 ~ 0.00024 cm/sec, respectively (Figure 2.6(b)). To calculate a blob velocity, an isolated blob size is varied from 0.005 to 0.04 cm. As shown in Figure 2.6, two velocities u_{o5} and u_{o6} would have positive values since the velocities are evaluated without considering the effect of soil capillarity. From the results, it is proven that a capillary tension force exerted on a NAPL blob gives a significant effect to blob entrapment. In our system, the capillarity would not be negligible since NAPL blobs are remained at soil pores.

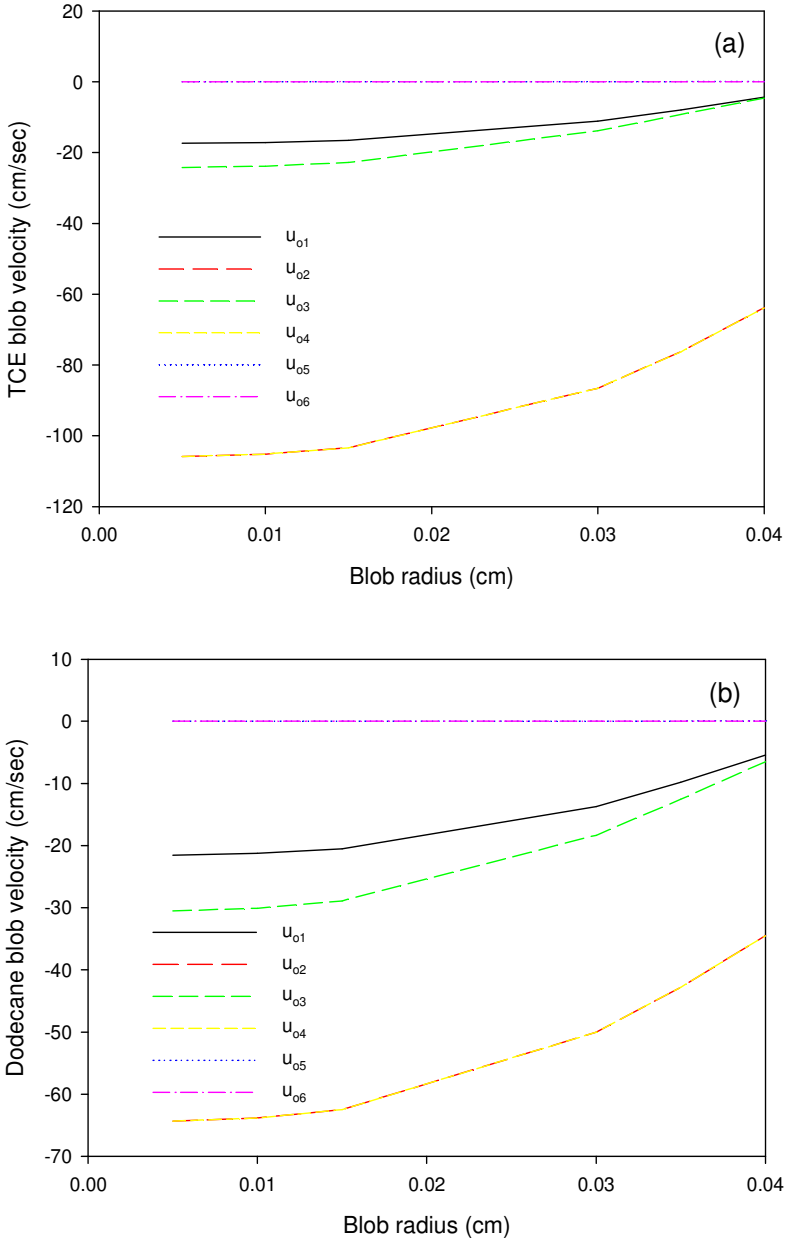

Figure 2.6 Velocities of isolated (a) TCE and (b) dodecane blobs at pore-scale.

Therefore, blob mobilization would require that driving forces (buoyant or push forces) increase or a resisting force (capillary tension force) decrease. However, during water flooding, a push force would be more easily controlled than a capillary tension force acting on a NAPL blob.

Figure 2.6 also shows that blob velocities increase with increasing blob size. It follows a general theory in which droplet velocity flowing through a porous medium is proportional to its size. In the Figure, the result of u_{o6} does not correspond to the general theory. In u_{o2} and u_{o4} proposed under some assumptions, the absolute value of u_{o2} and u_{o4} is greater than the water velocity. This does not reasonably explain the flow velocity of a NAPL blob displaced by the water phase. In the cases of u_{o1} and u_{o3}, they would closely approach a description of a blob motion. However, u_{o3} ignores the drag force and is limited in its description of blob motion obstructed by pore sidewalls. Therefore, it seems that $\sum F_l$ is a pertinent equation to describe mobilized blob velocity at pore-scale.

2.5. Effect of Parameters on Mobility of Trapped NAPL Blobs

2.5.1. Characteristics of a Porous Medium

In this study, a constricted tube is chosen as a prototype of idealized porous medium models. In the tube, all fluids are assumed to be dominated by Darcy's law and on the basis of Kozeny's equation, intrinsic permeability is obtained as (Gioia et al. 2003),

$$k = \frac{d_s^{\,2}}{150}\frac{n^3}{(1-n)^2} \tag{2.32}$$

In Equation (2.32), the intrinsic permeability $k(\,d_s^{\,2}\,)$ is a function of solid grain diameter d_s at pore-scale and at REV-scale, $k(\,L^2\,)$ is a function of a characteristic length of a porous medium L. At pore-scale, the value of k is 7.50×10^{-5} cm^2 according to the data given in Table 4.2.

The porosity n used in Equation (2.32) would be obtained by a ratio of pore volume V_p to total volume of a porous medium V_t as (Gioia et al., 2003),

$$n = V_p / V_t \tag{2.33}$$

To identify wettability in our system, correlated relationships between relative permeabilities and their saturation are investigated. k_{rw} is only dependent on saturation and a constitutive relationship between relative permeability and saturation is expressed by Irmay (1954) (Corey 1994).

$$k_{rw} = S_w^3 = (1 - S_o)^3 \tag{2.34}$$

k_{ro} is obtained by equilibrium relative permeability with k_{rw} as,

$$k_{ro} = 1 - k_{rw} \tag{2.35}$$

Theoretically, k_{rw} would be equal to zero at pore-scale, assuming that a NAPL blob completely filled within a soil pore. Hence, k_{ro} approaches the value of 1. However, at zero value of k_{rw}, k_{ro} would be greater than one due to the hydration of the soil minerals and migration of the soil particles. For this reason, relative permeability to

NAPL may be dependent on saturation as well as the viscosity ratio of a wetting to a non-wetting phase. However, in our system, k_{ro} is assumed to be equal to 1.0.

Saturations and relative permeabilities to NAPL and water computed by the equations above are shown in Figure 2.7. To obtain the result, it is assumed that a NAPL blob is trapped at a pore throat and its volume fraction (the ratio of a NAPL blob to a pore body volume) is almost equal to 1.0. Hence, its relative permeability would be almost 1.0 at NAPL entrapment. In the displacement process of NAPL blobs, NAPL saturation and its relative permeability decrease whereas water saturation and its relative permeability increase.

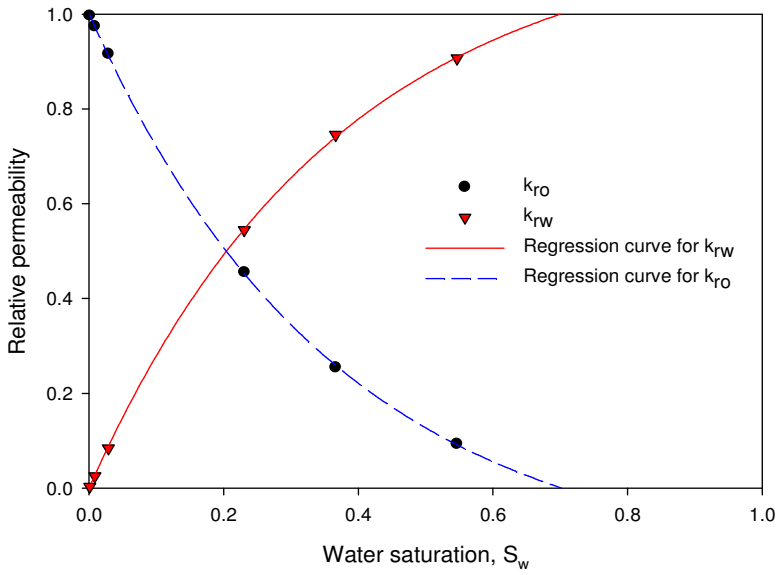

Figure 2.7 Constitutive relationships of relative permeabilities and saturations to NAPL and water. Two curves are fitted to exponential forms.

2.5.2 Pore Geometry Models

An understanding of solid packing and arrays is important in quantifying the mobility of NAPL blobs trapped in porous media. For pore-level investigation and comparison with the micromodel experiment, simple and orthorhombic closed-cubic packing as idealized porous medium models are discussed as shown in Figure 2.8. A simple cubic packing is chosen since its porosity is similar to that of the micromodel. Orthorhombic cubic packing employed frequently in studies of porous media is selected, in order to compare it with a simple cubic packing model.

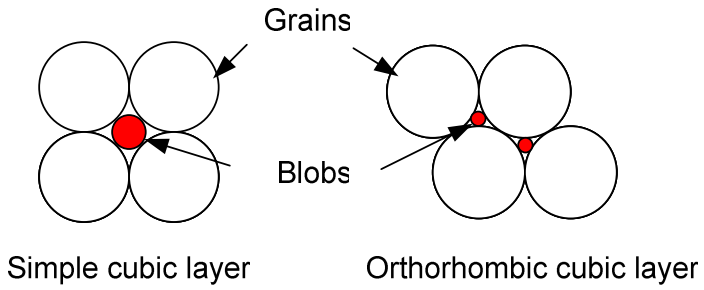

Figure 2.8 Representative diagrams for pore geometry models depicted as an ideal porous medium model.

Pore geometric factors for the micromodel are acquired by the experiment conducted by Chowdhury (1996) and the factors for the simple, and the orthorhombic-closed cubic packing models are obtained from previous studies (Graton and Fraser 1935; Al-Raoush et al. 2003). The values of the factors are shown in Table 2.3.

In Table 2.3, unit pore volumes for orthorhombic and simple cubic packing are calculated by $2.74(d_s/2)^3$ and $1.47(d_s/2)^3$, respectively (Graton and Fraser 1935).

Table 2.3 Characteristics of porous media.

Porous medium size	Micromodel	Orthorhombic-closed cubic packing	Simple cubic packing
Pore throat radius(mm)	0.13	0.12	0.31
Pore body radius(mm)	0.47	0.22	0.55
Unit pore volume(mm^3)	0.49~0.60	1.12	1.61
Unit cell volume(mm^3)	1.47	3.38	2.92
Porosity (%)	50.00	39.54	47.64
Aspect ratio	3.62	1.83	1.77

2.5.3 Critical Velocity of Water Flood

As discussed earlier, NAPL blob displacement occurs due to increasing push forces acting on the blobs during water flooding. The force is enhanced with increasing water velocity. Hence, understanding of the critical velocity of water phase u_w^c is important in order to drive the NAPL blob displacement from entrapment. Additionally, the study of u_w^c would be cost-effective.

In the idealized pore geometry models discussed above, some assumptions are suggested to obtain u_w^c.

(1) Generally, DNAPL and LNAPL blob mobilization occurs at 4.5×10^{-5} ~ 4.7×10^{-5} and 2×10^{-5} ~ 5×10^{-5} of the sum of N_{Ca} and N_{Bo}, respectively and represented as (Pennell et al., 1996; Boving and Brusseau, 2000; Dawson and Roberts, 1997),

$$\left|N_{Ca} + N_{Bo}\right| = 4.5\times10^{-5} \sim 4.7\times10^{-5} \quad \text{for LNAPL types}$$

and

$$\left|N_{Ca}+N_{Bo}\right| = 2\times10^{-5} \sim 5\times10^{-5} \text{ for DNAPL types} \tag{2.36}$$

where the Capillary N_{Ca} and the Bond numbers N_{Bo} are solved by $(\mu_w u_w / \sigma_{ow}\cos\theta_{ow})$ and $(\Delta\rho g \sin\alpha k k_{rw} / \sigma_{ow}\cos\theta_{ow})$, respectively.

(2) For satisfying blob mobilization, the maximum value of the sum of N_{Ca} and N_{Bo} are chosen to be 5×10^{-5}, regardless of NAPL types. In Equation (2.36), the critical velocity of water phase u_w^c replaces u_w and then, an expression for u_w^c is obtained as,

$$u_w^c = \frac{\sigma_{ow}\cos\theta_{ow}}{\mu_w}\left(mobilization\ value - \frac{\Delta\rho_{ow} g sin\alpha k k_{rw}}{\sigma_{ow}\cos\theta_{ow}} \right) \tag{2.37}$$

TCE (as a DNAPL type) blob mobilization occurs at 0.23, 0.19, and 0.22 cm/sec of u_w^c and for dodecane (as a LNAPL type), at 0.05, 0.07, and 0.06 cm/sec of u_w^c in the micromodel experiment, orthorhombic, and simple closed-cubic packing, respectively. However, at the values of u_w^c, the NAPL blobs are still trapped.

From our work, it is found that 1.5×10^{-2} of a critical blob mobilization value would displace simultaneously two trapped DNAPL and LNAPL blobs and u_w^c should be 27.32 cm/sec for TCE and dodecane blob displacement. After this, mobile blob velocities could be discovered (Figure 2.9). In the figure, an isolated NAPL blob is assumed to be a sphere in shape and the range of a blob size is 0.01 ~ 0.04 cm. The size is adapted by considering a soil pore body size and a pore throat size from each pore geometry model. Values of other factors are illustrated by Tables 2.1 and 2.3.

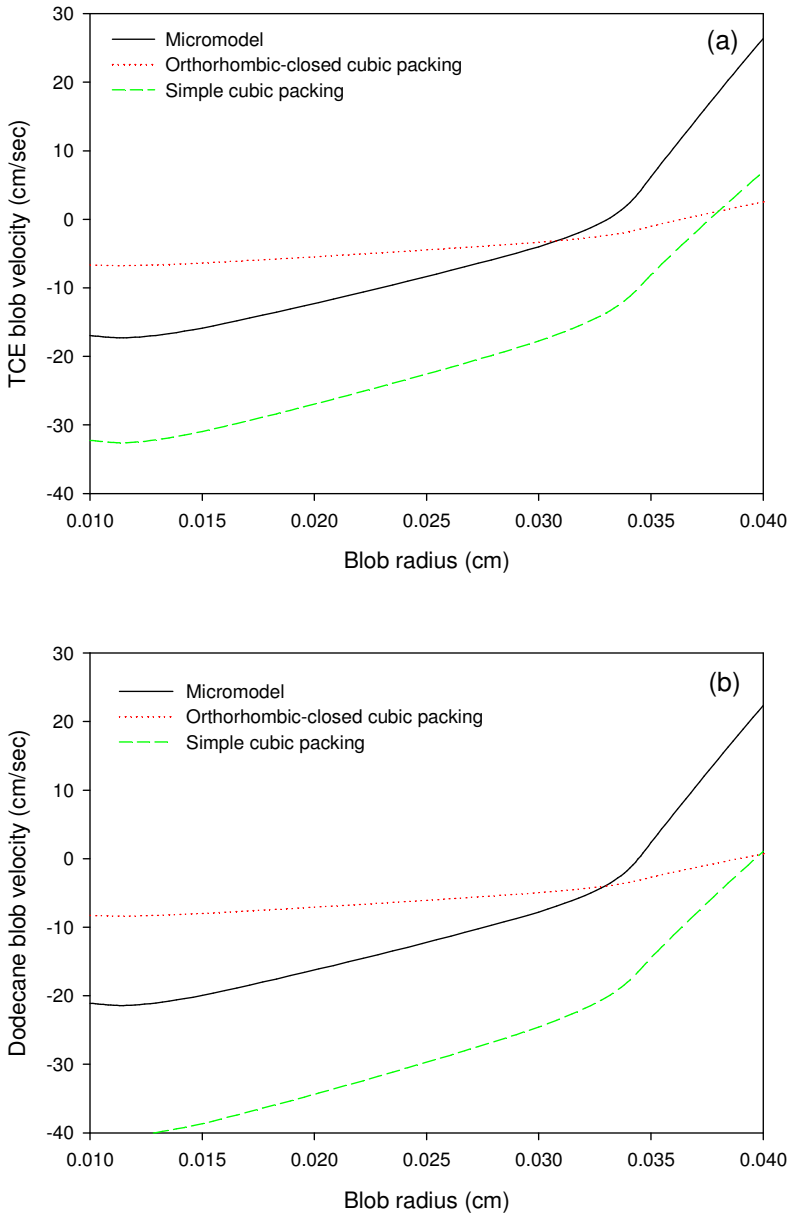

Figure 2.9 (a) TCE and (b) dodecane blob velocities for three different pore geometry models: micromodel experiment, orthorhombic-closed cubic packing, and simple cubic packing.

A surface inclination angle α does not greatly affect the determination of a mobile blob velocity, but it provides a small effect when evaluating the critical velocity of the water phase.

To obtain the results shown in Figure 2.9, we assume that water flows vertically upward through each model and $\sin\alpha$ in Equation (2.7) is equal to 1.0. The contact angle of TCE - or dodecane - water θ_{ow} in Equation (2.12) is assumed to be 60°. In reality, the contact angle between water and NAPL blobs would be a sensitive factor in determining a mobile blob's velocity. As the contact angle increases, the blob velocity is slower. Intrinsic permeabilities employed to obtain blob velocities are 7.50×10^{-5}, 2.54×10^{-5}, and 5.92×10^{-5} cm^2 for the micromodel, the orthorhombic, and the simple closed-cubic packing, respectively. Figure 2.9 shows that TCE and dodecane blobs begin to flow over 0.03 ~ 0.04 cm of a blob size. During blob displacement, blobs flow in the micromodel faster than in the other medium models due to higher intrinsic permeability and porosity values.

2.5.4 Interfacial Tension between NAPL and Water

The effect of interfacial tension of water-NAPL blobs is investigated based on residual NAPL blob displacement. It has been used as a component of the Capillary number and Bond number. As the value of the interfacial tension is low, the two dimensionless numbers increase and blob mobilization is expected. In order to decrease interfacial tension, surfactant solution (Tween 80, SDS, aerosol MA-80, and a mixture of surfonic PE-2594 and witconol NP-100) or co-solvent (50% EtOH) are employed as displacing fluids (Table 2.4). They have been used more effectively than the water phase

to displace NAPL blobs, lowering interfacial tension and increasing the two dimensionless numbers. In Table 2.4, the values of the interfacial tension between NAPL and various displacing fluids including water are shown. More information for properties of surfactant solutions and co-solvent is provided by Zhong et al. (2003) and Boving and Brusseau (2000).

Table 2.4 Interfacial tension of displacing fluids-TCE.

Displacing fluids	Composition	Interfacial tension (dyne/cm)
Water		33.34
Tween 80[1]	POE (Polioxyethylen Sorbitan Monooleate)	10.0
SDS[1]	Sodium Dodecyl Sulfate	3.0
50% EtOH[2]	Ethanol	3.3
Aerosol MA-80[1]	Sodium Dihexyl Sulfosuccinate	0.8
Surfonic PE-2594 + Witconol NP-100[1]		1.22

[1] Zhong et al. (2003); and [2] Boving and Brusseau (2000)

In Figure 2.10, a 1.5×10^{-2} mobilization value is applied for all displacing fluids flowing through an orthorhombic closed-cubic packing model. It shows that blob velocities increase as the interfacial tension between displacing fluids and TCE blobs decreases. Results of the effectiveness of displacing fluids indicate that TCE blob flows more rapidly in surfactant solutions including aerosol MA-80, and as expected, TCE blobs displaced by water move slowly since the interfacial tension of TCE - water is relatively high.

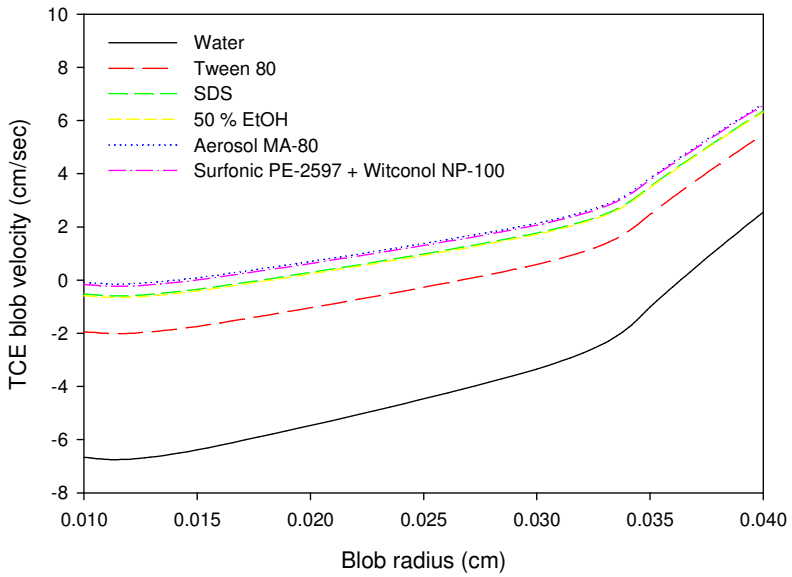

Figure 2.10 TCE blob displaced by various displacing fluids in orthorhombic-closed cubic packing.

CHAPTER III

DIMENSIONAL ANALYSIS OF BLOB MOBILIZATION IN A WATER-WET POROUS MEDIUM

3.1. Blob Mobilization Model

3.1.1 Development of a Trapping Number

As discussed in Chapter II, forces on NAPL blobs remained within soil pores were balanced at the pore-level. As balancing the forces, dimensional analysis would give a help to identify the flow regime of the NAPL blobs and quantify the moment of blob mobilization. As NAPL blob is transited from an immobile phase to a mobile phase, most previous studies had limitation to describe NAPL blob motion. Moreover, blob solubilization and mobilization were separately evaluated with an assumption that mobilization occurs only as solubilization is at or near equilibrium. To overcome these limitations, theoretical approaches and dimensional analysis which are able to simultaneously consider blob solubilization and mobilization are investigated in our study. For dimensional analysis, the total force balance in Equation (2.27) is assumed to be equal to zero and then, dimensionless forms and numbers are obtained by directly nondimensionalizing each force in Equation (2.27). They are represented as,

$$N_T^w = N_{Bo}^w + A_1 N_{Ca}^w - C_1 N_{Ca}^o \tag{3.1}$$

where $N_T^w \left(= 2\pi R_n k k_{rw} / V_o\right)$ is the modified Trapping number, which describes the onset of the blob mobilization during water flooding; $N_{Bo}^w \left(= \Delta\rho_{ow} g \sin\alpha k k_{rw} / \sigma_{ow} \cos\theta_{ow}\right)$ is

the Bond number; $N_{Ca}^{w}\left(=\mu_w u_w/\sigma_{ow}\cos\theta_{ow}\right)$ and $N_{Ca}^{o}\left(=\mu_o u_o/\sigma_{ow}\cos\theta_{ow}\right)$ are the Capillary numbers represent the water phase and the NAPL, respectively. C_1 is the dimensionless form $\left(=A_1\left(S_w/1-S_w\right)\left(\mu_w/\mu_o\right)+A_2\left(k_{rw}/k_{ro}\right)\right)$. Herein, the cross permeability, k_{wo}, is regarded as an effective permeability to the water phase $\left(=kk_{rw}\right)$.

3.1.2 Comparison between Previous and Modified Trapping Numbers

In the study of Pennell et al. (1996), their Trapping number, N_T, is expressed in terms of blob length and pore geometry factors such as the radii of the pore throat and body, and a formula for N_T is depicted by

$$N_T=\frac{2\beta kk_{rw}}{\Delta\ell R_n} \tag{3.2}$$

where $\Delta\ell$ is the blob average length; R_n [L] and R_p [L] are the pore throat and the pore body radii, respectively; β is the dimensionless form $\left(=1-R_n/R_p\right)$. However, in their studies, the value of N_T was obtained not by Equation (3.2) but by the sum of N_{Ca}^{w} and N_{Bo}^{w} (Pennell et al. 1996).

In this study, we compared the modified Trapping number N_T^w obtained by our theoretical approach with the Trapping number N_T expressed by Pennell et al. (1996). From Equations (3.1) and (3.2), it was observed that there are common physical properties. For example, the magnitudes of N_T and N_T^w are proportional to a pore throat or a body size, indicating that NAPL blobs would flow more easily through larger pore throats or pore bodies. It corresponds to previous studies (Saripalli et al. 1997). Saripalli

et al. (1997) observed that NAPL mobilization does not occur at small pore sizes. In the same manner, we can make a hypothesis that as a NAPL blob length or a blob radius is small enough to pass through pore throats N_T and N_T^w increase and thus the trapped blobs begin to be mobilized by displacing fluids.

3.1.3 Trapping Number Concepts for NAPL Blob Mobilization Analysis

Like Pennell et al. (1996), many researchers also employed the sum of N_{Ca}^w and N_{Bo}^w to evaluate NAPL blob motion (Morrow and Songkran 1981; Pennell et al. 1996; Hall et al. 1997; Padgett et al. 1999; Fu et al. 2002; Duffield et al. 2003; Childs et al. 2004; Schaerlaekens et al. 2005). As discussed in previous chapter, when the driving forces (buoyant and push forces) increase over the holding forces (capillary and drag forces), and finally the NAPL blobs would be released from entrapment. Based on our theoretical approach, it can suggest that blob mobilization would occur as the sum of the three dimensionless numbers in the RHS of Equation (3.1) is greater than the value of N_T^w (Dawson 1992; Gioia et al. 2003). In other words, NAPL blob mobilization commences as the absolute value of the RHS exceeds a critical value of N_T^w, and then they may rewritten as,

$$N_T^w < \left| N_{Bo}^w + A_1 N_{Ca}^w - C_1 N_{Ca}^o \right| \tag{3.3}$$

In Equation (3.3), if the RHS has a negative value, NAPL blobs would move downward and vice versa.

Table 3.1 shows that the value of N_T^w was obtained by using Equation (2.27) with micrormodel experiment data in Table 2.2. To compare the value of N_T discussed

in Chapter I with N_T^w, C_1 and A_1 in Equation (3.3) are assumed to be 1.0. Table 3.1 also shows the values of N_{Bo}^w and N_{Ca}^w calculated in our study. However, N_{Ca}^o is not represented in Table 3.1 since TCE blobs are still trapped at the specific discharges of the water phase q_w.

Table 3.1 Values of dimensionless numbers.

q_w (m/day)	N_T^w ($\times 10^{-2}$)	N_{Bo}^w ($\times 10^{-3}$)	N_{Ca}^w ($\times 10^{-6}$)	$\left\|N_{Bo}^w + N_{Ca}^w\right\|$ ($\times 10^{-3}$)
0.9	1.35	- 1.09	1.61	1.09
1.7	4.30	- 1.33	3.95	1.33
3.6	3.90	- 1.35	3.87	1.34
5.6	4.94	- 1.46	9.71	1.45

The result is also illustrated in Figure 3.1, which explains the possibility of TCE blob flow during water flooding. However, as the discussed in Equation (3.3), the RHS does not exceed the value of N_T^w. Therefore, it could conclude that TCE blob mobilization could be not expected under the micromodel experimental condition given by Chowdhury (1996). This result obtained in our theoretical models corresponds to the result observed by Chowdhury (1996). However, in the study of Chowdhury (1996), TCE blobs were reduced and TCE saturation decreased because the blobs are dissolved into water. If NAPL saturation decreases in a solubilization process, an uncertain contaminated area with a large scale may be occurred since the dissolved blobs would flow downward. Generally, experimental data employed to evaluate blob mobilization have a limitation because those data were collected from a batch system. Hence, models

have been developed to control various systems requiring a minimum investment to do a trial and error test. Therefore, it is expected that with experimental data acquired by a batch system the modified Trapping number, N_T^w, suggested in this study can evaluate closely NAPL blob motion. Furthermore, it can contribute to provide theoretical information to improve the removal efficiency of NAPL blobs trapped in porous media.

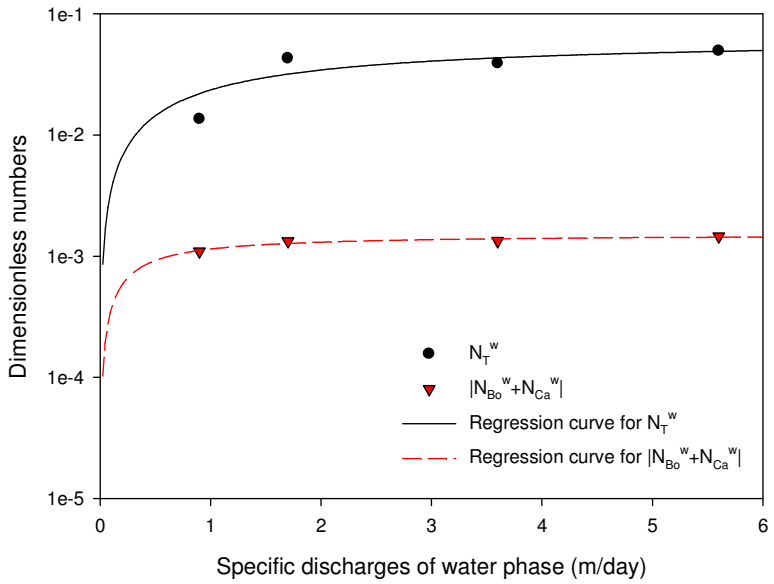

Figure 3.1 Comparison of the modified Trapping number N_T^w and the sum of Capillary and Bond numbers $\left|N_{Bo}^w + N_{Ca}^w\right|$.

3.2 Dimensional Analysis

As stated above, dimensionless numbers evaluate the magnitude of a force as compared to another force. The Bond number N_{Bo}^{w} and the Capillary numbers N_{Ca}^{w} are written in general form except for the modified Trapping number N_{T}^{w}. In previous studies, N_{Bo}^{w} and N_{Ca}^{w} were individually evaluated in order to predict NAPL blob mobilization (Gioia et al. 2003; Gioia and Urciuolo 2006). Herein, we will examine the dimensionless numbers in detail.

3.2.1 Bond Number

The Bond number N_{Bo}^{w} presented in Equation (3.1) is related to a buoyant force for blob mobilization and a capillary tension force for blob entrapment. As the density of water is lower than that of TCE, N_{Bo}^{w} becomes a negative value where the negative sign is not represented in Figure 3.2.

Table 3.2 Values of Bond number N_{Bo}^{w} and TCE saturation S_n.

q_w (m/day)	S_n (%)	N_{Bo}^{w} ($\times 10^{-3}$)
0.9	7 ~ 20	1.55 ~ 0.85
1.7	2 ~ 24	1.91 ~ 0.68
3.6	2 ~ 23	1.91 ~ 0.74
5.6	2 ~ 20	1.90 ~ 0.85

As shown in Table 3.2, the value of N_{Bo}^{w} varies from 0.85×10^{-4} to 1.55×10^{-3} in the range of 2 ~ 24 % of TCE saturation. However, at the given value of N_{Bo}^{w}, blob mobilization is not expected to occur.

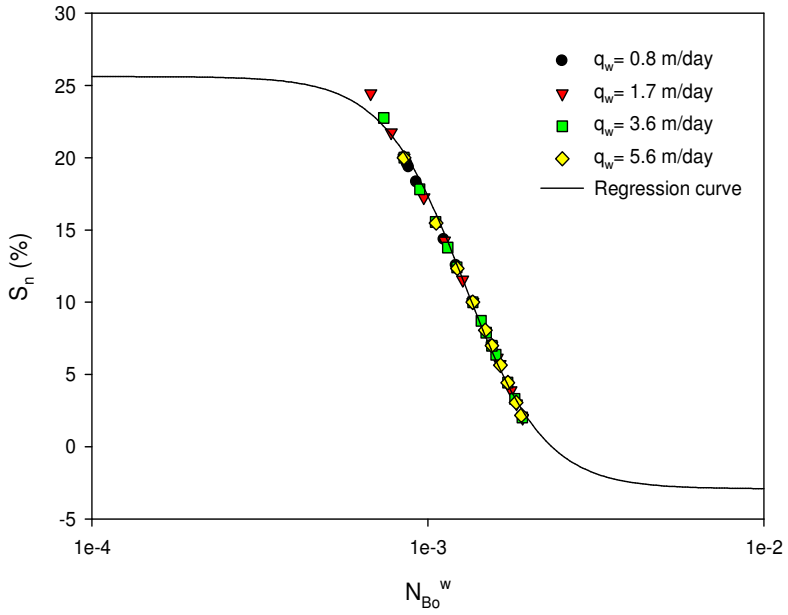

Figure 3.2 Change in TCE saturation S_n with respect to Bond number N_{Bo}^{w}.

Figure 3.2 illustrates that TCE saturation S_n decreases with increasing the Bond number, N_{Bo}^{w}, suggesting that N_{Bo}^{w} could be a good sign for NAPL blob dissolution or mobilization. During a decrease in S_n, if N_{Bo}^{w} is below 10^{-3}, blob dissolution occurs whereas N_{Bo}^{w} is over 10^{-3}, blob mobilization occurs. Also, it could be expected that N_{Bo}^{w} is not affected by specific discharges of the water phase, q_w.

3.2.2. Capillary Number for Water Phase

The Capillary number for the water phase N_{Ca}^{w} signifies the ratio of a push force to a capillary retention force on a NAPL blob. Generally, for a NAPL singlet mobilization, N_{Ca}^{w} should be greater than 10^{-3} (Morrow and Chatzis 1982; Payatakes

1982). However, Gioia et al. (2003) suggested that during water flooding, the trapped droplets were displaced at 10^{-6} ~ 10^{-5} of N_{Ca}^{w} regardless of the droplet size. In Table 3.3, N_{Ca}^{w} values calculated in our work belong to the value of the droplet mobilization proposed by Gioia et al. (2003) but blobs are still trapped. In this study, N_{Ca}^{w} should be over 10^{-3} for blob mobilization since the blob is assumed to be a singlet.

Table 3.3 Values of capillary number N_{Ca}^{w} and TCE saturation S_n.

q_w (m/day)	S_n (%)	N_{Ca}^{w} (× 10^{-6})
0.9	7 ~ 20	2.3 ~ 1.3
1.7	2 ~ 24	6.7 ~ 2.4
3.6	2 ~ 23	12.9 ~ 5.0
5.6	2 ~ 20	14.5 ~ 6.5

Figure 3.3 shows that S_n decreases with increasing N_{Ca}^{w}, and N_{Ca}^{w} is strongly dependent on q_w unlike N_{Bo}^{w}. As q_w increases, N_{Ca}^{w} increases, causing a decrease in S_n.

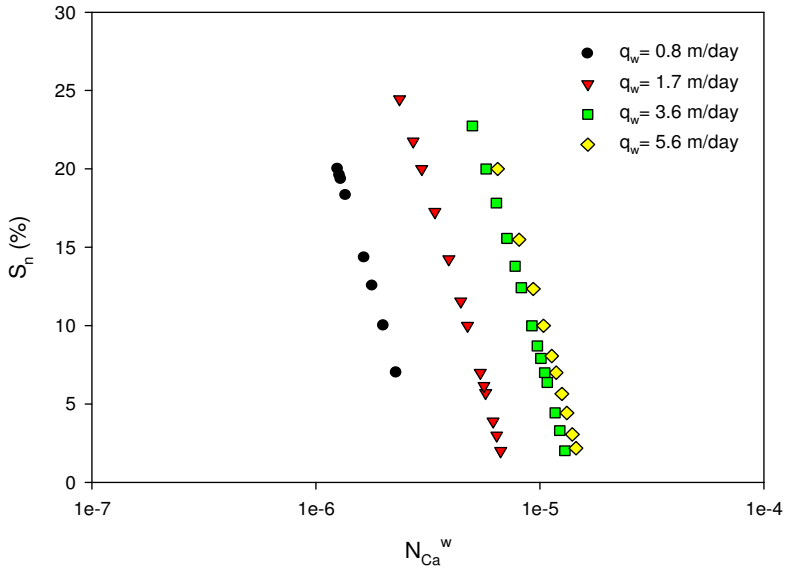

Figure 3.3 Change in TCE saturation S_n with respect to Capillary number N_{Ca}^{w}.

3.3 Development of a Correlation Model

To predict residual saturation of NAPL blobs spreading over a large region, correlation models which describe relationships between NAPL saturation and dimensionless numbers should be used. Residual saturation has been predicted in terms of N_{Ca}^{w}, N_{Bo}^{w} or the sum of the two dimensionless numbers (Morrow and Songkran 1981; Chatzis et al. 1983; Pennell et al. 1996; Dawson and Roberts 1997; Padgett and Hayden 1999; Fu and Imhoff 2002; Childs et al. 2004). Study on the relationship between

dimensionless numbers and residual saturation would provide a better understanding in order to evaluate an uncertain area contaminated by NAPL blobs, choose adaptable remediation technologies, and perform further risk assessment (Chevalier 2006). Therefore, a model being able to describe a correlated relation of residual saturation and dimensionless numbers would be an important and convenient tool to describe the flow of residual NAPL in a contaminated area.

In this study, residual NAPL saturation is correlated to a Trapping number. We found that previous correlation models follow the van Genuchten or Corey types (Delshad 1990; Delshad et al. 1996; Saripalli et al. 1997; White and Oostrom 1998; Pope et al. 2000; Chevalier and Fonte 2000; Childs et al. 2004; Bang et al. 2006; Chevalier 2006). The types are represented by two nonlinear methods such as exponential decay (single, 3 parameters) and standard curves (four parameter logistic curve) (Sigma-Plot®). The previous correlation models are shown in Table 3.4. More details are explained in previous studies (Delshad 1990; Delshad et al. 1996; Saripalli et al. 1997; White and Oostrom 1998; Pope et al. 2000; Chevalier and Fonte 2000; Childs et al. 2004; Bang et al. 2006; Chevalier 2006).

Table 3.4 Correlation models.

	NAPL Saturation-Trapping number	Fluids	Porous Media
White and Oostrom (1998)	$\bar{S}_{rn}^{\max} = \min\left(S_n \, , \frac{\bar{S}_{rn}^{\max}\big\vert_{N_T=0}}{1+(N_T/N_T^c)} \right)$	PCE/surfactant solution (Pennell et al. 1996)	Soil columns
Saripalli et al. (1997)	$S_n = 0.5 S_{ni}\left[1+erf(-\ln N_T - y)/z)\right]$	n-decane/surfactant/cosolvent solution	Glass beads columns
Delshad (1990); Delshad et al. (1996); Pope et al. (2000); Bang et al. (2006)	$S_{rn} = \min\left(S_n, high\ S_{rn} + \frac{low\ S_{rn} - high\ S_{rn}}{1+T_n(N_T)} \right)$	Gas/condensate/water PCE/surfactant/solution (Pennell et al. 1996)	Rock type
Childs et al. (2004)	$S_n = 0.02 + 0.22\left[1+\left(\frac{N_T}{4.85\times10^{-5}} \right)^{2.6} \right]^{-3.2}$	PCE/surfactant solution	Dover soil column
Chevalier and Fonte (2000)	$S_{rn} = 3.71 C_u^{-0.112} C_c^{0.107} N_{T1}^{-0.142}$	Soltrol/water	Glass/complex soil columns
Chevalier (2006)	$S_{rn} = 1.63 - 0.42 C_u + 0.01 N_{T1} - 0.6 C_u^2 + 12.81 N_{T1}^2$ $S_{rn} = 3.61 C_u^{-0.13} C_c^{0.1} N_{T1}^{-0.14}$ $S_{rn} = 3.98 C_u^{-0.2} C_c^{0.12} N_{T2}^{-0.14}$	Same as above	Complex soil columns

Where $N_{T1} = N_{Ca} + 0.001412 N_{Bo(R^2)}$; $N_{T2} = \sqrt{N_{Ca}^2 + N_{Bo(k)}^2}$ (if horizontal flow)

In our work, a correlation model describing the relation of TCE saturation and the modified Trapping number is fit into the values calculated from the expression for N_T^w and it follows a standard regression curve, as shown in Fig 3.4. The result shows that our correlation model follows the Corey type and the model can be expressed as follows.

$$S_o = S_o^{\min} + \frac{S_o^{\max} - S_o^{\min}}{1 + \left(N_T^w / \beta\right)^{\delta}} \tag{3.4}$$

Equation (3.4) is similar to the models proposed by White and Oostrom (1998), Pope et al. (2000), and Bang et al. (2006). In Equation (3.4), the minimum values of NAPL saturation $S_o^{\min}$ are 0.73, 1.89, 1.55, and 1.16 for 0.8, 1.7, 3.6, and 5.6 m/day of q_w, respectively. The maximum values of NAPL saturation $S_o^{\max}$ are 25.2, 25.9, 25.5, and 25.2 at the same values of q_w. The empirical constant β is 0.0165, 0.0151, 0.0155, and 0.0162 and the values of δ is 1.5 over the entire ranges of q_w. As a result, the value of N_T^w is $7.2 \times 10^{-3} < N_T^w < 3.7 \times 10^{-2}$. Its value is nearly two or three orders of magnitude greater than previous values. The reason is found in the studies of Lenormand and Zarcone (1988) and Saripalli et al. (1997). According to their explanation, the N_T^w would be different since N_T^w value depends on the types of porous media and the NAPL blobs, for example, glass beads, sandstone, micromodel, or rock types have different N_T^w values. Furthermore, NAPL singlet, doublet or complex blobs would be displaced by different N_T^w values.

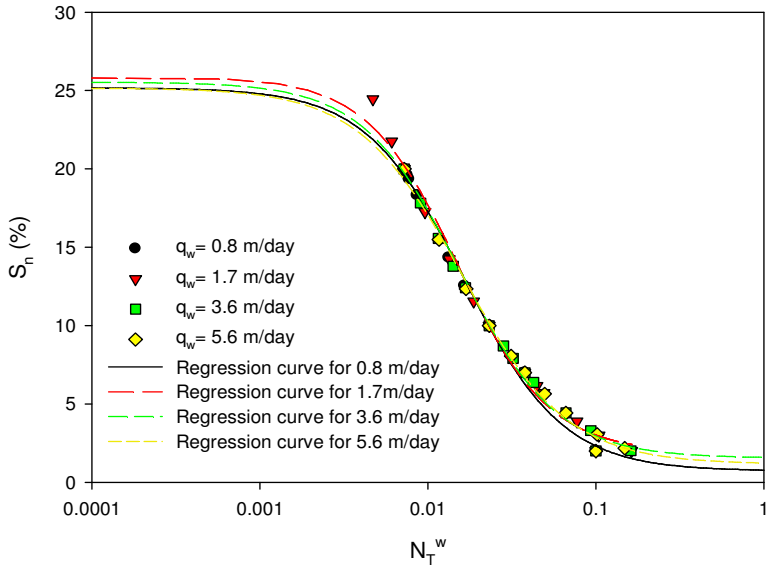

Figure 3.4 Representation of TCE saturation S_n as a function of modified Trapping number N_T^w, which is fitted by a correlation model in Equation (3.4).

3.4 Quantification of Critical Conditions of Blob Mobilization

3.4.1 Prediction of Blob Mobilization

As the sum of three dimensionless numbers or at least one of a dimensionless numbers in the RHS of Equation (3.2) exceeds N_T^w, blob mobilization can be expected to occur. For a NAPL singlet mobilization from entrapment, specifically, a critical specific discharge of the water phase q_w^c of 7.4×10^4 m/day is necessary. The value is obtained by using Equation (3.1) in which the maximum value of N_T^w is 4.94×10^{-2}, as shown in Figure 3.1. The result shows that as blob size gets smaller, it is more difficult to observe blob mobilization. Therefore, for mobilization, small blobs require a higher flow

velocity of the water phase than do large blobs. It also follows a general theory that the value of N_{Ca}^{w} is higher for a NAPL singlet mobilization than that of residual NAPL mobilization. Furthermore, N_{T}^{w} or the sum of the dimensionless numbers represented in Equation (3.1) would be higher than previous values being able to quantify residual NAPL mobilization. In other words, the dimensionless numbers should be higher for the flow of a NAPL blob trapped at a pore throat than a large NAPL blob extending through two or more pore throats. Accordingly, they should have a greater value at a pore-scale than at a micro-scale, in order to drive blob mobilization. However, increase in q_w for blob mobilization may be impractical and inefficient to remove NAPL blobs trapped within a porous medium.

3.4.2 Critical Capillary Number for Blob Mobilization

With the value of q_w^c using Equation (3.1), the critical Capillary number for the water phase, $N_{Ca}^{w,c}$, is obtained, as shown in Figure 3.5. It compares between the general N_{Ca}^{w} and the critical Capillary number $N_{Ca}^{w,c}$. The critical Capillary number $N_{Ca}^{w,c}$ in Figure 3.5 would be expressed in terms of a critical velocity of the water phase, u_w^c, as follows.

$$N_{Ca}^{w,c} = \frac{\mu_w u_w^c}{\sigma_{ow} \cos\theta_{ow}} \tag{3.5}$$

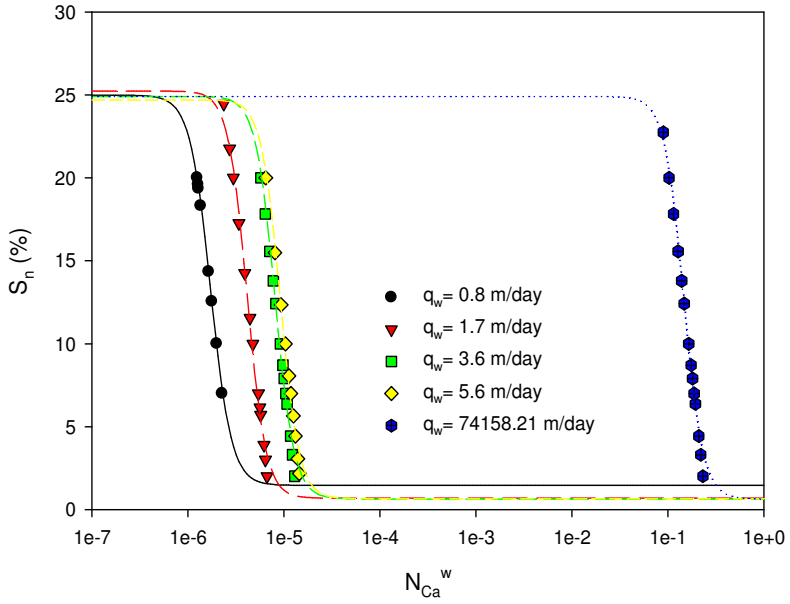

Figure 3.5 Variation of TCE saturation S_n over the Capillary number N_{Ca}^{w} as affected by the Capillary number $N_{Ca}^{w,c}$.

Figure 3.5 plots variation of S_n values between N_{Ca}^{w} and $N_{Ca}^{w,c}$. As the value of $N_{Ca}^{w,c}$ is $8.96 \times 10^{-2} \sim 2.32 \times 10^{-1}$, blob mobilization can occur. It also demonstrates that S_n decreases even though N_{Ca}^{w} is lower than $N_{Ca}^{w,c}$. As mentioned earlier, reduction of S_n occurred not because of blob mobilization but because of its dissolution. Generally, N_{Ca}^{w} would explain blob mobilization but would not identify two removal mechanisms (dissolution and mobilization) of NAPL blobs. However, from this study, the mechanisms would be recognized by comparing N_{Ca}^{w} and $N_{Ca}^{w,c}$. If $N_{Ca}^{w} < N_{Ca}^{w,c}$ and S_n decreases, blob dissolution would be expected whereas blob mobilization would be expected at $N_{Ca}^{w} > N_{Ca}^{w,c}$. From the evaluation, it is known that an understanding of the

relationship between N_{Ca}^{w} and S_n would be important in identifying the mechanism of mobilization and/or dissolution during the removal of the trapped NAPL blobs.

CHAPTER IV

MECHANISMS OF NAPL BLOB DISPLACEMENT BY DISCRETE FOAM BUBBLE FLOW

4.1. Overview

In the previous chapters, the forces exerted on NAPL blobs displaced by waterflood were investigated and the displacement efficiency of the blobs was evaluated. Despite water flooding, most of the NAPL blobs were still trapped and they are rarely displaced. Complete displacement of NAPL blobs requires raising the driving (push and buoyant) forces or lowering a capillary tension force by several orders of magnitude. Practically, the addition of a surfactant solution to soil pores trapping NAPL blobs decreases the capillary tension force by lowering the interfacial tension between the surfactant solution and NAPL blobs. However, surfactant flushing is considered an inefficient method because it induces NAPL blobs to move downward and to enlarge the area contaminated with NAPL. As an alternative operation to displace NAPL blobs upward, steam or gas flooding can be suggested. However, these operations also have problems such as viscous fingering, gravity override, or low contact to residual NAPL-contaminated areas due to the low viscosity and the low density of the gases (Schramm and Novosad 1990; Yan et al. 2006). Recently, as an alternative technology, surfactant foam flooding or surfactant-alternating gas injection is utilized to drive the transport of NAPL blobs upward resulting in higher displacement efficiency (Chu 1996; Jeong and Corapcioglu 2003). During the injection of surfactant foam, NAPL blobs are displaced

by discrete air bubbles dispersed in the surfactant solution (Chu 1996). To displace NAPL blobs more effectively, unstable foam would be strongly recommended than a stable foam because the unstable foam simultaneously transports two immiscible phases (discrete air bubbles and continuous liquid phase) by rupture and/or coalescence processes (Hahn 1985; Owete and Brigham 1987).

In this study, blob mobilization by unstable surfactant foam is investigated. Our main concern is the interaction between surfactant foam and NAPL blobs in a porous medium. Because the interaction between the phases is somewhat complex in a porous medium and the application of the foam used in oil reservoir is limited to studies of foam flow displacing NAPL blobs (Dalland et al 1994; Sagar and Castainer 1997). Additionally, studies of surfactant foam flow behavior have been focused only on its phenomenological configurations in porous media contaminated by residual NAPL. Even though some technical papers have successfully discussed the role of foam on residual NAPL, they are inadequate to develop a quantitative relationship between two immiscible phases with use of unstable foam on NAPL blobs (Llave et al. 1990). Therefore, to predict NAPL blobs displacement by surfactant foam in porous media, a mathematical model quantifying the interaction of two immiscible phases of surfactant foam **-** NAPL blobs at pore-scale is necessarily required. In addition to the work, development of a conceptual model is essential to determine the motion of NAPL blobs displaced by surfactant foam.

4.2 Configuration of Discrete Foam Bubble–NAPL Blob Displacement

As discussed above, surfactant foam would disperse into discrete foam bubbles (air bubbles) and foaming solution (surfactant solution) in porous media. After breakage of a liquid film (called lamellae) connecting two air bubbles, the air bubbles more freely flow through pore throats than foam flow. Then, as the free bubbles confront to NAPL blobs trapped within water-wet pores, the bubbles push the blobs, causing blob displacement. Otherwise, the blobs would spread at the interface of the air bubbles and the surfactant solution. Then, they would create NAPL films surrounding the bubbles and NAPL film displacement would occur. When air bubbles, blobs, and surfactant solution are present together in soil pores, their ideological configurations may be similar to pore-scale displacement mechanisms occurring among three immiscible fluids (gas, oil and liquid). For that reason, the flow configurations of the gas-oil-liquid phases are discussed here in detail, based on pore-scale displacement processes studied by previous chapter.

4.2.1 Negative vs. Positive Spreading Mechanisms

To elucidate configured fluid distributions among three immiscible phases (NAPL blobs, air bubbles, and surfactant solution), a spreading coefficient, S_{aow}, is considered as (Oren and Pinczewki 1992; Oren et al. 1994; Pereira et al. 1996),

$$S_{aow} = \sigma_{aw} - \sigma_{ao} - \sigma_{wo} \tag{4.1}$$

where S_{aow} is the spreading coefficient; the subscripts a, w, and o denote an air bubble, surfactant solution instead of the water phase used in the Chapter II and III, and a NAPL blob, respectively; σ_{aw} [M T^{-2}], σ_{ao} [M T^{-2}] and σ_{wo} [M T^{-2}] are the interfacial tensions

between a bubble and a surfactant solution, between a bubble and a blob, and between a blob and a surfactant solution, respectively. Spreading coefficient S_{aow} shows the possibility of NAPL blobs spreading between two displacing phases (air bubbles and surfactant solution). If S_{aow} has a positive sign (called a positive spreading equilibrium coefficient, $S_{aow} > 0$), we expect that a NAPL blob will spread between the two displacing phases (Oren et al. 1994; Keller et al. 1997). In other words, it could be supposed that a NAPL blob continuously spreads between the two immiscible phases in which there may be a NAPL film surrounding a bubble. If the system has a negative spreading coefficient (called a negative spreading equilibrium coefficient, $S_{aow} < 0$), there is no spreading NAPL blob or a NAPL film occluding an air bubble. (Oren et al. 1994; Keller et al. 1997)

Next, we see how a blob would flow in two different spreading systems. If there is a positive spreading system, a spreading NAPL blob may partially or entirely engulf a free bubble (Oren et al. 1994; Keller et al. 1997). In the case of partial engulfment, there are three contact lines among a spreading blob, an air bubble and a surfactant solution. However, the spreading blob may attempt to completely surround the bubble. For entire engulfment, a NAPL film is formed and it completely surrounds a mobile bubble. Thus, the bubble is separated from the surfactant solution due to a NAPL film and there are two contact lines between a bubble and a NAPL film, and between NAPL film and surfactant solutions. The NAPL film would be transported by a mobile bubble and be smaller in size due to bubble breakage. For a negative spreading system, consider that a mobile air bubble invades a pore throat capturing a non-spreading blob. The mobile

bubble meets the front of the blob and pushes it, causing blob displacement (Oren et al. 1994; Keller et al. 1997). It is called the first displacement (Oren et al. 1994; Keller et al. 1997). Surfactant solution surrounding surfaces of solid pores flows very slowly or stagnantly. Therefore, the front of the blob displaced by the mobile bubble faces the surfactant solution and may push it, resulting in the second displacement. More details for the first and the second displacement of the NAPL blob are discussed in the next section.

4.2.2. Double Drainage vs. Direct Drainage Systems

To understand two or three immiscible phases flowing through a porous medium, a term of wettability is employed. As a liquid phase (water, surfactant solution or co-solvent) invades a non-wetting phase remaining within soil pores (oil - wet or gas wet - medium), the mechanism of imbibition occurs. While a gas phase enters into a liquid (oil or water) - wet medium, a drainage mechanism is anticipated in the system. If oil, gas, and liquid phases are simultaneously present in a porous medium, the liquid phase imbibes and the gas phase drains into the oil-wet medium. Because the gas phase is a non-wetting phase and the liquid phase is a wetting phase against the oil as an intermediate-wetting phase. Therefore, several displacement sequences may occur such as double drainage, drainage-imbibition, imbibition-drainage, or double imbibition among a three-immiscible phase flow (Suicmez et al. 2006). In this study, we suppose that discrete foam bubbles drains into NAPL blobs entrapped in soil pores saturated with surfactant solution, resulting in two different drainage types such as double and direct drainage. If a mobile bubble directly contacts and pushes a NAPL blob, a first drainage

occurs as a direct drainage. After that, the displaced blobs would push surfactant solution present to the rear of the NAPL blob, causing the second drainage. This sequence is called the double drainage system (Oren et al. 1994).

4.3 Mechanistic Force Balance Approach

4.3.1 Equilibrium Forces

Equilibrium force among three immiscible phases (air bubble, surfactant solution, NAPL blob) depends on capillary pressures based on a spreading coefficient. Suppose that there is a double drainage system with a negative spreading coefficient. Under this assumption, a capillary pressure is expressed by (Øren and Pinczewski 1992; Øren et al. 1994),

$$P_c = \sigma_{ao} \cos\theta_{ao} R_{c1} + \sigma_{wo} \cos\theta_{wo} R_{c2} \tag{4.2}$$

where R_{c1} [L^{-1}] and R_{c2} [L^{-1}] denote the threshold curvatures at the interfaces of air bubble-NAPL blob and water-NAPL blob, respectively. They can also be expressed in terms of pore sizes using the Laplace's equation.

$$R_{c1} = 2\left(\frac{\cos\theta_{ao,f}}{R_n} - \frac{\cos\theta_{ao,b}}{R_p} \right) \text{ and}$$

$$R_{c2} = 2\left(\frac{\cos\theta_{wo,f}}{R_n} - \frac{\cos\theta_{wo,b}}{R_p} \right) \tag{4.3}$$

where the subscript f and b denote the front and the rear sides, respectively; θ_{ao} [$M\ T^{-2}$] and θ_{wo} [$M\ T^{-2}$], are the contact angles of an air bubble and a NAPL blob, respectively.

For simplification, the contact angles of the front $\theta_{ao,f}$ and the rear ends $\theta_{ao,b}$ of an air bubble are assumed to be similar. If this assumption is applied to the NAPL blob, Equation (4.3) can be rewritten as,

$$P_c = 2\sigma_{ao}\left(\frac{\cos\theta_{ao}}{R_n}\right) + 2\sigma_{wo}\left(\frac{\cos\theta_{wo}}{R_n}\right) \tag{4.4}$$

In Equation (4.4), a hypothesis of which an air bubble and a blob are trapped by pore constrictions, an equilibrium force could simply be represented by multiplying the surface area of a pore throat by Equation (4.4).

$$F_C^{awo} = 2\pi R_n(\sigma_{ao}\cos\theta_{ao} + \sigma_{wo}\cos\theta_{wo}) \tag{4.5}$$

Equation (4.5) can also account for describing the double drainage displacement between foam and a non-spreading blob, which corresponds to studies of Øren and Pinczewski (1994).

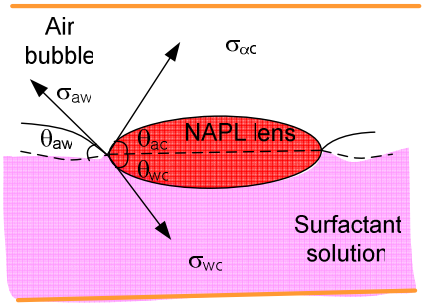

Figure 4.1 Interfacial tensions among three immiscible phases (an air bubble, NAPL lens, and surfactant solution.

Figure 4.1 depicts the relationships among three immiscible phases. The equilibrium condition among three immiscible phases would be represented by the relationship between the three immiscible phases as (Bear 1972),

$$\sigma_{ao}\cos\theta_{ao} = \sigma_{wo}\cos\theta_{wo} + \sigma_{aw}\cos\theta_{aw} \tag{4.6}$$

More detail in Equation (4.6) is provided by Bear (1972).

For a direct drainage system with a negative spreading coefficient, a capillary pressure is signified by Øren et al. (1994),

$$P_c = \sigma_{ao}\frac{2\cos\theta_{ao}}{R_n} \tag{4.7}$$

If an air bubble directly pushes a NAPL blob from a pore throat to an adjacent pore throat and there is no second drainage, an equilibrium force would be obtained in a similar way as in Equation (4.5)

$$F_C^{ao} = 2\pi R_n \sigma_{ao}\cos\theta_{ao} \tag{4.8}$$

If there is a double drainage system with a positive spreading coefficient, it would be more complex and difficult to express an equilibrium force.

For the system, Øren et al. (1994) attempted to express a capillary pressure as,

$$P_c = \sigma_{ao}\cos\theta_{ao}R_{c1} + \sigma_{wo}\cos\theta_{wo}R_{c2} + \Delta P \cdot n \tag{4.9}$$

where ΔP is the viscous pressure drop describing NAPL film flow and n is the number of pores connecting the first drainage and the second drainage.

By the viscous pressure drop defined by Øren et al. (1994), Equation (4.9) would be rewritten for an equilibrium force.

$$F_C^{awo} = 2\pi R_n(\sigma_{ao}\cos\theta_{ao} + \sigma_{wo}\cos\theta_{wo}) + nf\frac{\mu_o u_{of}}{k}V_{of} \quad (4.10)$$

where f is the flow resistance factor; u_{of} [L T^{-1}] is the NAPL film velocity; V_{of} [L^3] is the equivalent volume of the NAPL film.

For a direct drainage system with a positive spreading coefficient, a capillary pressure is represented as, based on the theory proposed by Øren et al. (1994)

$$P_c = \left(\sigma_{ao}\cos\theta_{ao} + \sigma_{wo}\cos\theta_{wo}\right)R_{c2} \quad (4.11)$$

Using Equation (4.11), an equilibrium force for explaining a direct drainage system could be obtained. It could be expressed as the same as the force in Equation (4.5). From the process above, it is supposed that a double drainage system with a negative spreading coefficient and a direct drainage system with a positive spreading coefficient have the same expression for their equilibrium forces. However, the expression is limited in describing homogeneous and regular solid packing layers.

4.3.2 Buoyant Forces

As discrete foam bubbles and surfactant solution are injected into pores trapping NAPL blobs, a non-spreading NAPL blob is surrounded by surfactant solution as a continuous phase. As a blob is removed, the pore occupied with the blob would be filled with the surfactant solution. While a blob is vertically displaced by a surfactant solution flowing through a pore, a net upward force on the blob, F_B^{wo}, can be represented by,

$$F_B^{wo} = (\rho_w - \rho_o)g\sin\alpha V_o \quad (4.12)$$

In the case of a spreading NAPL film, it would partially or completely engulf an air bubble in the surfactant solution. Thus, the NAPL film and the bubble could be

regarded as an object. However, the net upward forces on the NAPL film, F_B^{wo}, and the air bubble, F_B^{aw}, occluded by the surfactant solution would differently represented as,

$$F_B^{awo} = F_B^{aw} + F_B^{wo} = (\rho_w - \rho_a) g \sin\alpha V_{aw} + (\rho_w - \rho_o) g \sin\alpha V_{wo} \quad (4.13)$$

Where the volume of an engulfed air bubble, V_{aw} [L^3], and a spreading blob, V_{wo} [L^3], at three contact lines among three immiscible phases could be calculated by the methods suggested by Johnson and Sadhal (1985), Torza and Mason (1970), Bloom and Heindel (1997), and Hey and Kingston (2006). Equation (4.12) means that a discrete bubble and a non-spreading blob in flowing surfactant solution are at separation and have no contact line between them. It would be employed for a negative spreading system. Contrary to Equation (4.12), Equation (4.13) describes a positive spreading system.

4.3.3 Driving and Retaining Forces

To investigate a driving and retaining force acting on a trapped NAPL blob, some assumptions are suggested as follows.

(1) During surfactant foam flooding, air bubbles behave as a bubbly flow in a porous medium.

(2) A discrete or isolated foam bubble rather than a surfactant solution pushes a NAPL blob since the flow rate of a surfactant solution is, generally, far slower than that of discrete bubbles in the process of surfactant foam injection (Chu 1996).

(3) A direct and a double drainage system occur when pressure in the surfactant solution between an air bubble and a blob is too low to be present in the two immiscible phases (air bubble and NAPL blob).

Based on the assumptions above, recall Equations (2.14) and (2.15). They describe a push and a drag force acting on a NAPL blob. On the basis of the equations, forces acting on a NAPL blob in three-immiscible phase flow would be derived as,

$$F_D^{awo} = F_D^o + F_D^{wo} + F_D^{ao}$$
$$= -A_3 \frac{\mu_o u_o}{k k_{ro}} V_o - A_4 \frac{\mu_w \left(\frac{V_p - V_o - V_a}{V_o} u_o - u_w \right)}{k k_{rwo}} V_o - A_5 \frac{\mu_a \left(\frac{V_p - V_o}{V_o} u_o - \frac{V_p - V_a}{V_a} u_a \right)}{k k_{rao}} V_o \quad (4.14)$$

where F_D^o is the drag force acting on a blob; F_D^{wo} and F_D^{ao} indicate the momentum-flux force acting on a blob with a surfactant solution and with an air bubble, respectively. Again, F_D^{wo} and F_D^{ao} simultaneously consider an attractive and a repulsive force on a NAPL blob with a surfactant solution and an air bubble, respectively. They also indicate frictions occurring on a NAPL blob surface; A_3, A_4 and A_5 are the correction factors. In our definition, they may be the friction coefficients, which would be controlled by the operators or users on a per-NAPL blob basis; k_{rwo} and k_{rao} are the cross permeability between a surfactant solution and NAPL, and between air bubbles and NAPL, respectively. However, we assume k_{rwo} and k_{rao} are equal to relative permeabilities to surfactant solution k_{rw} and air bubbles k_{ra}, respectively, for quantifying NAPL blob displacement. In Equation (4.14), the other parameters were explained in Chapters II and III. To obtain Equation (4.14), a liquid-gas interfacial drag model (Tung and Dhir 1988) and Darcy's law expressing a relationship among flux, pressure gradient and body force (Brutsaert and El-Kadi 1984) were employed.

4.3.4 Total Force Balance Acting on a NAPL Blob

In Section 4.2, each force acting on a NAPL blob during the injection of air bubbles and a surfactant solution was investigated, based on displacement configurations occurring among three immiscible phases. In the present text, the forces are balanced under the some assumptions below.

(1) NAPL blobs may or may not spread between air bubbles and a surfactant solution however there are no NAPL films completely engulfing or surrounding air bubbles.

(2) Air bubbles rather than a surfactant solution displace trapped NAPL blobs and the displaced NAPL blobs may push the surfactant solution, causing second drainage.

(3) In the system, a double and a direct drainage mechanism occur with a negative and a positive spreading system, respectively.

With the assumptions above and adding up Equations (4.5), (4.12), and (4.14), a force balance exerting on a NAPL blob is obtained as

$$\sum F^{total} = F_B^{wo} - F_C^{awo} - F_D^{awo} \tag{4.15}$$

Herein, we assume that the NAPL blob has no mass. By the consequence of the assumption, the sum of the forces acting on the NAPL blob has to be 0, that is,

$$\sum F^{total} = 0 \tag{4.16}$$

By employing Equations (4.15) and (4.16), finally, the forces are rewritten as,

$$\Delta\rho_{ow} g V_o - A_4 \frac{\mu_w \left(\frac{V_p - V_o - V_a}{V_o} u_o - C_1 u_w \right)}{k k_{rwo}} V_o - A_5 \frac{\mu_a \left(\frac{V_p - V_o}{V_o} u_o - C_2 \frac{V_p - V_a}{V_a} u_a \right)}{k k_{rao}} V_o$$
$$= 2\pi R_n (\sigma_{ao} \cos\theta_{ao} + \sigma_{ow} \cos\theta_{ow}) + A_3 \frac{\mu_o u_o}{k k_{ro}} V_o \tag{4.17}$$

4.4 Effect of Parameters on Flow Velocity of a NAPL Blob

4.4.1 Velocity of a NAPL Blob

Employing Equation (4.17), an expression for a blob velocity is given by,

$$u_o = \frac{\Delta\rho_{ow} g \sin\alpha V_o - 2\pi R_n (\sigma_{ao} \cos\theta_{ao} + \sigma_{ow} \cos\theta_{ow}) + A_4' \frac{\mu_w u_w}{k k_{rwo}} V_o + A_5' \frac{\mu_a \left(\left(V_p - V_a / V_a \right) u_a \right)}{k k_{rao}} V_o}{A_3 \frac{\mu_o V_o}{k k_{ro}} - A_4 \frac{\mu_w \left(V_p - V_o - V_a \right)}{k k_{rwo}} - A_5 \frac{\mu_a \left(V_p - V_o \right)}{k k_{rao}}} \tag{4.18}$$

where A_4' and A_5' are the correction factors and they are made outside the two brackets of the two and the third terms in the LHS of Equation (4.17).

Before a blob velocity is computed, some assumptions are recommended.

(1) An air bubble and a blob are spherical objects in shape.

(2) For all NAPL types, injected bubble size and the interfacial tension between NAPL and air bubbles are given under the same condition since the values are similar in the experiment. However, if the concentration of a surfactant solution or the temperature is changed, the interfacial tension will be greatly different.

(3) Velocities of a surfactant solution and air bubbles are constant at steady-state.

(4) Air bubbles and a surfactant solution concurrently flow upward.

To investigate the flow behaviors of NAPL blobs during surfactant foam operation, some data are employed from the micromodel experiment conducted by Jeong et al. (1999) (Table 4.1).

Table 4.1 Properties of a micromodel used as a porous medium.

	k (cm^2) $\times 10^{-7}$	V_p (cm^3) $\times 10^{-5}$	n	R_n (cm) $\times 10^{-3}$
Micromodel	1.70	8.70	0.27	3.31

To compare DNAPL and LNAPL blob velocities, properties of three different DNAPL types and two different LNAPL types are chosen, as shown in Table 4.2. With the data shown in Tables 4.1 and 4.2, blob velocities could be calculated using Equation (4.18). Herein, it is assumed that the interfacial tension between air (nitrogen) and all NAPLs is the same. Flow velocities of an air bubble and a surfactant solution are fixed at

Table 4.2 Physical and chemical properties of NAPL and two displacing phases.

	Density (g/cm^3)	Viscosity (cp)	Interfacial tension (NAPL-SOS) (dyne/cm)	Interfacial tension (NAPL-Nitrogen) (dyne/cm)
NAPL types				
DNAPL;				
TCE	1.47	0.59	4.9[1]	26.0[1]
Bromobenzene	1.50	1.05	3.7[2]	
4-Chlorotoluene	1.07	0.89	4.1[2]	
LNAPL;				
Dodecane	0.75	1.51	4.6[2]	
Soltrol-130	0.75	1.42	4.0[2]	
Fluids			Surface tension (dyne/cm)	
Gas (nitrogen)	0.0012	0.0179		
Liquid-surfactant solution (SOS; Bioterge 2% AS-40 as anionic)	1.062	1.029	34.5	

By Jeong et al. (1999)[1]; Chu et al. (1997)[2]

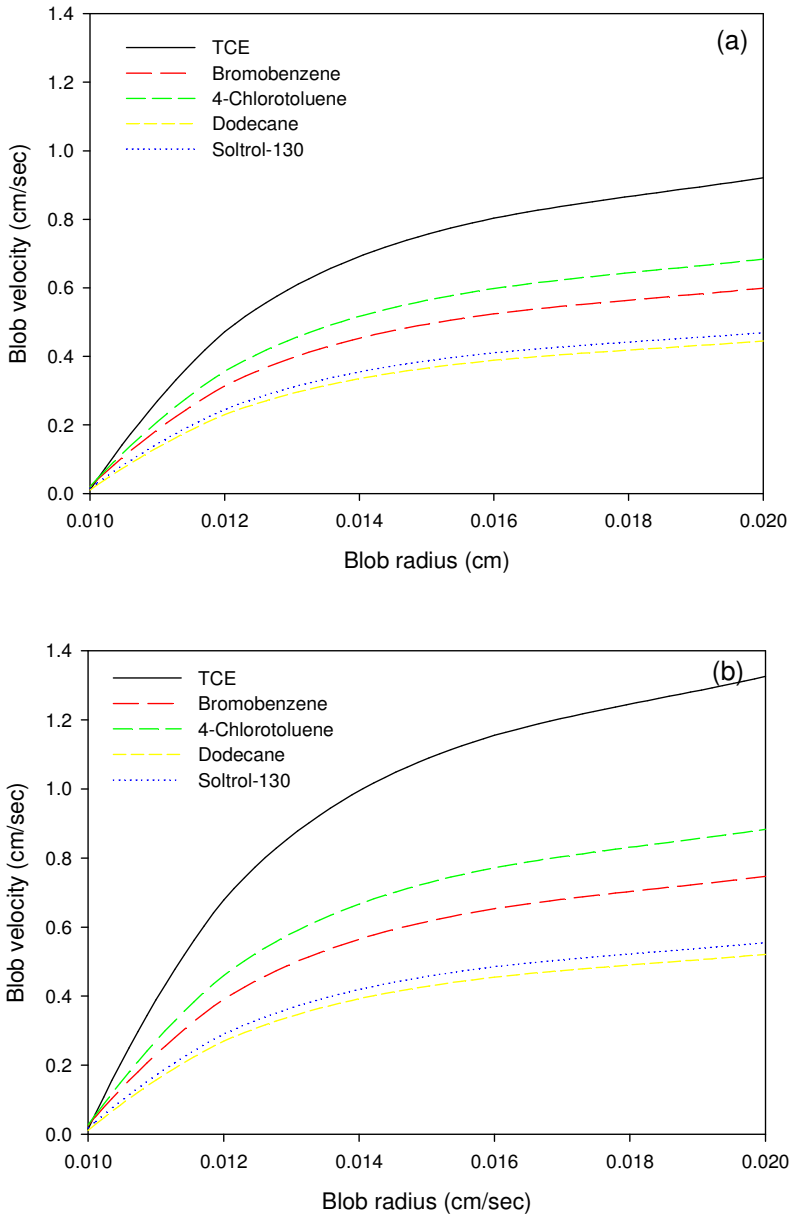

Figure 4.2 Change in NAPL blob velocities as a function of NAPL blob radius in a micromodel; (a) with relative motions and (b) without relative motions between a NAPL blob - a surfactant solution and a NAPL blob - an air bubble.

4 and 0.094 cm/sec, respectively and the air bubble size is 12 mm (Jeong 1999). For investigating effect of relative motion on a blob velocity, relative permeabilities to NAPL blobs, air bubbles and a surfactant solution are fixed at 0.35, 0.48, and 0.16, respectively since relative permeability affects to the relative motion between NAPL blobs and displacing phases.

Figure 4.2 shows that the calculated velocities of the NAPL blobs increase with increasing a NAPL blob size. In the figure, the velocities are also compared (a) with and (b) without relative motions between NAPL blobs and two displacing phases (surfactant solution and air bubbles). In the result, it is proved that NAPL blobs flow faster in the absence of relative motions than in the presence of relative motions, which indicate NAPL blobs resisted by a surfactant solution and air bubbles. The result also illustrates that three different DNAPL (TCE, 4-chlorobenzen and bromobenzene) blobs flow faster than two LNAPL (dodecane and soltrl-130) blobs. The reason is that the viscosity of DNAPL is relatively very low compared to that of two displacing phases (air bubble and surfactant solution).

4.4.2 Velocity of Displacing Phases

To observe the effect of the velocities of the surfactant solution and the air bubbles on NAPL blobs, we assume three different conditions with relative permeability.

(1) Constant relative permeability

During the injection of bubbles and a surfactant solution used as displacing phases, entrapped NAPL blobs may still remained or be mobilized. To consider the effect of bubbles and a surfactant solution on NAPL blob motion, velocities of the displacing fluids are studied. Based on the data provided by Jeong and Corapcioglu (2003), NAPL blob motion is scrutinized (Table 4.3).

Table 4.3 Mobilization experimental conditions.

u_w (cm/sec)	u_a (cm/sec)	k_{rw}	k_{ra}	k_{ro}
0.094	4.00	0.165	0.485	0.350
	9.20	0.276	0.566	0.158
	15.71	0.194	0.709	0.097
	19.90	0.161	0.814	0.025
	22.34	0.248	0.746	0.006

In Table 4.3, velocity of a surfactant solution, u_w, is fixed at 0.094 cm/sec. k_{rw}, k_{ra} and k_{ro} are fixed at 0.165, 0.485, and 0.350, respectively. Herein, the value of k_{ro} shown in Table 4.3 is obtained by the relationship among relative permeabilities of three phases.

$$k_{ro} = 1 - k_{rw} - k_{ra} \tag{4.19}$$

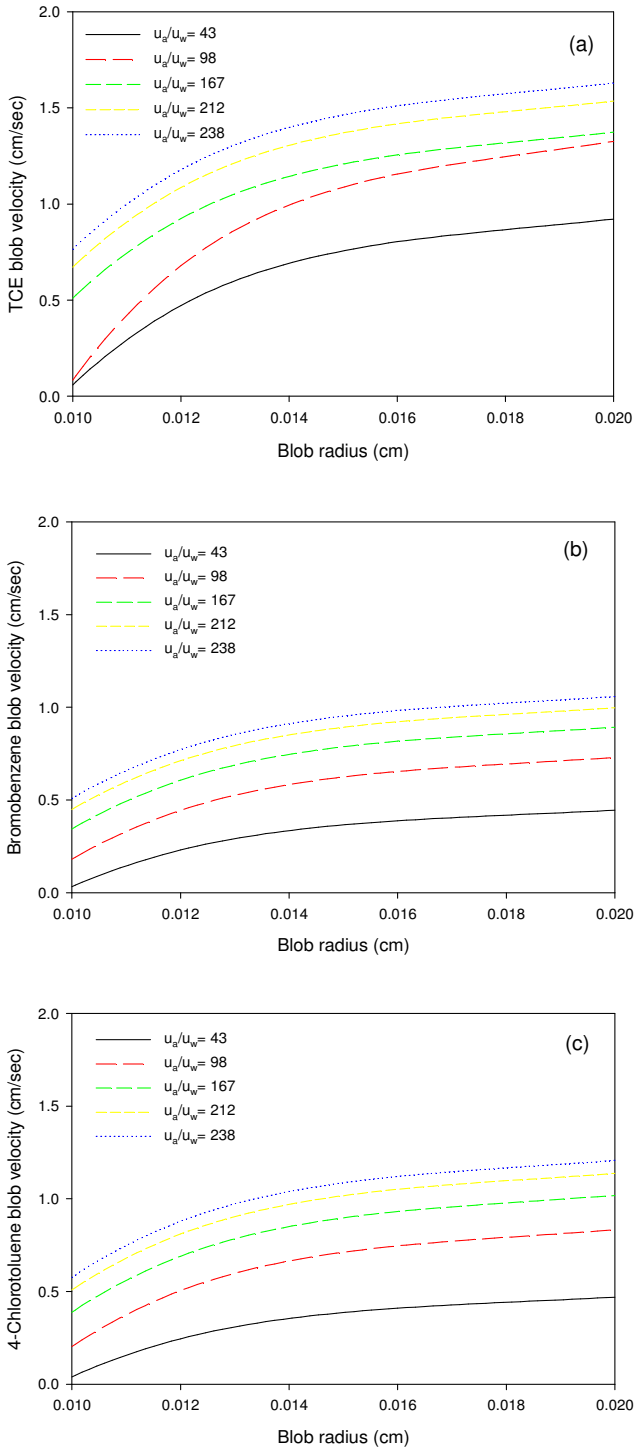

Figure 4.3 DNAPL blob motion under constant relative permeabilities to NAPL blobs, a surfactant solution, and bubbles; (a) TCE, (b) bromobenzene, and (c) 4-chlorotoluene.

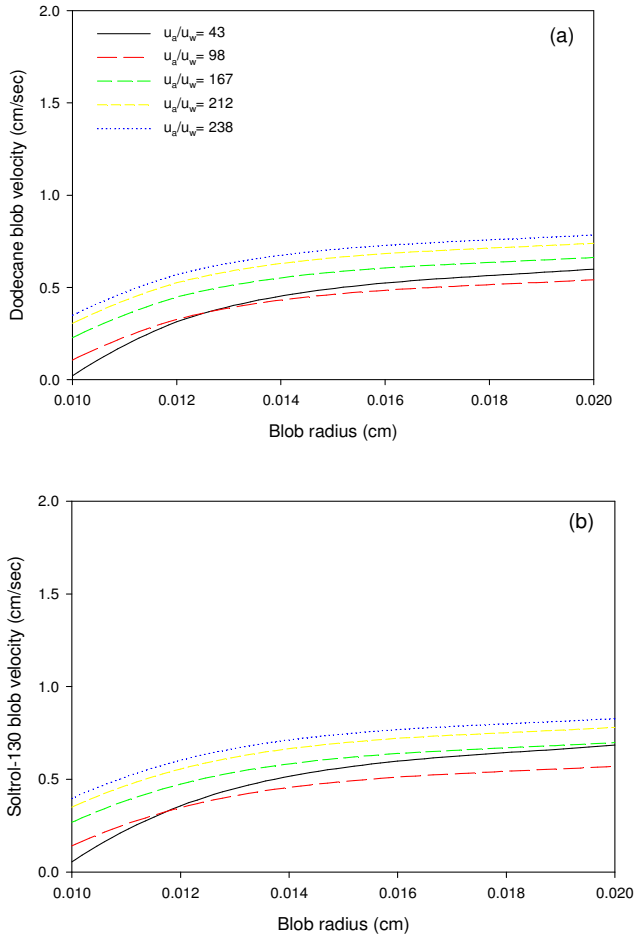

Figure 4.4 LNAPL blob motion under constant relative permeabilities to NAPL blobs, a surfactant solution, and bubbles; (a) dodecane and (b) soltrol-130.

Figures 4.3 and 4.4 show that DNAPL and LNAPL blobs follow the same tendency. DNAPL (TCE, bromobenzene, and 4-chlorobenzene) blob and LNAPL (dodecane and soltrol-130) blob velocities increase as blob size increases. In the Figures above, it is also illustrated that a blob velocity increases as an air bubble velocity increases relative to a surfactant solution velocity. For comparison of all NAPL types, a DNAPL blob velocity is greater than that of a LNAPL blob and specifically, a TCE blob tends to flow much faster than the others.

(2) Change in relative permeabilities to NAPL blobs and air bubbles

Next, u_w and k_{rw} are still fixed at 0.096 and 0.165, respectively and k_{ra} and k_{ro} are changed. Herein, we assume that relative permeability to water k_{rw} is almost constant. According to Kalaydjian et al. (1993), saturation of a liquid phase is always less than 20 % regardless of a positive or a negative spreading coefficient among three immiscible phases. In their experimental results describing relative permeabilities to three immiscible phases, it is inferred that the value of k_{rw} is not greatly changed in the displacement mechanism.

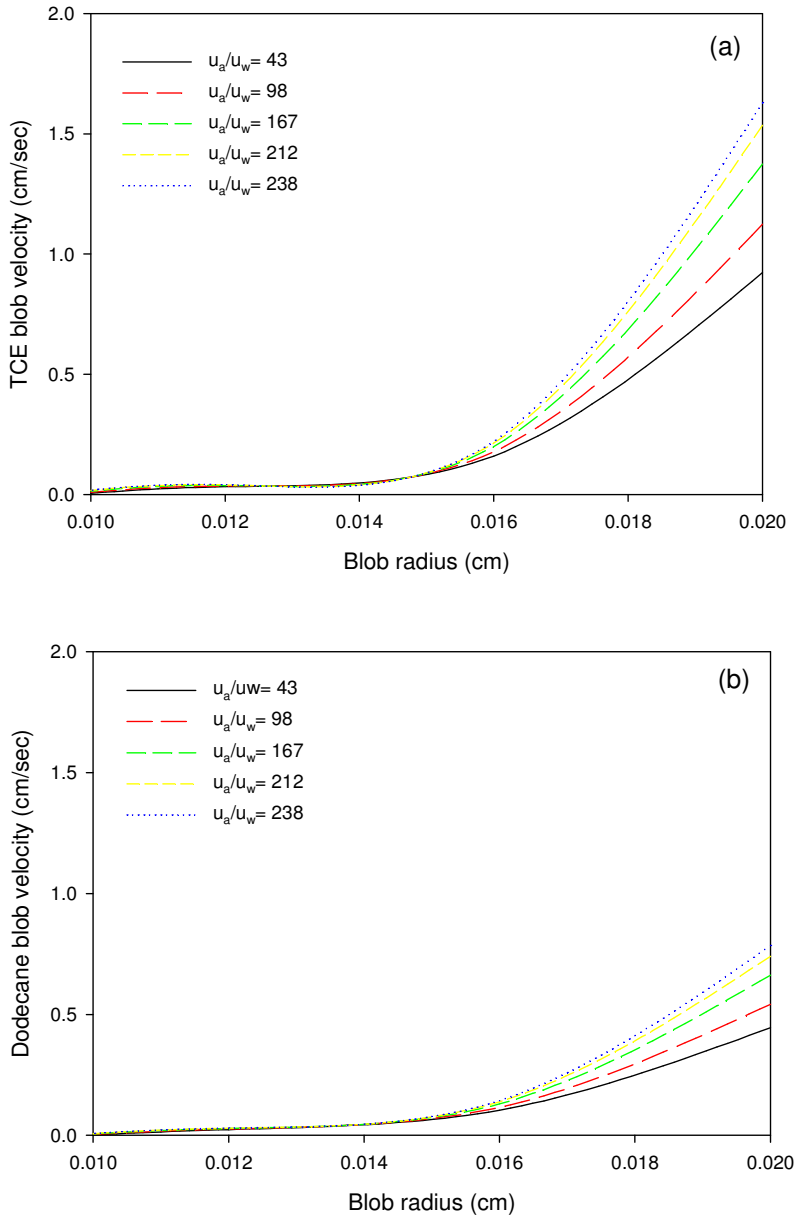

Figure 4.5 Velocities of (a) a TCE blob (DNAPL type) and (b) a dodecane blob (LNAPL type) under constant relative permeability to a surfactant solution.

In a free gas phase, k_{ra} is higher for a positive spreading condition than for a negative one, and for saturation of a trapped gas phase, it has 25 % and 9 % for a positive and a negative spreading condition, respectively (Kalaydjian et al. 1993). From their studies, it is also known that relative permeabilities may be affected by spreading conditions.

In Figure 4.5, TCE and dodecane are chosen as a typical DNAPL type and as a typical LNAPL type, respectively. They have the same tendency and a blob velocity increases with increasing a blob size, regardless of NAPL types. Additionally, for comparison of NAPL types, a TCE blob velocity is greater than that of dodecane blob.

(3) Influence of relative permeabilities to three immiscible phases

By considering relative permeabilities to three immiscible phases, each blob velocity is calculated as shown in Figure 4.6. It is similar to the result shown in Figure 4.5. As a NAPL blob gets bigger, the blob flows faster through pores. The magnitude of blob velocities is not greatly different between the results shown in Figures 4.5 and 4.6.

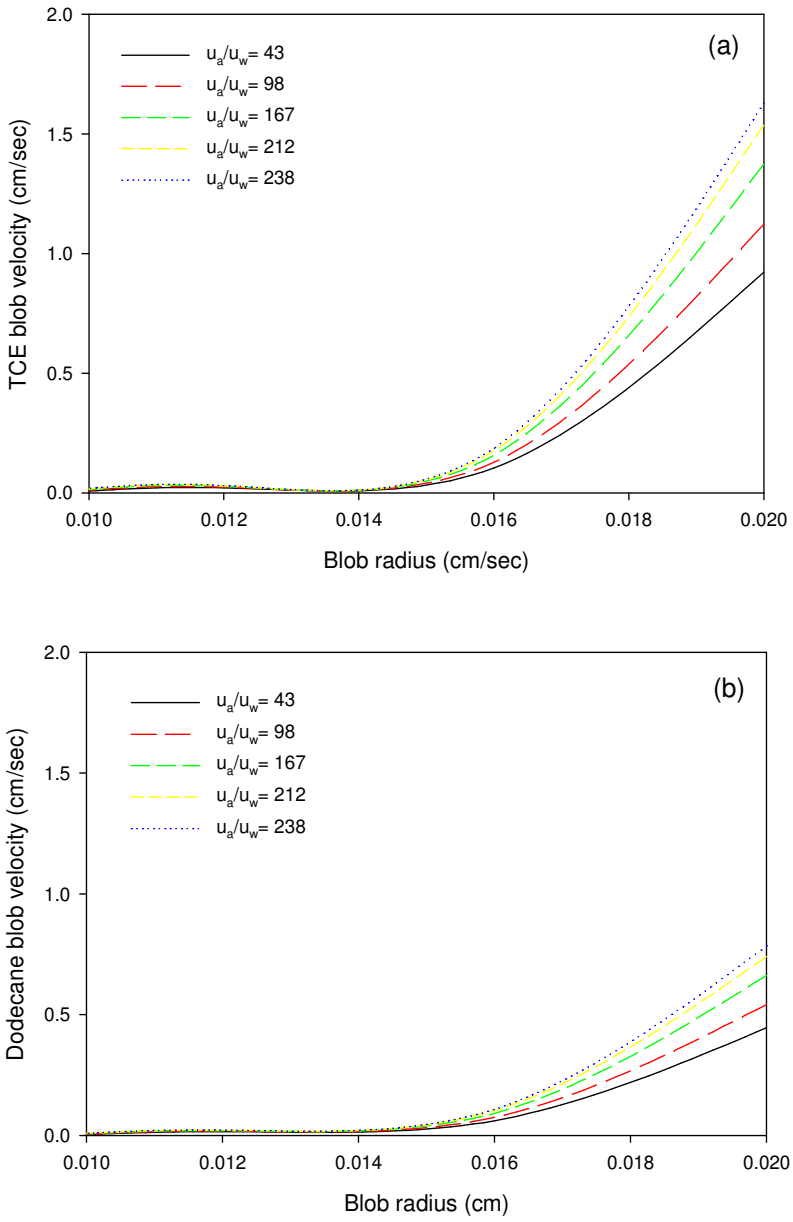

Figure 4.6 Velocities of (a) a TCE blob and (b) a dodecane blob under different relative permeabilities of three immiscible phases (NAPL, a surfactant solution, and air bubbles).

4.4.3. Viscosity of a Gas Phase

To investigate the effect of an apparent gas viscosity on NAPL blob motion, some data are obtained in the pack 3 experiment conducted by Falls et al. (1989). At the given condition, intrinsic permeability is 8.83×10^{-7} cm^2 and air bubble size is fixed at 0.054 cm. Apparent gas viscosities with changes in gas velocities and liquid velocities are given in Figure 4.7. It shows that as apparent gas viscosity decreases, gas velocity

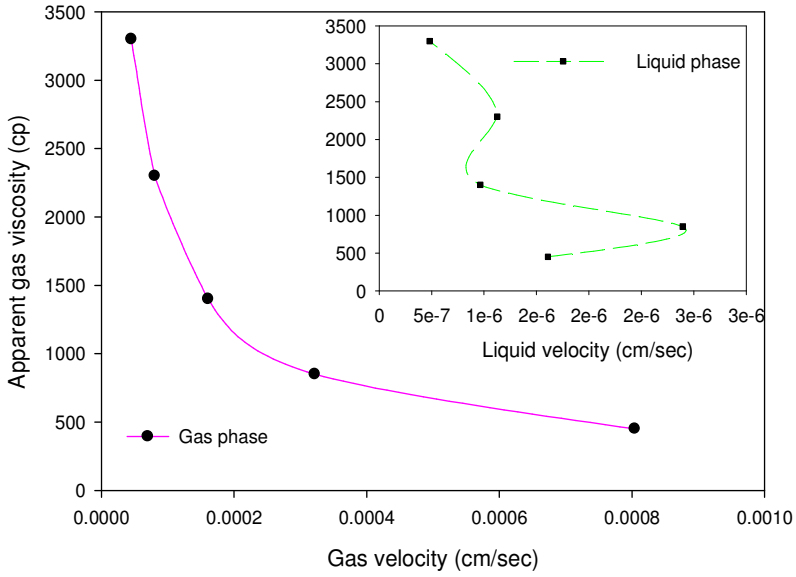

Figure 4.7 Effect of apparent gas viscosity on gas velocity and liquid velocity (adapted from Falls et al. 1989).

increases and liquid velocity is not affected by the apparent gas viscosity. From the results above, it may indicate that blob mobilization is expected as apparent gas viscosity decreases and gas velocity increases.

By using the data demonstrated in Figure 4.7, we attempt to compute a NAPL blob velocity. At the given data, the DNAPL and LNAPL blob velocities had negative values in the range of 0.008 ~ 0.02 cm of a blob size. It may imply that they do not flow or move downward through a porous medium. The results are also compared with Figures 4.2 ~ 4.6. In the Figures, as the apparent gas viscosity is 0.0179 cp and the gas velocity is 4 cm/sec, NAPL blobs were mobilized. From the result, it is clear that for NAPL displacement, lower apparent gas viscosity and higher gas velocity are required.

4.4.4 Surfactant Types

To observe the effect of the properties (i.e., density, viscosity, surface tension) of surfactants on a NAPL blob motion, nonionic, anionic, and amphoteric surfactants are selected (Tables 4.4 and 4.5). However, cationic surfactants are not employed for this study because they cause strong complexation with soil minerals (Abdul et al. 1990).

Table 4.4 Properties of surfactants for TCE.

Surfactant solution	Composition	Type	Density (g/cm^3)	Viscosity (cp, at 20~25℃)	Initial interfacial tension (dyne/cm)
Tween 80	POE(Polioxyethylen Sorbitan Monooleate)	Nonionic	1.06~1.08	1.33	9.2~11.0[1]
SDS	Sodium Dodecyl Sulfate	Anionic	1.006±0.001	0.96	1.2~4.4[1], 4.4±0.5[2]
SOS	Sodium $C_{14\text{-}16}$ olefin sulfonate	Anionic	1.62	1.03	4.9[3]
DOWFAX 8390	Disodium hexadecyldiphenyloxide disulfonate + disodium dihexadecyl–diphenyloxide disulfonate	Anionic	1.16[4]	10[4]	8.5±0.6[2]

[1] Zhong et al., 2003; [2] Boving and Brusseau, (2000); [3] Jeong (1999); and [4] Flick, (1993)

Table 4.5 Properties of surfactants for dodecane.

Surfactant solution	Composition	Type	Density (g/cm^3)	Viscosity (cp, at 20~25℃)	Initial interfacial tension (dyne/cm)
NaDBS[1]	Linear alkyl sulfate	Anionic	1.006±0.001	0.96	0.09
SOS[2]	Sodium $C_{14\text{-}16}$ olefin sulfonate	Anionic	1.62	1.03	4.6
C1215 AE30[1]	Ethoxylated alcohol	Nonionic	1.005±0.005	6.5	9.4
Atlas CD-413[3]	Dodecyldimethylamine N-oxide	Amphoteric	0.806	2.0	2.40

[1] Schramm and Novosad (1990) and Shcramm et al. (1993); [2] Lobo and Wasan (1993); and [3] Chu et al. (1997)

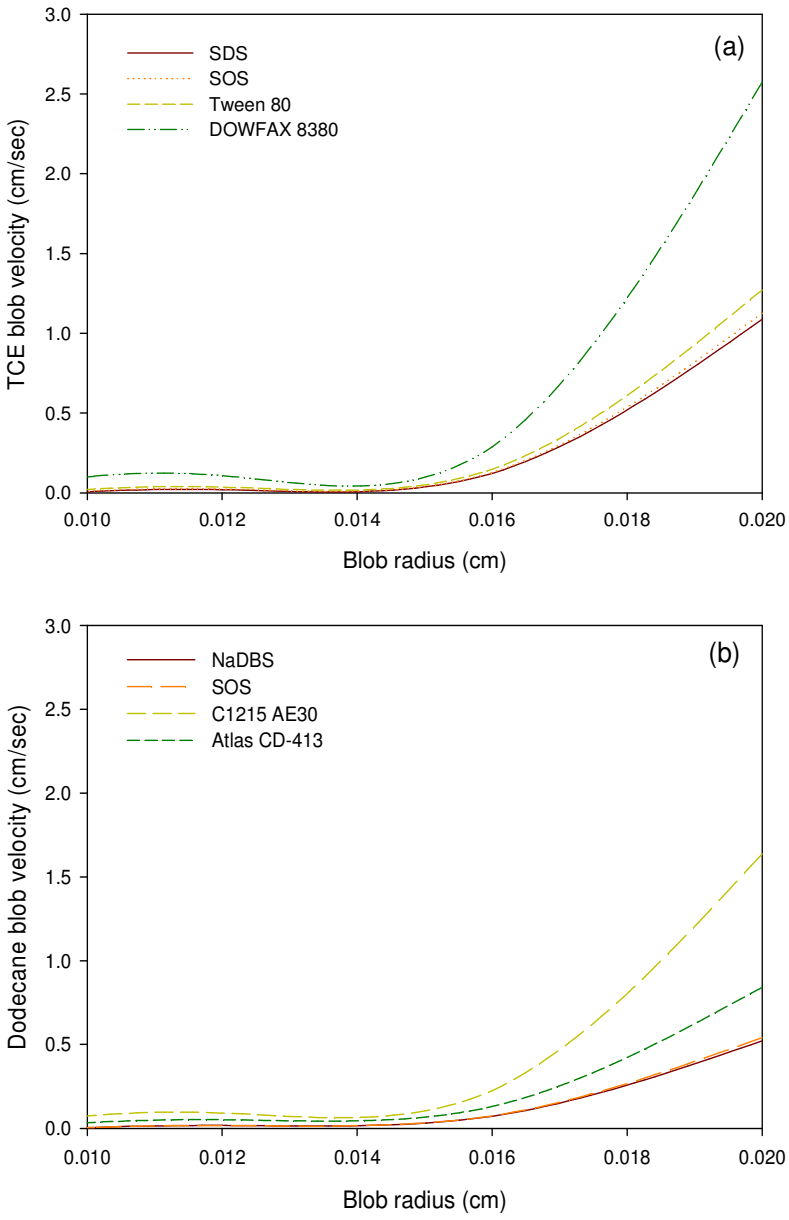

Figure 4.8 Velocities of (a) a TCE blob and (b) a dodecane blob under different surfactant types.

Figure 4.8 shows that TCE and dodecane blob velocities increase with increasing blob radius. In comparison to surfactant types, Figure 4.8 (a) shows that a TCE blob flows faster in a surfactant solution including the surfactant DOWFAX 8390 than in the other surfactant solutions (Tween 80, SDS, and SOS). The reason is that DOWFAX 8390 viscosity is greater than the others, regardless of the magnitude of the interfacial tensions between TCE and the surfactant solutions. In Figure 4.8 (b), a dodecane blob velocity is larger in a C1215 AE 30 solution than the other surfactant (NaDBS, Atlas CD-413, and SOS) solutions. The reason is the same as the reason for the TCE blob motion. From the two results above, it is proved that in properties of surfactants, surfactant viscosity greatly affects blob mobilization.

4.5 Dimensional Analysis

4.5.1 Modified Trapping Numbers

From Equation (4.17), we suggest two different expressions for modified Trapping numbers in terms of relative permeabilities to a gas phase (air bubble) and a

liquid phase (surfactant solution), respectively.

(1) Modified Trapping number on a gas phase

Dividing each term by $\sigma_{ao}\cos\theta_{ao}+\sigma_{ow}\cos\theta_{ow}$ and V_o then, multiplying by kk_{rao} in Equation (4.17), a dimensionless form is obtained as,

$$\frac{\Delta\rho_{ow} g \sin\alpha kk_{rao}}{(\sigma_{ao}\cos\theta_{ao}+\sigma_{ow}\cos\theta_{ow})} - A_3\left(\frac{kk_{rao}}{kk_{ro}}\right)\frac{\mu_o u_o}{(\sigma_{ao}\cos\theta_{ao}+\sigma_{ow}\cos\theta_{ow})}$$
$$-A_4\left(\frac{kk_{rao}}{kk_{rwo}}\right)\left(\frac{V_w}{V_o}\right)\frac{\mu_w u_o}{(\sigma_{ao}\cos\theta_{ao}+\sigma_{ow}\cos\theta_{ow})} + A_4'\left(\frac{kk_{rao}}{kk_{rwo}}\right)\frac{\mu_w u_w}{(\sigma_{ao}\cos\theta_{ao}+\sigma_{ow}\cos\theta_{ow})}$$
$$-A_5\left(\frac{V_a}{V_o}\right)\frac{\mu_a u_o}{(\sigma_{ao}\cos\theta_{ao}+\sigma_{ow}\cos\theta_{ow})} + A_5'\left(\frac{V_o}{V_a}\right)\frac{\mu_a u_a}{(\sigma_{ao}\cos\theta_{ao}+\sigma_{ow}\cos\theta_{ow})} = \frac{2\pi R_n kk_{rao}}{V_o} \tag{4.20}$$

Then, the third and the fifth terms in the LHS of Equation (4.20) are multiplied by ratio of phase velocity for dimensionless forms and then Equation (4.20) would be rewritten as,

$$\frac{\Delta\rho_{ow} g \sin\alpha kk_{rao}}{(\sigma_{ao}\cos\theta_{ao}+\sigma_{ow}\cos\theta_{ow})} - A_3\left(\frac{kk_{rao}}{kk_{ro}}\right)\frac{\mu_o u_o}{(\sigma_{ao}\cos\theta_{ao}+\sigma_{ow}\cos\theta_{ow})}$$
$$-A_4'\left(\frac{V_w}{V_o}\right)\left(\frac{u_o}{u_w}\right)\left(\frac{kk_{rao}}{kk_{rwo}}\right)\frac{\mu_w u_w}{(\sigma_{ao}\cos\theta_{ao}+\sigma_{ow}\cos\theta_{ow})} + A_4\frac{\mu_w u_w}{(\sigma_{ao}\cos\theta_{ao}+\sigma_{ow}\cos\theta_{ow})}$$
$$-A_5\left(\frac{V_a}{V_o}\right)\left(\frac{u_o}{u_a}\right)\frac{\mu_a u_a}{(\sigma_{ao}\cos\theta_{ao}+\sigma_{ow}\cos\theta_{ow})} + A_5'\left(\frac{V_o}{V_a}\right)\frac{\mu_a u_a}{(\sigma_{ao}\cos\theta_{ao}+\sigma_{ow}\cos\theta_{ow})} = \frac{2\pi R_n kk_{rao}}{V_o} \tag{4.21}$$

After this, Equation (4.21) would be represented by dimensionless numbers as,

$$N_{Bo}^a - C_1 N_{Ca}^o - C_2 N_{Ca}^w - C_3 N_{Ca}^a = N_T^a \tag{4.22}$$

where C_1, C_2, and C_3 are the dimensionless forms and it may be expressed as,

$C_1 = A_3\left(kk_{rao}/kk_{ro}\right); C_2 = A_4\left(V_w/V_o\right)\left(u_o/u_w\right)\left(kk_{rao}/kk_{rwo}\right) - A_4\left(kk_{rao}/kk_{rwo}\right)$; and $C_3 = A_5\left(V_a/V_o\right)\left(u_o/u_a\right) + A_5'\left(V_o/V_a\right)$. In Equation (4.22), the dimensionless numbers developed in our study are shown in Table 4.6.

(2) Modified Trapping number on a liquid phase

In the similar way, an expression for a modified Trapping number on a surfactant solution is obtained as,

$$\frac{\Delta\rho_{ow} g \sin\alpha kk_{rwo}}{(\sigma_{ao}\cos\theta_{ao} + \sigma_{ow}\cos\theta_{ow})} - A_3\left(\frac{kk_{rwo}}{kk_{ro}}\right)\frac{\mu_o u_o}{(\sigma_{ao}\cos\theta_{ao} + \sigma_{ow}\cos\theta_{ow})}$$
$$-A_4\left(\frac{V_w}{V_o}\right)\left(\frac{u_o}{u_a}\right)\frac{\mu_w u_w}{(\sigma_{ao}\cos\theta_{ao} + \sigma_{ow}\cos\theta_{ow})} + A_4'\frac{\mu_w u_w}{(\sigma_{ao}\cos\theta_{ao} + \sigma_{ow}\cos\theta_{ow})}$$
$$-A_5\left(\frac{V_a}{V_o}\right)\left(\frac{u_o}{u_a}\right)\left(\frac{kk_{rwo}}{kk_{rao}}\right)\frac{\mu_a u_a}{(\sigma_{ao}\cos\theta_{ao} + \sigma_{ow}\cos\theta_{ow})} + A_5'\left(\frac{V_o}{V_a}\right)\left(\frac{kk_{rwo}}{kk_{rao}}\right)\frac{\mu_a u_a}{(\sigma_{ao}\cos\theta_{ao} + \sigma_{ow}\cos\theta_{ow})}$$
$$= \frac{2\pi R_n kk_{rwo}}{V_o} \tag{4.23}$$

Equation (4.23) would be rewritten by dimensionless numbers as,

$$N_{Bo}^{w} - C_4 N_{Ca}^{o} - C_5 N_{Ca}^{w} - C_6 N_{Ca}^{a} = N_T^{w} \tag{4.24}$$

where the dimensionless numbers are shown in Table 4.6 and three dimensionless forms (C_4, C_5, and C_6) are represented as, $C_4 = A_3\left(kk_{rwo}/kk_{ro}\right); C_5 = A_4\left(V_w/V_o\right)\left(u_o/u_w\right) + A_4$; and $C_6 = A_5\left(V_a/V_o\right)\left(u_o/u_a\right)\left(kk_{rwo}/kk_{rao}\right) - A_5'\left(V_o/V_a\right)\left(kk_{rwo}/kk_{rao}\right)$.

Table 4.6 Collection of dimensionless numbers.

Dimensionless numbers	Formulations	
Bond numbers	For NAPL on air bubbles ,	$N_{Bo}^{a} = \frac{\Delta\rho_{ow} g \sin\alpha k k_{rao}}{(\sigma_{ao}\cos\theta_{ao} + \sigma_{ow}\cos\theta_{ow})}$
	for NAPL on surfactant solution,	$N_{Bo}^{w} = \frac{\Delta\rho_{ow} g \sin\alpha k k_{rwo}}{(\sigma_{ao}\cos\theta_{ao} + \sigma_{ow}\cos\theta_{ow})}$
Capillary numbers	for NAPL,	$N_{Ca}^{o} = \frac{\mu_o u_o}{(\sigma_{ao}\cos\theta_{ao} + \sigma_{ow}\cos\theta_{ow})}$
	for surfactant solution,	$N_{Ca}^{w} = \frac{\mu_w u_w}{(\sigma_{ao}\cos\theta_{ao} + \sigma_{ow}\cos\theta_{ow})}$
	for air bubbles,	$N_{Ca}^{a} = \frac{\mu_a u_a}{(\sigma_{ao}\cos\theta_{ao} + \sigma_{ow}\cos\theta_{ow})}$
Modified Trapping numbers	for air bubbles,	$N_{T}^{a} = \frac{2\pi R_n k k_{rao}}{V_o}$
	for surfactant solution,	$N_{T}^{w} = \frac{2\pi R_n k k_{rwo}}{V_o}$

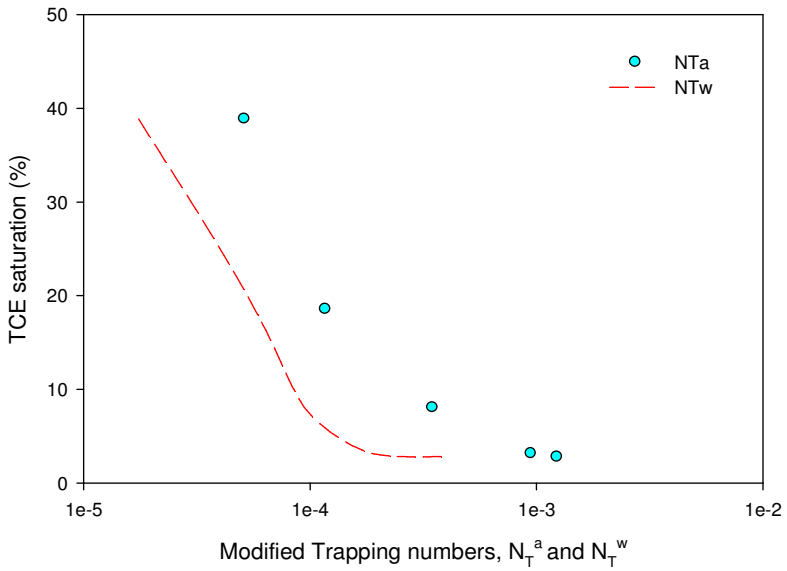

Figure 4.9 Change in TCE saturation at two different modified Trapping numbers on air bubbles, N_T^a, vs. surfactant solutions, N_T^w.

In Figure 4.9, the velocities of an air bubble and a surfactant solution are 4 and 0.096 cm/sec, respectively. It shows that two modified Trapping numbers for air bubbles, N_T^a, and a surfactant solution, N_T^w, have a similar trend. TCE saturation decreases as N_T^a and N_T^w increase. It corresponds to the results for the modified Trapping number discussed in Chapter III.

4.5.2 Critical Condition for Blob Mobilization

As discussed in Chapter III, trapped NAPL blobs are mobilized or displaced as the sum value of the Capillary number and the Bond number over the value of the modified Trapping number. The theoretical concept would also be applied in describing blob mobilization during surfactant foam operation. From Equations (4.22) and (4.24), the conditions for blob mobilization would be signified as,

$$\left| N_{Bo}^a - C_1 N_{Ca}^o - C_2 N_{Ca}^w - C_3 N_{Ca}^a \right| \geq N_T^a \tag{4.25}$$

$$\left| N_{Bo}^w - C_4 N_{Ca}^o - C_5 N_{Ca}^w - C_6 N_{Ca}^a \right| \geq N_T^w \tag{4.26}$$

As shown in Equations (4.25) and (4.26), the sum of the dimensionless numbers in the LHS should exceed the values of the modified Trapping numbers N_T^a or N_T^w, in order to determine blob mobilization. They are depicted in Figure 4.10.

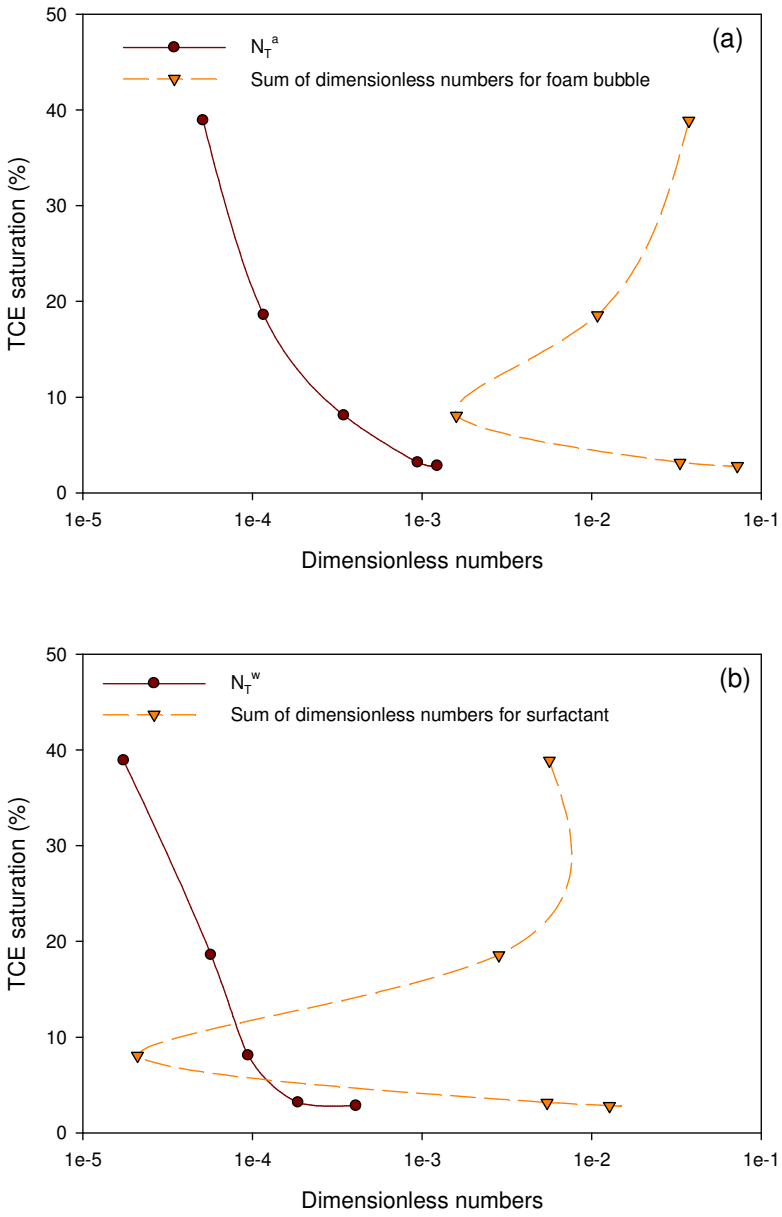

Figure 4.10 Sum of dimensionless numbers vs. modified Trapping numbers for (a) air bubbles and (b) surfactant solutions.

Figure 4.10 (a) shows that the sum of the dimensionless numbers in the LHS of Equations (4.25) and (4.26) is placed over the N_T^a and the TCE saturation continuously decreases from 38.88 to 2.8 %. In Figure 4.10 (b), the sum of the dimensionless numbers exceeds the N_T^w in the range of 38.88 ~ 2.8 % of the TCE saturation, except for around 8% of TCE saturation. It may imply that at around 8 % of TCE saturation, TCE blobs tends to be re-entrapped. In Equations (4.25) and (4.26), two Bond numbers, N_{Bo}^a, and N_{Bo}^w vary from 2.16×10^{-5} to 2.10×10^{-5} and from 6.34×10^{-5} to 9.76×10^{-5}, respectively but their values have a negative sign. The values of N_{Ca}^o are 2.88×10^{-2} ~ 4.92×10^{-4} in the range of 38.88 ~ 2.8 % of TCE saturation. N_{Ca}^w and N_{Ca}^a are 1.64×10^{-3} and 1.22×10^{-3} in the same range of the TCE saturation, respectively.

CHAPTER V

EFFECT OF FOAM BUBBLE-TRAIN ON NAPL BLOB MECHANISTIC DURING SURFACTANT FOAM OPERATION

5.1. Theoretical Background

5.1.1 Foam Structure

As discussed in Chapter IV, surfactant foam consists of a surfactant solution enclosing air bubbles and its structure depends on the surfactant solution content. For instance, if air bubbles are separated by a large amount of surfactant solution, it is called wet foam and in the case of dry foam, air bubbles are separated by thin films of surfactant solution. According to the extent of a surfactant solution, it is known that shapes of air bubbles are determined. Generally, in wet foam, air bubbles are spherical and in dry foam, they are a polyhedral shape (Breward and Howell 2002).

5.1.2 Foam Film vs. Pseudoemulsion-film

If surfactant foam is present in a porous medium without NAPL, a foam film (called lamellae) is formed. The film consists of surfactant solution and connects two air bubbles. The lamellae thickness typically varies from a few to a number of microns. However, if a NAPL blob is present in the lamella, it is called pseudoemulsion-film (Manlowe and Radke 1990; Hanssen and Dalland 1990; Aveyard et al. 1993). The film bridges a NAPL blob on one side and an air bubble on the other (Manlowe and Radke 1990; Hanssen and Dalland, 1990). In a surfactant solution present between a NAPL blob and an air bubble, surfactant hydrophobic tails start to be solubilized by chemical

binding with the NAPL blob, however, they are not dissolved into the air bubbles (Hanssen and Dalland 1990). Therefore, a pseudoemulsion-film connecting a dissolved NAPL blob and an air bubble may be more unstable than the foam film connecting two bubbles (Manlowe and Radke 1990; Hanssen and Dalland 1990).

5.1.3 Foam Bubble-Train Model

Another type of surfactant foam flowing through a porous medium is a bubble-train model. The bubble-train is a prototype of surfactant foam. Where, discrete bubbles displaced NAPL blobs trapped within pores and surfactant solutions lowered the interfacial tension between the trapped NAPL blobs and the surfactant solutions, respectively. Additionally, the flow configuration for the three immiscible fluids (NAPL blobs, air bubbles, and surfactant solution) in the bubble-train model was similar to the air-water-oil displacement mechanism proposed by Øren et al. (1994) and Keller et al. (1997).

There is a theoretical concept being able to describe foam flow developed by Rossen (1988). As surfactant foam is injected into a porous medium, bubble-trains are formed and they flow through pore spaces trapping air bubbles (Rossen 1988). In a bubble-train, air bubbles would be displaced by lamellae which are formed by a snap-off mechanism (Rossen 1988). A bubble-train consists of trains of at least two bubbles separated by lamellae flowing concurrently inside soil pores. The size of the air bubbles may vary up to several times a pore diameter (Thulasidas et al. 1995), and for foam stability, the minimum thickness of lamellae should be greater than 0.005 ~ 0.01 μm

(Chu 1997). Generally, lamella in a bubble-train is 5 ~ 50 μm thick (Thulasidas et al. 1995).

A bubble-train flow would be comparable to the motion of individual bubbles and surfactant solution displacing NAPL blobs. Discrete foam bubbles require more pressure to displace NAPL blobs than does a bubble-train since lamellae in a bubble-train plays a role in reducing the overall capillary resistance. Therefore, displacement of a bubble-train requires a minimum pressure gradient. The apparent viscosity of individual bubbles is small whereas that of bubble-trains dispersed in foam is greater than that of NAPL and water. Thus, the mobility of bubble-trains comes to be very much slower than that of individual bubbles (Yan et al. 2006). This means that discrete bubbles are more difficult to control than are bubble-trains in a porous medium. Thus, the motion of a bubble-train could be a valuable study on blob displacement compared to the motion of discrete air bubbles.

Surfactant foam applied in an oil recovery (EOS) process is more useful than other technologies in displacing NAPL blobs, as mentioned in Chapter I. However, surfactant foam is limited in NAPL blob displacement since a predictive model being able to describe foam-NAPL blob flowing in porous media has not been well organized and their flow has not well understood in porous media (Vikingstad et al. 2005). Furthermore, study on the interaction between bubble-trains and NAPL blobs could be challengeable. However, if the model is developed, it may provide useful and quantitative information on the entire phenomena between foam and NAPL blobs in porous media.

5.2 Descriptive Configurations of Blob Displacement by Foam Bubble-Train

When surfactant foam is injected into a porous medium to displace trapped NAPL blobs, its shapes or displacement configurations may be varied. For identifying its flow configuration, a spreading coefficient and an entering coefficient need to be discussed. According to Schramm (1994) and Jha et al. (2000), the flow configurations of surfactant foam-NAPL blobs would be classified, as shown in Table 5.1.

Table 5.1 Four possible flow configurations of a foam bubble-train and NAPL blobs.

Entering coefficient, E_f	Spreading coefficient, S_f	
	Negative (–)	Positive (+)
Negative (–)	Nothing (Type A)	Possibility of NAPL films (Spreading along pore wall) (Type B)
Positive (+)	NAPL lens (Drawn up through lamellae) (Type C)	NAPL films (NAPL blob is drawn up and then spread as a film along the lamellae surfaces: Possibility of lamellae ruptures (Type D)

Two coefficients, a spreading coefficient (S_f) and an entering coefficient (E_f), could determine descriptive concepts for the complex interactions between foam bubble-trains and NAPL blobs. The mathematical expressions related to the two coefficients are depicted as follows (Schramm et al. 1993; Schramm 1994).

$$S_f = \sigma_f - \sigma_{fo} - \sigma_o \tag{5.1}$$

$$E_f = S_f + 2\sigma_{fo} \tag{5.2}$$

where σ_f [M T^{-2}] and σ_o [M T^{-2}] denote the surface tension of surfactant solution in lamellae and NAPL, respectively. σ_{fo} [M T^{-2}] is the interfacial tension between the surfactant solution in lamellae and NAPL. If S_f and E_f are negative, blobs do not spread and move through the lamellae/air bubble interface. At $S_f \leq 0$, specifically, flow configuration is dominated by balance of buoyant and capillary forces acting on the NAPL lens (Schramm 1994). However, if the two coefficients are positive, blobs spread at the interface after being drawn into the lamellae. If S_f and E_f are negative and positive, respectively, blobs could move into the lamellae but they could not spread at the interface (Schramm et al. 1993). Schramm et al. (1993) also observed foam and oil flow behaviors qualitatively and proposed three types (Type B, C, and D). Herein, it is known that study of spreading and entering behaviors and the film stability of foam bubble-trains are significantly treated with the phase configurations of NAPL blobs and foam bubble-trains, in order to discover the complex interactions of NAPL blob-surfactant foam. Based on the concept of the flow configurations shown in Table 5.1, the interactive flow of a foam bubble-train and a NAPL blob is depicted in Figure 5.1.

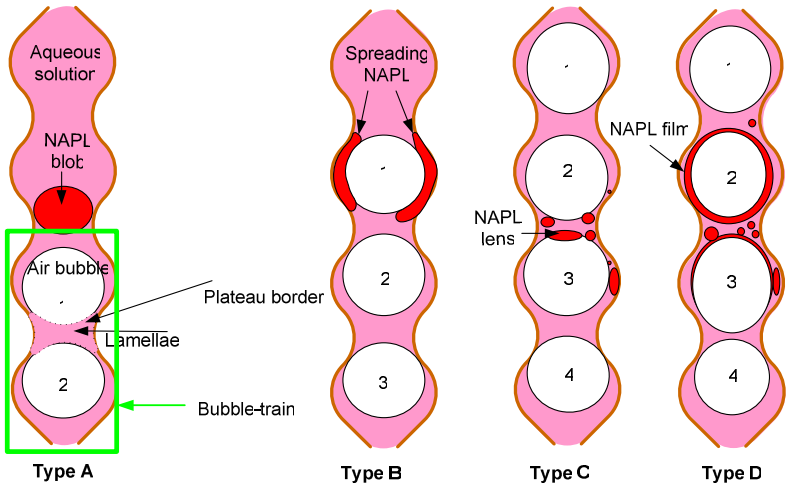

Figure 5.1 Schematic diagrams for the flow configuration of surfactant foam bubble-train (in rectangle) and a NAPL blob.

5.3 Mathematical Development

The fate of a bubble-train flowing through a porous medium needs to be mathematically explained in order to investigate the displacement efficiency of the bubble-train to displace NAPL blobs. First, a mathematical model for describing the foam bubble-train displacement is developed. Second, expressions for the average velocities of air bubbles and lamellae in a bubble-train flowing through pore throats are developed.

5.3.1 Movement of Foam Bubble-Train: Drawing-in

The flow pattern for bubble-trains flowing through soil pores is called drawing-in. A bubble-train in a drawing-in motion requires a minimum pressure gradient, $\nabla P_{\min}$, in order to transport or displace lamellae (Mast 1972; Rossen 1988; 1989; Vassenden and Holt 1998). The flow pattern could be represented by a pressure difference as,

$$\nabla P_{\min} = \Delta P X_n = 0.126 P_c^e X_n \tag{5.3}$$

where ΔP is the difference in pressure between bubbles to the front and rear over lamellae in the bubble-train; P_c^e is the least or the entry capillary pressure to pass through pore throats (Rossen 2003); X_n is the number of lamellae (n_L) per length of total bubble-train (L_T). More detail for Equation (5.3) is provided in the study of Rossen (1988).

In Equation (5.3), ΔP and P_c^e are expressed in terms of interfacial tension through the Young-Laplace equation (Mast 1972; Vassenden and Holt 1998)

$$\Delta P = \frac{4\sigma_{al} \sin\alpha}{R_c} \tag{5.4}$$

$$\Delta P = \frac{4\sigma_{al}}{R_l} \tag{5.5}$$

$$P_c^e = \frac{2\sigma_{al}}{R_n} \tag{5.6}$$

where σ_{al} [M T^{-2}] is the interfacial tension between air bubble and lamellae; α is the contact angle of the pore wall to the pore axis; R_c [L] and R_n [L] are the capillary and the pore throat radii, respectively; R_l [L] is the radius of an equivalent lamellae perpendicular to the pore wall. From Equations (5.3) and (5.6), a capillary retention force would be represented by,

$$F_C^f = 0.126 P_c^e X_n V = 0.126 \frac{2\sigma_{al}}{R_n} X_n \left(\pi R_n^2 L_T\right) = 0.252 \pi R_n \sigma_{al} n_L \tag{5.7}$$

As a foam bubble-train flows through a porous medium, a drag force takes place along pore walls saturated with surfactant solution. From Equation (2.15) discussed in Chapter II, a drag force acting on a foam bubble-train could be obtained as,

$$F_D^f = A_6 \frac{\mu_f u_f}{k k_{rfa}} V_f \tag{5.8}$$

where μ_f [M L^{-1} T^{-1}] is the apparent foam viscosity which will be discussed in detail later; u_f [L T^{-1}] is the foam bubble-train velocity. k_{rfa} is the relative permeability to a flowing foam bubble-train; V_f [L^3] is the volume of a foam bubble-train. Since an air bubble volume is considerably larger than that of lamellae, V_f could be almost same as the volume of total air bubbles in a bubble-train.

Therefore, a foam bubble-train volume could be expressed in terms of total gas volume as bellows,

$$V_f = \sum V_a + \sum V_\ell \approx \sum V_a \tag{5.9}$$

where V_a [L^3] and V_ℓ [L^3] are the volume of a discrete bubble and lamellae, respectively; $\sum V_a$ and $\sum V_\ell$ are the volume of the total air bubbles and the lamellae, respectively, which could be represented as,

$$\sum V_a = N_{bubble} V_a = N_{bubble} \left(\frac{4}{3} \pi R_a^3 \right) \tag{5.10}$$

$$\sum V_\ell = (N_{bubble} - 1) V_l = N_{bubble} \left(\frac{4}{3} \pi R_l^3 \right) \tag{5.11}$$

where N_{bubble} is the number of bubbles; R_a [L] is the air bubble radius.

In observation or visualization tests conducted by previous studies, it is known that a foam bubble-train moved through soil pores as the pressure gradient on lamellae exceeds a capillary pressure coming from pore constrictions. Therefore, study on lamellae transport would be an important addition to determine a bubble-train flowing through pores. Furthermore, evaluation for a relative motion between lamellae in a foam bubble-train and a liquid film (surfactant solution) wetting pore walls would be required to understand a bubble-train displaced at pore-scale. Based on theory for the relative motions discussed in Chapter II, a momentum force considering relative motions would be represented as,

$$F_m^f = \left[A_7 \frac{\mu_l u_l}{kk_{rl}} - A_7' \frac{\mu_l \left(V_l / V_f\right) u_f}{kk_{rl}} \right] V_f \tag{5.12}$$

Assuming that a foam bubble-train is flowing in the vertical direction, a buoyant force acting on a bubble-train should be considered. The buoyant force is simply represented as,

$$F_B^f = (\rho_w - \rho_f) g V_f \tag{5.13}$$

Then, forces acting on a bubble-train are balanced as,

$$\sum F_{BT} = F_B^f + F_m^f - F_D^f - F_C^f \tag{5.14}$$

For a foam bubble-train transport, the trapping (a capillary retention and a drag) forces should be less than the other two driving (a momentum and a buoyant) forces because the trapping forces obstruct the bubble-train flow and it is stated as,

$$(\rho_w - \rho_f) g V_f + \left[A_7 \frac{\mu_l u_l}{kk_{rl}} - A_7' \frac{\mu_l \left(V_l / V_f\right) u_f}{kk_{rl}} \right] V_f - A_6 \frac{\mu_f u_f}{kk_{rf}} V_f > 0.252 \pi R_n \sigma_{al} n_L \tag{5.15}$$

where A_6, A_7, and A_7' are the correction factors. Their values are discussed in foam bubble-train velocity. Equation (5.15) can express whether a foam bubble-train mobilization occurs or not. Use of the equation above would give important information on the application of foam to displacement of trapped NAPL blobs in porous media.

5.3.2 Balance of Forces Acting on a NAPL Blob during Bubble-Train Flow: Pushing-out

As a foam bubble-train confronts a NAPL trapped at a pore throat, the front of the bubble-train pushes the blob from the pore throat to an adjacent pore throat. This flow configuration was well demonstrated in Schramm and Novosad (1990), Schramm et al. (1993), and Denkov (2004). For the stability of a bubble-train displacing NAPL blobs, a liquid pressure in lamellae connecting two air bubbles should be high enough to be present in the bubble-train.

In a pushing-out flow pattern of air bubbles, NAPL blobs move upward and downward between mobile bubbles in a bubble-train. It is mathematically described as,

$$\sum F = (\rho_w - \rho_o)\, g \sin\alpha V_o - 2\pi R_n (\sigma_{of} \cos\theta_{of}) - A_8 \frac{\mu_o u_o}{k k_{ro}} V_o - \mu_f \left(A_9 \frac{V_f}{V_o} u_o - A_9' u_f \right) V_o \Big/ k k_{rfo} \tag{5.16}$$

As Equation (5.16) is unified, three dimensionless groups A_8, A_9, and A_9' are obtained as,

$$A_8 = n \left(\frac{V_p}{V_o} \right)^2 \tag{5.17}$$

$$A_9 = n \left(\frac{V_p}{V_f} \right)^3 \tag{5.18}$$

$$A_9' = n\left(\frac{V_o}{V_f}\right)\left(\frac{V_P}{V_f}\right) \tag{5.19}$$

5.4 Quantitative Analysis of Relationship between Foam Bubble-Train and NAPL Blob Interaction

5.4.1 Measured vs. Calculated Apparent Viscosity of Foam Bubble-Train

Based on a formulation suggested by Hirasaki and Lawson (1985) and Falls et al. (1989), the apparent viscosity of surfactant foam is made as,

$$\mu_f = \left[\begin{array}{l} L_s\left(X_n\right) + \left(\dfrac{0.85 X_n R_{cap}}{R_{PB}/R_{cap}}\right)\left(\dfrac{3\mu_w u_a}{\sigma}\right)^{-1/3}\left[1+\left(\dfrac{R_{PB}}{R_{cap}}\right)^2\right] \\ +\left(X_n\right) R_{cap}\left(\dfrac{3\mu_w u_a}{\sigma}\right)^{-1/3}\sqrt{N_s}\,\tanh(\dfrac{L_{BD}}{2}) + \xi\left(X_n\right) R_{cap}\left(\dfrac{3\mu_w u_a}{\sigma}\right)^{-1} \end{array}\right]\mu_w \tag{5.20}$$

In Equation (5.20), Hirasaki et al. (1985) proposed three terms to obtain the apparent viscosity of surfactant foam for a straight capillary tube: (1) the viscosity of the surfactant solution in lamellae between the air bubbles, (2) the friction between discrete foam bubbles and pore walls during foam bubble-train flow, (3) the capillary tension gradient due to the surfactant concentration gradient. Herein, Falls et al. (1989) added a term to express the apparent viscosity of foam flowing through a glass tube packed homogeneously with beads as a type of a constricted tube: (4) the retardation due to pore constrictions

Equation (5.20) is rewritten in terms of μ_{app}^{shape}

$$\mu_f = L_s\left(X_n\right)\mu_w + \left(C\mu_{app}^{shape}\right)\left[1+\left(\frac{R_{PB}}{R_{cap}}\right)^2\right] + \mu_{app}^{shape}\left(\frac{R_{PB}}{R_{cap}}\right)\sqrt{N_s}\tanh(\frac{L_{BD}}{2}) + \xi\mu_{app}^{shape}\left(\frac{R_{PB}}{R_{cap}}\right) \tag{5.21}$$

where C is the constant and would represent a foam characteristic. C was 0.85 for a typical constricted tube (Falls et al. 1989) and 0.57 for a straight tube (Yan et al. 2006); μ_{app}^{shape} is the apparent shape viscosity being able to explain the deformation of foam bubbles flowing through a porous medium (Yan et al. 2006). From the plane-Poiseuille flow, it is derived as

$$\mu_{app}^{shape} = \frac{\mu_w\left(X_n\right)R_{cap}}{\left(R_{PB}/R_{cap}\right)}\left(\frac{3\mu_w u_a}{\sigma}\right)^{-1/3} \tag{5.22}$$

To obtain a theoretical apparent foam viscosity, experimental data conducted by Chu (1997) are employed, as shown in Table 5.2.

Table 5.2 Characteristics of a porous medium and properties of surfactant foam.

	Definition	Value
Porous medium	d_m, mean grain size [cm]	0.066
(Ottawa sand)	n, porosity [-]	0.3954
	R_n, pore throat size [cm]	0.0051
Displacing fluid-surfactant foam		
Bioterge As-40 as surfactant	μ_w, viscosity as surfactant solution [cp]	1.22
	σ, surface tension [dyne/cm]	34.5
	R_a, an equivalent air bubble radius [cm]	
Air bubble as gas		0.02

From Table 5.2, each component in Equation (5.21) is calculated and it is shown in Table 5.3. Velocity of air bubbles u_a represented in L_{BD} is 0.024 cm/sec (Table 5.3).

Table 5.3 Values of factors calculated for an apparent foam viscosity.

Symbols	Definitions	Equations	Values
R_{cap}	equivalent capillary radius [cm]	$nd_m/[3(1-n)+2d_m/R_n]$	0.0009
R_{PB}	radius of plateau border curvature in a foam lamella [cm]	$\left[(1-\Gamma)(R_a/R_{cap})^3/3(1-\pi/4)\Gamma\right]^{0.5} R_{cap}$	0.0134
$\sqrt{N_s}$	dimensionless group [-]	$(\beta/R_{PB})^{0.5}$	19.300
L_B	foam bubble length [cm]	$\Gamma/X_n - 4/3R_n$	0.0343
L_{BD}	dimensionless group for bubble length [-]	$\left[(L_B/R_{PB})(3\mu_w u_a/\sigma)^{(-1/3)}\right]/\sqrt{N_s}$	4.4986
X_n	number of lamella per unit length [lamella/cm]	if $R_n \ll R_a$, $\left[(3/4)\Gamma R_n^2\right]/R_a^3$ if $R_n \gg R_a$, $\left[(3/2)\Gamma\right]/R_a$	21.41
L_s	length of a liquid slug between the two air bubbles [cm]	Without touching between bubbles, $[1-\Gamma]/X_n - 2/3R_n$ With touching between bubbles, the value is zero, $L_s = 0$	0.0022
β	empirical factor for surface tension gradient [cm]	for smooth-tube viscosity model	5
Γ	foam quality [-]	$\sum V_a/V_f$	0.88
ξ	geometric factor [-]		0.56

In Table 5.3, a tube diameter proposed as a component in R_{cap}, L_B, X_n and L_s (Falls et al. 1989) is modified to a pore throat size for our system since the four factors

are affected by pore constriction. By using Equation (5.21) and data shown in Table 5.2, a theoretical apparent foam viscosity is obtained to be 26.53 cp. It is in good agreement with 26.14 cp observed by Chu (1997).

From Equation (5.22), the apparent shape viscosity for deformation of foam bubbles, μ_{app}^{shape}, is determined to be 0.059 cp. The sum of μ_{app}^{shape} and μ_w is 1.279 cp which is much lower than 26.53 cp of μ_f. The result would be compared with the study of Yan et *al.* (2006). According to the difference between the μ_f and the sum of the μ_{app}^{shape} and the μ_w, it could be postulated that effect of the surface tension gradient on the foam bubbles is negligible in our system.

5.4.2 Flow Velocity of Foam Bubble-Train

To improve the displacement or the removal efficiency of NAPL blobs, the velocity of a foam bubble-train flowing through a porous medium should be predicted. By using Equation (5.15), a minimum bubble-train velocity, u_f, is derived. For practical application to get a bubble-train velocity, four different approaches ($u_f^{\,1}, u_f^{\,2}, u_f^{\,3}$ and $u_f^{\,4}$) are suggested as shown in Table 5.4.

Table 5.4 Theoretical velocities for a foam bubble-train under different conditions.

	Flowing foam bubble-train velocity , u_f (cm/sec)	Correction factors
$u_f^{\,1}$	$\left[(\rho_w-\rho_f)gV_f-0.252\pi R_n\sigma_{al}n_L+A_7\frac{\mu_l u_l}{kk_{rl}}V_f\right]\Big/\left(A_6\frac{\mu_f V_f}{kk_{rf}}+A_7'\frac{\mu_l V_l}{kk_{rl}}\right)$	$A_6=10$ $A_7=78.49\sim234.3$ $A_7'=21.52$
$u_f^{\,2}$	$\left[(\rho_w-\rho_f)gV_f-0.252\pi R_n\sigma_{al}n_L+A_7\frac{\mu_l u_l}{kk_{rl}}V_f\right]\Big/\left(A_6\frac{\mu_f V_f}{kk_{rf}}\right)$	
$u_f^{\,3}$	$\left[(\rho_w-\rho_f)gV_f-0.252\pi R_n\sigma_{al}n_L+\frac{\mu_l u_l}{kk_{rl}}V_f\right]\Big/\left(\frac{\mu_f V_f}{kk_{rf}}+\frac{\mu_l V_l}{kk_{rl}}\right)$	$A_6=1$ $A_7=1$ $A_7'=1$
$u_f^{\,4}$	$\left[(\rho_w-\rho_f)gV_f-0.252\pi R_n\sigma_{al}n_L+\frac{\mu_l u_l}{kk_{rl}}V_f\right]\Big/\left(\frac{\mu_f V_f}{kk_{rf}}\right)$	

Foam bubble-train velocities, $u_f^{\,1}$ and $u_f^{\,3}$, consider the relative motion between a bubble-train and surfactant solution flowing along pore walls with and without the correction factors, respectively, whereas $u_f^{\,2}$ and $u_f^{\,4}$ did not consider the relative motion with and without correction factors, respectively. The difference is described in Figure 5.2 and Table 5.5. Figure 5.2 shows $u_f^{\,1}$ and $u_f^{\,2}$ values are much lower than those of $u_f^{\,3}$ and $u_f^{\,4}$ because they are affected by correction factors. In reality, since the correction factors are affected by the characteristics of a porous medium, a foam bubble-train velocity affected by the correction factors may be different, depending on the system conditions applied.

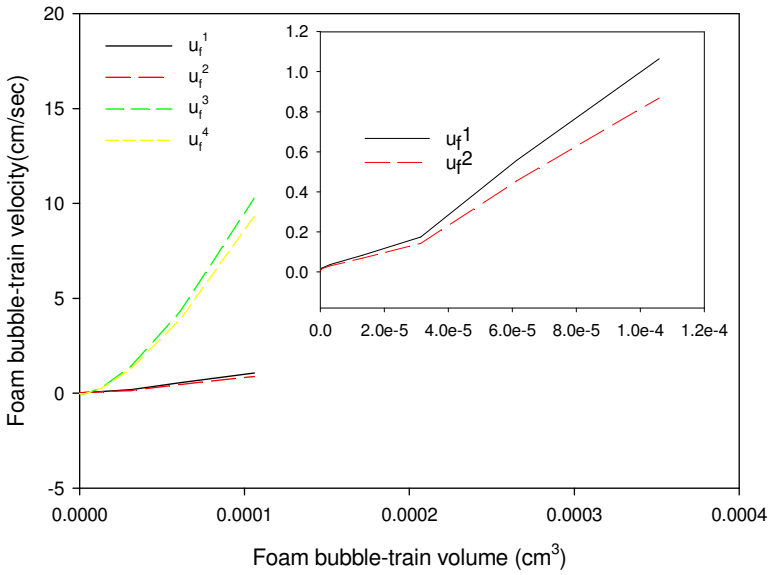

Figure 5.2 Flow velocities of a foam bubble-train over its volume.

Table 5.5 The theoretical values for four different foam bubble-train velocities.

V_f ($\times 10^{-6}$ cm^3)	$u_f{}^1$ (cm/sec)	$u_f{}^2$ (cm/sec)	$u_f{}^3$ (cm/sec)	$u_f{}^4$ (cm/sec)
0.06	0.011	8.857×10^{-3}	-0.013	-0.012
0.49	0.020	0.016	-0.036	-0.033
3.16	0.037	0.030	-0.047	-0.043
13.25	0.084	0.069	0.269	0.243
31.40	0.175	0.143	1.423	1.292
61.33	0.558	0.454	4.330	3.921
106	1.064	0.869	10.275	9.304

With 3.16×10^{-6} cm^3 of V_f, a mobile foam velocity measured by Chu (1996) is 0.03 cm/sec. In Table 5.5, the calculated value of $u_f{}^2$ is in close proximity to the value measured by Chu (1996). From the result, it is known that the relative motion between a

mobile foam bubble-train and liquid including surfactant on foam bubble-train flow would be negligible. However, to apply $u_f^{\,2}$ into the field scaled or the macro-scaled porous media, the empirical values for the correction factors would be required.

5.4.3 Pore Velocity of a NAPL Blob

During a foam bubble-train flow, a NAPL blob could be mobilized or not. To identify the physical condition for mobilization of a NAPL blob, a pore velocity of a NAPL blob trapped within soil pores needs to be studied precisely because it would be a significant factor for determining the displacement efficiency of foam. To obtain a pore velocity of a NAPL blob displaced by a foam bubble-train, Equation (5.15) is assumed to be zero as,

$$\sum F = 0 \tag{5.23}$$

Then, the pore velocity is expressed as

$$u_o = \frac{\left[\left(\rho_w - \rho_o \right) g \sin\alpha - 2\pi R_n (\sigma_{of} \cos\theta_{of}) / V_o - A_8' \mu_f u_f \Big/ kk_{rfo} \right]}{\left[A_7 \dfrac{\mu_o}{kk_{ro}} - A_8 \mu_f \left(\dfrac{V_f}{V_o} \right) \Big/ kk_{rfo} \right]} \tag{5.24}$$

For calculating the pore velocity of a NAPL blob, dodecane as a typical LNAPL type is chosen and from Equation (5.24), the result is shown in Figure 5.3.

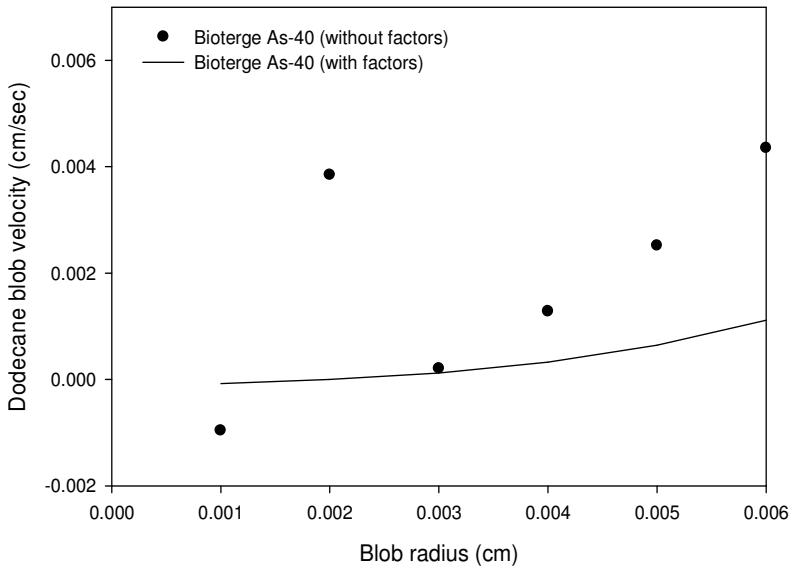

Figure 5.3 Comparison of a dodecane blob velocity displaced by a foam bubble-train using a surfactant (Bioterge As-40) solution with and without correction factors.

Figure 5.3 compares blob velocities controlled by the existence and nonexistence of the correction factors (A_8, A_9, and A_8') in Equation (5.24). In the case of considering the factors, A_8, A_9, and A_8' are 258.32, 12.33, and 3.16, respectively. In the absence of the factors, the blob velocity is higher than in the presence of the factors. Since the correction factors are related to the relative motion between a blob and a bubble-train flowing through pores, the relative motion with the high values of the factors can lead to the resistance for a blob flow.

5.4.4 Dimensional Analysis

Until now, foam efficiency for NAPL blob displacement has been described by using dimensional analysis. However, it is limited in explaining for foam–blob interaction. Thus, we attempt to quantify the foam efficiency by considering interactive relation between a bubble-train and a blob.

For dimensional analysis, Equation (5.15) is nondimensionalized by multiplying by kk_{rfo}, then dividing V_o and $\sigma_{of}\cos\theta_{of}$ into each term. Then, a dimensionless form is obtained as,

$$N_{Bo}^{f} - A_6\left(\frac{kk_{rfo}}{kk_{ro}}\right)N_{Ca}^{o} - \left[A_7\left(\frac{V_f}{V_o}\right)\left(\frac{u_o}{u_f}\right) - A_7'\right]N_{Ca}^{f} = N_T^{f} \tag{5.25}$$

where N_{Bo}^{f} is the Bond number for a bubble-train ($=(\rho_w-\rho_o)\,g\sin\alpha/\sigma_{of}\cos\theta_{of}$); N_{Ca}^{o} is the Capillary number for a NAPL blob ($=\mu_o u_o/\sigma_{of}\cos\theta_{of}$); N_{Ca}^{f} is the Capillary number for a bubble-train ($=\mu_f u_f/\sigma_{of}\cos\theta_{of}$); and N_T^{f} is the modified Trapping number for a bubble-train ($=2\pi R_n kk_{rfo}/V_o$). The values of the dimensionless numbers are listed in Table 5.6. N_{Bo}^{f} and N_{Ca}^{f} are constant for residual dodecane saturation because of the density differences in N_{Bo}^{f}, and the foam bubble-train viscosity and the velocity in N_{Ca}^{f} are constant.

Table 5.6 Dimensionless numbers.

Residual Saturation of dodecane	N_{Bo}^{f} ($\times 10^{-10}$)	N_{Ca}^{o} ($\times 10^{-6}$)	N_{Ca}^{f}	N_{T}^{f} ($\times 10^{-6}$)
0.52	2.10	7.31	0.003	0.122
0.30		4.23		0.211
0.15		2.16		0.411
0.06		0.080		0.975
0.02		0.016		3.291
0.002		-0.49		26.33

In Figure 5.4, residual dodecane displaced by a bubble-train is evaluated by the relationship between the dimensionless numbers shown in Equation (5.25).

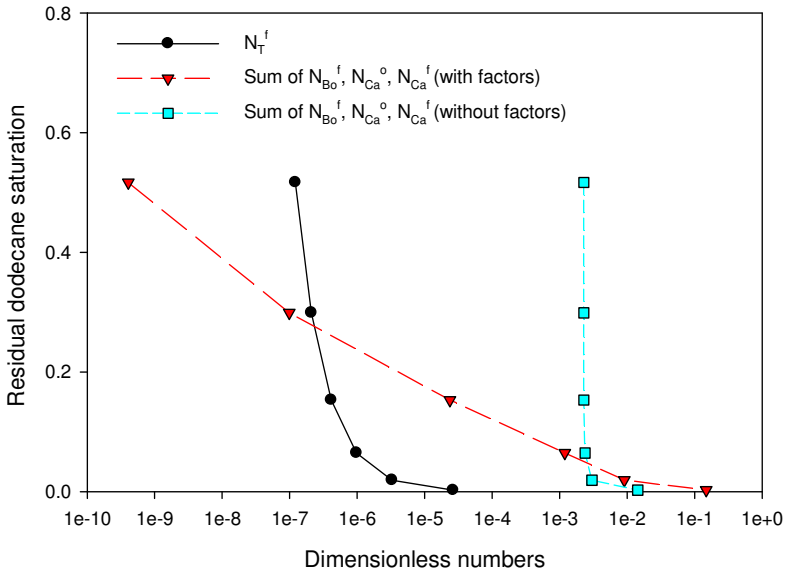

Figure 5.4 Change in residual dodecane saturation during injection of a surfactant foam.

The sum of N_{Bo}^{f}, N_{Ca}^{o}, and N_{Ca}^{f} with the correction factors in the LHS of Equation (5.25) decreases with decreasing residual dodecane saturation. The sum value increases at around 8×10^{-7} of N_{T}^{f}. This indicates that dodecane blobs would mobilize in the system. The sum value without considering the factors shows a similar tendency of N_{T}^{f} and from initial residual saturation, the value starts to go over the N_{T}^{f} value. To satisfy blob mobilization, the LHS of Equation (5.25) should be greater than the N_{T}^{f} value. In the LHS of Equation (5.25), the sum value of N_{Bo}^{f}, N_{Ca}^{o}, and N_{Ca}^{f} with the factors is reasonable because the sum value without the factors should not be greater than the N_{T}^{f} value at initial dodecane saturation. By comparing the sum value with the factors to the N_{T}^{f} value, dodecane blob displacement could be evaluated. The blob displacement would be expected from about 0.3 of dodecane saturation.

5.5 Characteristics of Foam Bubble-Train Affecting Blob Mobilization

5.5.1 Lamellae Number

Lamellae number is a major factor in determining NAPL blob displacement in a bubble-train flow. The lamellae number would be represented by the balance of forces between a capillary suction within a plateau boarder and a capillary resisting force at the lamellae-blob interface when NAPL blobs enter into the lamellae (Schramm and Novosad 1990; 1992).

The lamellae number is expressed in terms of two pressure drops occurred at a plateau boarder and a lamellae-blob interface (Schramm and Novosad 1990; 1992).

$$n_L = \frac{\nabla P_{RB}}{\nabla P_{of}} \tag{5.26}$$

Assumption for which NAPL blobs are small enough to enter into foam lamellae is suggested to use Equation (5.26) above. Schramm and Novosad (1990) assumed a blob diameter moving through lamellae is equal to lamellae thickness $L_s = 2R_o$.

With that hypothesis, the pressure drops in Equation (5.26) would be expressed in terms of capillary tensions using Young-Laplace (Schramm and Novosad 1990).

$$\nabla P_{RB} = \frac{2\sigma_{fs}}{R_{PB}} \tag{5.27}$$

$$\nabla P_{of} = \frac{2\sigma_{of}}{R_o} \tag{5.28}$$

where R_{PB} [L] and R_o [L] are the radii of a plateau boarder and a blob, respectively. As a consequence, the lamellae number is expressed as (Schramm and Novosad 1992).

$$n_L = \frac{\sigma_{fs} R_o}{\sigma_{of} R_{PB}} \tag{5.29}$$

Schramm et al. (1993) observed that the resulting ratio of a blob and a plateau boarder size R_o / R_{PB} was almost equal to 0.15 which is always constant for all foams. By employing the ratio, the value of the lamellae number is obtained (Table 5.7). Three interfacial tensions σ_{fs}, σ_{of}, and σ_{os} are given by Chu (1996).

Table 5.7 Calculated lamellae number.

	σ_{fs} (dyne/cm)	σ_{of} (dyne/cm)	σ_{os} (dyne/cm)	S	E	B	n_L
Bioterge As-40	34.5	4.6	24.5	5.4	14.6	611.16	1.1

From Table 5.7, the flow configuration between a bubble-train and a blob would be evaluated by using Equations (5.1) and (5.2). It follows Type D, as shown in Table 5.1. In Table 5.7, it also shows that the lamellae number is at $1 < n_L < 7$ in which NAPL blobs can be emulsified into smaller droplets and thereby blob displacement is highly expected (Schramm and Novosad 1992). However, if $n_L < 1$, there is no emulsified droplet and blob displacement is rarely expected (Schramm and Novosad 1992). In the case of $n_L > 7$, blob emulsification occurs and blob displacement efficiency is higher than at $n_L < 1$ but lower than $1 < n_L < 7$ (Schramm and Novosad 1992). In the case of foam breakage, it occurs faster at $n_L > 7$ than at $1 < n_L < 7$ (Schramm and Novosad 1992). The value of the lamellae number obtained in Table 5.7 was calculated using the experimental data given by Chu (1996) who observed that NAPL blobs were displaced during foam flooding. In his experiment, the lamellae number is at $1 < n_L < 7$ and the theory about the lamellae corresponds to his experimental result. Consequently, it is known that the lamellae number could determine whether NAPL blobs are emulsified or not, and whether blob displacement occurs or not. Additionally, it could also be used to explain NAPL blob transport within the lamellae (Vikingstod et al. 2005).

In Table 5.7, a bridging coefficient B also describes a blob role in a bubble-train. If B > 0 and a NAPL blob enters into the lamellae without spreading, an unstable blob would be present as a bridge connecting two bubbles. An expression of the bridging coefficient B is obtained as (Aveyard et al. 1993)

$$B = \sigma_{fs}^2 + \sigma_{of}^2 - \sigma_{os}^2 \tag{5.30}$$

5.5.2 Foam Bubble-Train Size

To calculate the apparent viscosity of a bubble-train, a bubble size is required. The bubble size is assumed be same as an equivalent sphere in shape. In reality, air bubbles in a bubble-train may be lengthened due to the effect of pore constrictions. Thus, we attempt to calculate a bubble length by comparing lamella numbers proposed by Schramm and Novosad (1992) and Falls et *al.* (1989).

By using Equation (5.29) and an expression for X_n in Table 5.3, a total bubble-train length would be obtained as,

$$L_T = \frac{number\ of\ lamellae}{X_n} = \frac{\left(\sigma_{fs} R_o / \sigma_{of} R_{PB}\right)}{X_n} \tag{5.31}$$

The total length is also equal to sum of a bubble length and lamellae thickness and is expressed as

$$L_T^{'} = L_B + L_s \tag{5.32}$$

For comparison of two expressions for the total length, some data in Tables 5.3 and 5.7 are employed. Calculated L_T and $L_T^{'}$ values are 0.053 and 0.037 at $R_o / R_{PB} = 0.15$ proposed by Schramm and Novosad (1992), respectively. Unfortunately,

they do not correspond. However, when R_o/R_{PB} is equal to 0.104, they correspond to each other. With the result and the value of R_{PB} in Table 5.3, an equivalent blob radius flowing into the lamellae could be predicted. At 0.104 of R_o/R_{PB}, the R_o value is equal to 0.0134 cm since R_{PB} is 0.0139 cm. From the result, it is known that the blob size does not move through the lamella because the R_o value is greater two times than the lamellae thickness.

5.5.3 Foam Quality

As shown in Table 5.3, foam quality is calculated by a ratio of volume of total bubbles to that of a foam bubble-train. Foam quality plays an important role in improving the removal or the displacement efficiency of NAPL blobs and the sweep efficiency of foam bubble-trains since foam quality is used to determine an apparent foam viscosity.

Table 5.8 shows that the apparent foam viscosity increases as the foam quality increases. Table 5.8 also demonstrates that the apparent foam viscosity increases as total liquid volume in the lamellae decreases and the total volume of the bubbles increases. From the result, it is known that the apparent foam viscosity is proportional to the volume of the total bubbles in a foam bubble-train. The result is also illustrated in Figure 5.5.

Table 5.8 Theoretical apparent foam viscosity for foam quality.

	Air bubble radius R_a = 0.0093 cm Average total bubble volume $V_a = 2.53 \times 10^{-6}$ cm^3			Average foam bubble-train volume $V_f = 3.16 \times 10^{-6}$ cm^3		
Γ	V_f ($\times 10^{-6}$ cm^3)	V_l ($\times 10^{-6}$ cm^3)	μ_f (cp)	V_a ($\times 10^{-6}$ cm^3)	V_l ($\times 10^{-6}$ cm^3)	μ_f (cp)
0.58	4.35	1.83	22.5	1.83	1.33	31.71
0.68	3.71	1.19	23.77	2.15	1.01	31.66
0.78	3.24	0.71	24.96	2.46	0.70	31.43
0.88	2.87	0.34	26.53	2.78	0.38	31.43
0.93	2.72	0.19	27.69	2.94	0.22	32.21

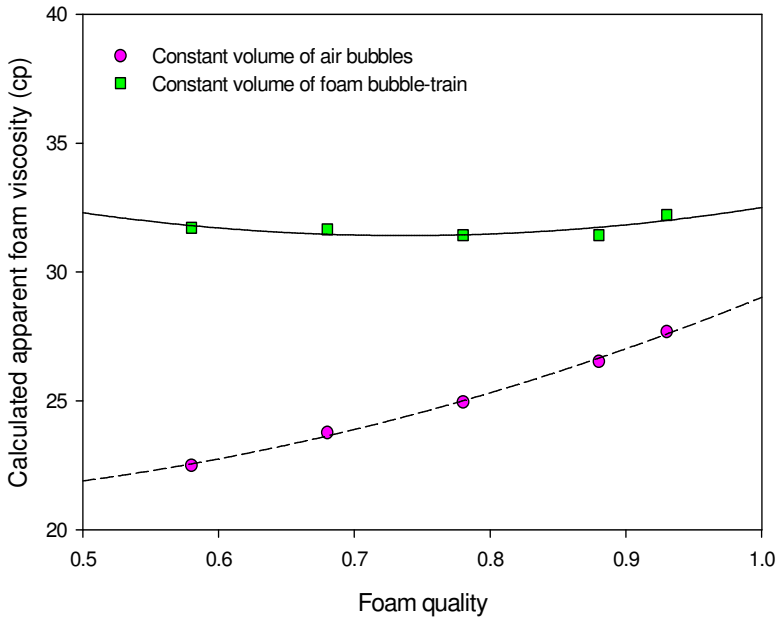

Figure 5.5 Change in calculated apparent foam viscosity over foam quality.

As shown in Table 5.8 and Figure 5.5, the theoretical apparent foam viscosity increases with increasing foam quality and total bubbles volume. Specifically, the result indicates that high foam quality enhances blob mobilization because foam viscosity increases the push force represented in Equation (5.5). Hence, foam quality could be regarded as a significant factor in evaluating blob mobilization or displacement.

CHAPTER VI

SUMMARY AND CONCLUSION

The objective of this research is to develop theoretical analysis and pore-level models predicting two removal mechanisms (dissolution or solubilization and mobilization) of NAPL blobs during the injection of displacing phases (water and surfactant foam) in water-wet porous media. The pore-level models consist of a solubilization model and a mobilization and they are based on the mass and the force balances (buoyant, push, capillary retention, and drag forces) acting on a NAPL blob at pore-scale, respectively. The solubilization model was developed to estimate total volume of NAPL blobs dissolved in water and to describe the relationship between residual NAPL saturation and the total volume of the NAPL blobs. In the mobilization model, the blob volume was employed as a parameter in a buoyant, a push, a drag and an additional force. Specifically, the additional force which describes the relative motion between displaced NAPL blobs and displacing phases would explain NAPL blob flow from the blob mobilization moment.

To observe NAPL blob dissolution, TCE was chosen as a typical DNAPL type. Residual TCE saturation and total volume of TCE blob were investigated under four different specific charges of the water phase, 0.8, 1.7, 3.6, and 5.6 m/day. At a high velocity of the water phase, the residual TCE saturation and the dissolving TCE volume greatly decrease. In the relationship between residual TCE saturation and the TCE blob

volume, the change in the dissolving blob volume was proportional to that in the residual saturation.

In this research, NAPL blob motion was determined by a NAPL blob flow velocity quantified by developed mobilization models. To predict the NAPL blob motion, different displacing phases (water and surfactant foam) and two NAPL types (DNAPL and LNAPL) were employed. During water flooding, velocities of TCE blobs as DNAPL and dodecane blobs as LNAPL were considered under the same specific discharges of the water phase, respectively. At the give condition, the NAPL blob displacements were not expected. Thus, a critical velocity of the water phase displacing a NAPL blob was derived by applying the 5×10^{-5} mobilization value proposed by previous studies but blob mobilization did not occur at the velocity. To expect a NAPL blob mobilization, at least a 1.5×10^{-2} mobilization value was required and the critical water velocity was 27.32 cm/sec. At the given velocity, micromodel, orthorhombic-closed cubic packing, and simple-cubic packing were chosen for observing the effect of the pore geometry model on blob mobilization. TCE and dodecane blobs moved faster in the micromodel than in the other pore geometry models because porosity and intrinsic permeability in the micromodel were relatively higher than the others. However, the NAPL blobs did not flow below 0.035 cm of blob size. For comparison of NAPL types, the TCE blob has a greater velocity than the dodecane blob at the same range of blob size. Herein, for pore-level quantification, a NAPL blob size was selected in the range of 0.005 ~ 0.04 cm regardless of NAPL types since the range of their pore body sizes in three different pore geometry models varied from 0.022 to 0.055 cm. A trapped NAPL

blob volume was calculated, assuming that a NAPL blob was a sphere in shape and it was present at a pore body connecting two pore throats. To conclude, a high velocity of the water phase did not effectively displace NAPL blobs, so a surfactant (Tween 80, SDS, aerosol MA-80, surfonic PE-2594 and witconol NP-100) and co-solvent (50 % EtOH) solution was selected to drive TCE blob mobilization. The blob mobilization first caused at a 0.015 cm of blob size. The blob traveled faster through pores in the surfactant solution including aerosol MA-80 than in the other surfactant solutions, TCE blob because the interfacial tension between TCE and aerosol MA-80 was the lowest.

To predict a NAPL blob flow regime in porous media, dimensional analysis was carried out. In the analysis, a previous Trapping number was developed to describe onset of blob mobilization, comparing it with the sum of dimensionless numbers (Capillary and Bond numbers). Additionally, a correlation model describing the relationship between the Trapping number and residual TCE saturation was produced to give a better understanding of the fate of the NAPL blobs spreading in an area contaminated by residual NAPL. For blob mobilization, the maximum value of the Trapping number was calculated to be 4.94×10^{-2} and as the value was less than the sum of the Capillary number and the Bond number, NAPL blob mobilization could be expected.

In the case of using surfactant foam as a displacing phase, NAPL blob flow was investigated by assuming two different types of surfactant foam traveling through a porous medium.

First, we assumed that surfactant foam acted individually as discrete foam bubbles and surfactant solution in porous media. Thus, to approach a quantitative

analysis on blob mobilization, force acting on a NAPL blob was investigated and they were balanced to explain the three-immiscible fluid flow (NAPL blob as oil, foam bubble as gas, and surfactant solution as liquid). From the force balance, velocities of TCE, bromobenzene, and 4-chlorotoluene blobs as DNAPL, and dodecane and soltrol-130 blobs as LNAPL were computed at 4 cm/sec of a bubble and 0.094 cm/sec of surfactant solution. DNAPL blob velocities were relatively greater than LNAPL blob velocities and of the NAPL types, the TCE blob moved more rapidly. The effect of the ratio of a bubble velocity to a surfactant solution velocity on a blob mobilization was evaluated by controlling relative permeabilities for three-immiscible fluids. The velocity of the surfactant solution was fixed at 0.094 cm/sec and ratios of a bubble velocity to a surfactant solution velocity were 43, 98, 167, 212, and 238. As expected, NAPL blobs traveled faster through pore throats at the higher ratio. The effect of the properties of an air bubble and a surfactant solution on a blob mobilization was also studied. For discrete foam bubbles, an apparent gas viscosity decreased with increasing bubble velocity and it indicated that low gas viscosity and high bubble velocity could cause blob mobilization. To examine the effect of surfactant types on NAPL blob mobilization, Tween 80, SDS, SOS, and DOWFAX 8390 were chosen for TCE blobs. NaDBS, SOS, C1215 AE30, and Atlas CD-413 as surfactants were selected for dodecane blobs. In a surfactant solution with DOWFAX 3890, the TCE blob velocity was the highest and in the C1214 AE 30 solution, the dodecane blob moved more rapidly since the two surfactant viscosities were greater than the other surfactants. To predict blob mobilization during surfactant foam flooding, the relative magnitude between two different modified Trapping numbers and

the sum of dimensionless numbers (Capillary and Bond numbers) were compared. The Trapping numbers for surfactant solutions and foam bubbles were derived by the force balance obtained in our work. The two Trapping numbers for surfactant solutions and foam bubbles were calculated to be $5.11 \times 10^{-5} \sim 1.20 \times 10^{-3}$ and $1.75 \times 10^{-5} \sim 4.09 \times 10^{-4}$, respectively which were relatively low compared to water flooding for blob mobilization. In comparison to the sum of the dimensionless numbers, it was generally greater than the two modified Trapping numbers, resulting in blob mobilization.

Second, in the operation of surfactant foam, it was assumed that the foam could behave as a foam bubble-train consisting of lamellae connecting discrete bubbles in porous media. To investigate foam bubble-train flow in porous media, a balance of forces acting on a foam bubble-train was formulated and from the force balance, foam bubble-train velocity was obtained, which was in good agreement with previous experimental data. The influence of the foam bubble-train on NAPL blob mobilization was scrutinized using a model developed in our work where dodecane as a NAPL type was selected to compare with experimental data. Similar to the discrete foam bubbles dispersed in a surfactant solution, the dodecane blob began to be displaced at from 0.001 cm of its blob size. However, the blob displaced by the foam bubble-train moved more slowly than by individual foam bubbles and a surfactant solution since the foam bubble-train moved more slowly than discrete foam bubbles in porous media. In this research, characteristics (lamellae number, bubble-train size, and foam quality) of a foam bubble-train affecting blob mobilization were examined. For blob mobilization, the modified Trapping number for a foam bubble-train was calculated to be $1.22 \times 10^{-7} \sim 2.63 \times 10^{-5}$.

It was the lowest, with respect to another type of surfactant foam flooding and water flooding discussed above. Compared to the sum of dimensionless numbers, it passed the Trapping number value as residual dodecane saturation approached around 30 %.

Finally, as compared with water and two different types of surfactant foam, it is concluded that individual foam bubbles and surfactant solution is the most effective treatment in displacing NAPL blobs trapped within pores. However, in reality, it could be more difficult to control individual air bubble and surfactant solution flow than the others in field-scale. Therefore, the study for discrete foam bubbles and surfactant solution flowing through a porous medium is still required to improve removal efficiency of NAPL blobs.

REFERENCES

Abdul, S. A., Thomas, L. G., and Devi, N. R. "Selection of surfactants for the removal of petroleum products from shallow sandy aquifers." *Ground Water*, 28(6), 920-926.

Al-Gharbi, M. S., and Blunt, M. J. (2005). "Dynamic network modeling of two-phase drainage in porous media." *Physical Review E*, 71, 1-16.

Al-Raoush, R., Thompson, K., and Willson, C. S. (2003). "Comparison of network generation techniques for unconsolidated porous media." *Soil Sci. Soc. Am. J.* 68, 1687-1700.

Aveyard, R., Binks, B. P., Fletcher, P. D. I., Peck, T. G., and Garrett, P. R. (1993). "Entry and spreading of alkane drops at the air/surfactant solution interface in relation to foam and soap film stability." *J. Chem. Soc. Faraday Trans.*, 89(24), 4313-4321.

Babchin, A. J., and Nasr, T. N. (2006). "Analytical model for the capillary pressure gradient in oil-water-rock system." *Transport in Porous Media*, 65(2), 359-362.

Bang, V., Kumar, V., Ayyalasomayajula, P. S., Pope, G. A., and Sharma, M. M. (2006). "Relative permeability of gas-condensate fluids: a general correlation." *SPE 102741*, 1-8.

Bear, J. (1972). *Dynamics of fluids in porous media*, American Elsevier Publishing Company, New York.

Bergeron, V., Fagan, M. E., and Radke, C. J. (1993). "Generalized entering coefficients: a criterion for foam stability against oil in porous media." *Langmuir*, 9, 1704-1713.

Bloom, F., and Heindel, T. J. (1997). "Mathematical modeling of the flotation deinking process." *Mathematical and Computer Modeling*, 25(5), 13-58.

Boving, T. B., and Brusseau, M. L. (2000). "Solubilization and removal of residual trichloroethene from porous media: comparison of several solubilization agents." *J. Contam. Hydrol.*, 42, 51-67.

Breward, C. J. W., and Howell, P. D. (2002). "The drainage of a foam lamella." *Journal of Fluid Mechanics*, 458, 379-406.

Brown, C. L., and Pope, G. A. (November 1994). "Simulation of surfactant-enhanced aquifer remediation." *Water Resour. Res*, 30(11), 2959-2977.

Brutsaert, W., and El-Kadi, A. I. (March 1984). "The relative importance of compressibility and partial saturation in unconfined groundwater flow." *Water. Resour. Res.*, 20(3), 400-408.

Chatzis, I., Morrow, N. R., and Lim, H. T. (1983). "Magnitude and detailed structure of residual oil saturations." *Soc. Pet. Eng. J.*, 22(2), 311-326.

Chen, W. L., Twu, M. C., and Pan, C. (2002). "Gas-liquid two-phase flow in micro-channels." *Int. J. Multiphase Flow*, 28(7), 1235-1247.

Chevalier, L. R. (2003). "Surfactant dissolution and mobilization of LNAPL contaminants in aquifers." *Environmental Monitoring and Assessment*, 84, 19-33.

Chevalier, L. R. (2006). "Use of optimization to develop a correlation model for predicting residual NAPL saturation." *Civil Engineering and Environmental Systems*, 23(2), 65-72.

Chevalier, L. R., and Fonte, J. M. (2000). "Correlation model to predict residual immiscible organic contaminants in sandy soils." *J. Hazard. Mater.*, B72, 39-52.

Childs, J. D., Acosta, E., Know, R., Harwell, J. H., and Sabatini, D. A. (2004). "Improving the extraction of tetrachloroethylene from soil columns using surfactant gradient systems." *J. Contam. Hydrol.*, 71, 27-45.

Chowdhury, S. (1996). Visualization and quantification of transport processes in porous media using micromodels, Ph.D. dissertation, Texas A&M University.

Chu, H. (1997). Displacement of nonaqueous phase organic liquids form saturated sands with surfactant foams, Ph.D. dissertation, University of Michigan.

Cinar, Y., Jessen, K., Berenblyum, R., Juanes, R., and Orr, F. M. (2006). "An experimental and numerical investigation of crossflow effects in two-phase displacements." *SPE Journal*, 11(2), 216-226.

Conrad, S. H., Wilson, J. L., Mason, W. R., and Peplinski, W. J. (February 1992). "Visualization of residual organic liquid trapped in aquifers." *Water. Resour. Res*, 28(2), 467-478.

Corapcioglu, M. Y., Cihan, A., and Drazenovic, M. (2004). "Rise velocity of an air bubble in porous media: Theoretical studies." *Water. Resour. Res.*, 40, 1-9.

Corey, A. T. (1994). *Mechanics of immiscible fluids in porous media*, Water Resources Publications, Highlands Ranch, Colorado.

Dalland, M., Hanssen, J. E., and Kristiansen, T. S. (1994). "Oil interaction with foams under static and flowing conditions in porous media." *Colloids Surf. A:Physicochem. Eng. Aspects*, 82, 129-140.

Dawson, H. E., and Roberts, P. V. (1997). "Influence of viscous, gravitational, and capillary forces on DNAPL saturation." *Ground Water*, 35(2), 261-269.

Delshad, M. (1990). *Trapping of micellar fluids in Berea Sandstone*. Ph.D. dissertation, University of Texas at Austin.

Delshad, M., Pope, G. A., and Sepehrnoori, K. (1996). "A compositional simulator for modeling surfactant enhanced aquifer remediation .1. Formulation." *J. Contam. Hydro.*, 23(4), 303-327.

Denkov, N. D. (2004). "Mechanisms of foam destruction by oil-based antifoams." *Langmuir*, 20, 9463-9505.

Dillard, L. A., and Blunt, M. J. (2000). "Development of a pore network simulation model to study non-aqueous phase liquid dissolution." *Water Resour. Res*, 36, 439-454.

Duffield, A. R., and Ramamurty, R. S. (2003). "Surfactant enhanced mobilization of mineral oil within porous media." *Water, Air, and Soil Pollution*, 143, 111-122.

Dullien, F. A. L. (1979). *Porous media. Fluid transport and pore structure*, Academic Press, New York.

ElSherbini, A., and Jacobi, A. (2006). "Retention forces and contact angles for critical liquid drops on non-horizontal surfaces." *J. Colloid Interface Sci.*, 299(2), 841-849.

Falls, A. H., Musters, J. J., and Ratulowski, J. (May 1989). "The apparent viscosity of foams in homogeneous bead packs." *SPE Reserv. Eng.*, 4, 155-164.

Flick, E. W. (1993). *Industrial surfactants*, William Andrew Inc, Park Ridge, New Jersey.

Franzetti, A., Di Gennaro, P., Bevilacqua, A., Papacchini, M., and Bestetti, G. (2006). "Environmental features of two commercial surfactants widely used in soil remediation." *Chemosphere*, 62(9), 1474-1480.

Fu, X., and Imhoff, P. T. (2002). "Mobilization of small DNAPL pools formed by capillary entrapment." *J. Contam. Hydrol.*, 56, 137-158.

Gauglitz, P. A., Stlaurent, C. M., and Radke, C. J. (1988). "Experimental-Determination of Gas-Bubble Breakup in a Constricted Cylindrical Capillary." *Industrial & Engineering Chemistry Research*, 27(7), 1282-1291.

Gioia, F., Alfani, G., Andreutti, S., and Murena, F. (2003). "Oil mobility in a saturated water-wetted bed of glass beads." *J. Hazard. Mater.*, B97, 315-327.

Gioia, F., and Urciuolo, M. (2006). "Combined effect of Bond and Capillary numbers on hydrocarbon mobility in water saturated porous media." *J. Hazard. Mater.*, 133(1-3), 218-225.

Graton, L. C., and Fraser, H. J. (1935). "Systematic packing of spheres-with particular relation to porosity and permeability." *Journal of Geology*, 43(8), 785-909.

Grattoni, C. A., Pingo Almada, M. B. and Dawe, R. A. (1997). "Pore and core-scale displacement mechanisms with spreading and wetting effects during three-phase flow." *SPE NV LACPEC*, Rio de Janeiro, 1-14.

Hahn, P. S., Ramamohan, T. R., and Slattery, J. C. (1985). "Mobility control in the displacement of residual oil by an unstable foam." *AIChE Journal*, 31(6), 1029-1035.

Hall, J. L., Imhoff, P. T., Wilson, C. S., and Miller, C. T. (1997). "Surfactant-enhanced mobilization of dense nonaqueous phase liquids in groundwater remediation." Technical Report, University of North Carolina at Chapel Hill.

Hanssen, J. E., and Dalland, M. (1990). "Foams for effective gas blockage in the presence of crude oil." *SPE/DOE 20193*, 209-222.

Hey, M. J., and Kingston, J. G. (2006). "Maximum stability of a single spherical particle attached to an emulsion drop." *J. Colloid Interface Sci.*, 298(1), 497-499.

Hilfer, R., and Oren, P. E. (1996). "Dimensional analysis of pore scale and field scale immiscible displacement." *Transport in Porous Media*, 22, 53-72.

Hirasaki, G. J., and Lawson, J. B. (1985). "Mechanisms of foam flow in porous media: Apparent viscosity in smooth capillaries." *SPE Annual technical conference, 1-21*.

Hitchens, L., Vane, L. M., and Alvarez, F. R. (2001). "VOC removal from water and surfactant solutions by evaporation: a pilot study." *Separation and Purification Technology*, 24(1-2), 67-84.

Imhoff, P. T., Jaffe, P. R., and Pinder, G. F. (1994). "An experimental-study of complete Dissolution of a nonaqueous phase liquid in saturated porous-media." *Water Resour. Res.*, 30(2), 307-320.

Jeong, S. (1999). Surfactant foam-enhanced remediation of nonaqueous phase liquids (NAPLs) in porous media: micromodel study, Ph.D. dissertation, Texas A&M University.

Jeong, S. W. (2005). "Evaluation of the use of capillary numbers for quantifying the removal of DNAPL trapped in a porous medium by surfactant and surfactant foam floods." *J. Colloid Interface Sci.*, 282(1), 182-187.

Jeong, S. W., and Corapcioglu, M. Y. (2003). "A micromodel analysis of factors influencing NAPL removal by surfactant foam flooding." *J. Contam. Hydrol.*, 60, 77-96.

Jeong, S. W., Corapcioglu, M. Y., and Roosevelt, S. E. (2000). "Micromodel study of surfactant foam remediation of residual trichloroethylene." *Environ. Sci. Technol.*, 34, 3456-3461.

Jha, B. K., Christiano, S. P., and Shah, D. O. (2000). "Silicone antifoam performance: Correlation with spreading and surfactant monolayer packing." *Langmuir*, 16(26), 9947-9954.

Johnson, R. E., and Sadhal, S. S. (1985). "Fluid-Mechanics of Compound Multiphase Drops and Bubbles." *Annual Review of Fluid Mechanics*, 17, 289-320.

Kam, S. I., and Rossen, W. R. (December 2003). "A model for foam generation in homogeneous media." *Soc. Pet. Eng. J.*, 417-425.

Keller, A. A., Blunt, M. J., and Roberts, P. V. (1997). "Micromodel observation of the role of oil layers in three-phase flow." *Transport in Porous Media*, 26, 277-397.

Kennedy, C. A., and Lennox, W. C. (1997). "A pore-scale investigation of mass transport from dissolving DNAPL droplets." *J. Contam. Hydrol.*, 24, 221-246.

Kim, H., Soh, H. E., Annable, M. D., and Kim, D. J. (2004). "Surfactant-enhanced air sparging in saturated sand." *Environ. Sci. Technol.*, 38, 1170-1175.

Kovscek, A. R., and Radke, C. J. (1996). "Gas bubble snap-off under pressure-driven flow in constricted noncircular capillaries." *Colloid Surf. A: Physicochem. Eng. Aspects*, 117, 55-76.

Kovscek, A. R., Patzek, T. W., and Radke, C. J. (1995). "A mechanistic population balance model for transient and steady-state foam flow in Boise sandstone." *Chemical Engineering Science*, 50(23), 3783-3799.

Larson, R. G., Davis, H. T., and Scriven, L. E. (1981). "Displacement of residual nonwetting fluid from porous media." *Chemical Engineering Science*, 36, 75-85.

Lenhard, R. J., Kacimov, A. R., Tartakovsky, A. M., and AbdelRahman, H. (2002). "Modeling residual NAPL in water-wet porous media." *Agricultural Sciences*, 7(2), 1-7.

Lenormand, R., and Zarcone, C. (1988). "Physics of blob displacement in a two-dimensional porous medium." *SPE Format. Eval.* , 3(1), 271-275.

Llave, F. M., Chung, F. T-H., Louvier, R. W., and Hudgins, D. A. (1990). "Foams as mobility control agents for oil recovery by gas displacement." *SPE/DOE 20245*, 689-701.

Lobo, L., and Wasan, D. T. (1993). "Mechanisms of aqueous foam stability in the presence of emulsified non-aqueous-phase liquids - structure and stability of the pseudoemulsion film." *Langmuir*, 9(7), 1668-1677.

Lovoll, G., Meheust, Y., Maloy, K. J., Aker, E., and Schmittbuhl, J. (2005). "Competition of gravity, capillary and viscous forces during drainage in a two-dimensional porous medium, a pore scale study." *Energy*, 30(6), 861-872.

Manlowe, D. J., and Radke, C. J. (November, 1990). "A pore-level investigation of foam/oil interactions in porous media." *SPE 18069*, 495-502.

Mast, R. F. (1972). "Microscopic behavior of foam in porous media." *SPE 3997*, 1-8.

Mayer, A. S., and Miller, C. T. (1993a). "An experimental investigation of pore-scale distributions of nonaqueous phase liquids at residual saturation." *Transport in Porous Media*, 10, 57-80.

Mayer, A. S., and Miller, C. T. (1993b). "An experimental investigation of pore-scale distributions of nonaqueous phase liquids at residual saturation." *Transport in Porous Media*, 10, 57-80.

Mayer, A. S., Zhong, L. and Pope, G. A. (1999). "Measurement of mass-transfer rates for surfactant-enhanced solubilization of nonaqueous phase liquids." *Environ. Sci. Technol.*, 33, 2965-2972.

Miller, C. T., Poirier-McNeill, M. M., and Mayer, A. S. (1990). "Dissolution of trapped nonaqueous phase liquids: mass transfer characteristics." *Water. Resour. Res.*, 26(11), 2783-2796.

Morrow, N. R., and Chatzis, I. (1982). "Measurement and correlation of conditions for entrapment and mobilization of residual oil." *USDOE Report*, 10310-20.

Morrow, N. R., and Songkran, B. (1981). Effects of trapping and buoyancy forces on nonwetting phase trapping in porous media, in D. O. Shah (ed.), Surface phenomena in enhanced oil recovery, Plenum press, pp. 387-411.

Morrow, N. R., Chatzis, I., and Taber, J. J. (1988). "Entrapment and mobilization of residual oil in bead packs." *SPE Reserv. Eng. 3,* 927-934.

Ng, K. M., Davis, H. T., and Scriven, L. E. (1978). "Visualization of blob mechanics in flow through porous media." *Chem. Eng. Sci.*, 33, 1009-1017.

Olbricht, W. L. (1996). "Pore-scale prototypes of multiphase flow in porous media." *Ann. Rev. Fluid Mech.*, 28, 187-213.

Øren, P. E., and Pinczewski, W. V. (1992). "Mobilization of waterflood residual oil by gas injection for water-wet conditions." *SPE Format. Eval.*, 7, 70-78.

Øren, P. E., and Pinczewski, W. V. (1994). "Effect of wettability and spreading on recovery of waterflood residual oil by immiscible gasflooding." *SPE Format. Eval.*, 9, 149-156.

Øren, P. E., Billiotte, J., and Pinczewski, W. V. (1994). "Pore-scale network modeling of waterflood residual oil recovery by immiscible gas flooding." *SPE/DOE 27814*, 345-359.

Owete, O. S., and Brigham, W. E. (August 1987). "Flow behavior of foam: a porous micromodel study." *SPE Reserv. Eng.*, 315-323.

Padgett, P. K., and Hayden, N. J. (1999). "Mobilization of residual tetrachloroethylene during alcohol flushing of clay-containing porous media." *J. Contam. Hydrol.*, 40(3), 285-296.

Payatakes, A. C. (1982). "Dynamics of oil ganglia during immiscible displacement in water-wet porous media." *Ann. Rev. Fluid. Mech*, 14, 365-393.

Pennell, K. D., Abriola, L. M., and Weber, W. J. (1993). "Surfactant-enhanced solubilization of residual dodecane in soil columns.1. Experimental investigation." *Environ. Sci. Technol.*, 27, 2332-2340.

Pennell, K. D., Jin, M., Abriola, L. M., and Pope, G. A. (1994). "Surfactant enhanced remediation of soil columns contaminated by residual tetrachloroethylene." *J. Contam. Hydrol.*, 16, 35-53.

Pennell, K. D., Pore, G. A., and Abriola, L. M. (1996). "Influence of viscous and buoyancy forces on the mobilization of residual tetrachloroethylene during surfactant flushing." *Environ. Sci. Technol.*, 30, 1328-1335.

Pereira, G. G., Pinczewski, W. V., Chan, D. Y. C., Paterson, L., and Oren, P. E. (1996). "Pore-scale network model for drainage-dominated three-phase flow in porous media." *Transport in Porous Media*, 24, 167-201.

Pope, G. A., Wu, W., Narayanaswamy, G., Delshad, M., Sharma, M. M., and Wang, P. (2000). "Modeling relative permeability effects in gas-condensate reservoirs with a new trapping model." *SPE Reserv. Eval. Eng.*, 171-178.

Powers, S. E., Abriola, L. M., and Weber, W. J. (1992). "An Experimental Investigation of Nonaqueous Phase Liquid Dissolution in Saturated Subsurface Systems - Steady-State Mass-Transfer Rates." *Water Resour. Res.*, 28(10), 2691-2705.

Powers, S. E., Abriola, L. M., Dunkin, J. S., and Weber, W. J. (1994). "Phenomenological models for transient NAPL-water mass-transfer processes." *J. Contam. Hydrol.*, 16, 1-33.

Powers, S. E., Loureiro, C. O., Abriola, L. M., and Weber, W. J. (April 1991). "Theoretical study of the significance of nonequilibrium dissolution of nonaqueous phase liquids in subsurface systems." *Water. Resour. Res.*, 27(4), 463-477.

Reddi, L. N., and Wu, H. (1996). "Mechanisms involved in vibratory destabilization of NAPL ganglia in sands." *Journal of Environmental Engineering-ASCE*, 122(12), 1115-1119.

Rezkallah, K. S. (1996). "Weber number based flow-pattern maps for liquid-gas flows at microgravity." *Int. J. Multiphase Flow*, 22(6), 1265-1270.

Rossen, W. R. (1988). "Theories of foam mobilization pressure gradient." *SPE/DOE 17358*, 393-412.

Rossen, R. H. (1989). "Simulation of gas/oil drainage and water/oil imbibition in naturally fractured reservoirs." *SPE Reserv. Eng.*, 4(4), 464-40.

Rossen, W. R. (2003). "A critical review of roof snap-off as a mechanism of steady-state foam generation in homogeneous porous media." *Colloids Surf. A:Physicochem. Eng. Aspects*, 225, 1-24.

Rossen, W. R., Zeilinger, S. C., Shi, J. X., and Lim, M. T. (Sep. 1999). "Simplified mechanistic simulation of foam processes in porous media." *SPE Journal*, 4(3), 279-287.

Sagar, N. S., and Castanier, L. M. (1997). “Oil-foam interactions in a micromodel.” Technical Report, Stanford University, CA.

Sahloul, N. A., Ioannidis, M. A., and Chatzis, I. (2002). "Dissolution of residual non-aqueous phase liquids in porous media: pore-scale mechanisms and mass transfer rates." *Adv. in Water Res.*, 25, 33-49.

Saripalli, K. P., Annable, M. D., and Rao, P. S. C. (1997). "Estimation of nonaqueous phase liquid-water interfacial areas in porous media following mobilization by chemical flooding." *Environ. Sci. Technol.*, 31, 3384-3388.

Schaerlaekens, J., and Feyen, J. (2004). "Effect of scale and dimensionality on the surfactant-enhanced solubilization of a residual DNAPL contamination." *J. Contam. Hydrol.*, 71(1-4), 283-306.

Schaerlaekens, J., Carmeliet, J., and Feyen, J. (2005). "Multi-objective optimization of the setup of a surfactant-enhanced DNAPL remediation." *Environ. Sci. Technol.*, 39, 2327-2333.

Schaerlaekens, J., Vanderborght, J., Merckx, R., and Feyen, J. (2000). "Surfactant enhanced solubilization of residual trichloroethene experimental and numerical analysis." *J. Contam. Hydrol.*, 46, 1-16.

Schramm, L. L. (1994). *Foams: fundamentals and applications in the petroleum industry*, Advances in Chemistry Series, Washington, DC.

Schramm, L. L., and Novosad, J. J. (1990). "Micro-visualization of foam interaction with a crude oil." *Colloid Surf. A: Physicochem. Eng. Aspects*, 46, 21-43.

Schramm, L. L., and Novosad, J. J. (1992). "The destabilization of foams for improved oil recovery by crude oils: effect of the nature of the oil." *Journal of Petroleum Science and Engineering*, 7, 77-90.

Schramm, L. L., Turta, A. T., and Novosad, J. J. (1993). "Microvisual and coreflood studies of foam interactions with a light crude oil." *SPE Reserv. Eng.*, 8, 201-206.

Simpkin, T., Sale, T., Kueper, B., Pitts, M., and Wyatt, K. (1999). *Surfactant and cosolvents for NAPL remediation: a technology practices manual*, Lewis Publishers.

Singh, G., Hirasaki, G. J., and Miller, C. A. (1997). "Dynamics of foam films in constricted pores." *Environmental and Energy Engineering*, 43(12), 3241-3252.

Slattery, J. C. (March 1979). "Interfacial effects in the displacement of residual oil by foam." *AIChE Journal*, 25(2), 283-289.

Suicmez, V. S., Piri, M., and Blunt, M. J. (April, 2006). "Pore-scale modeling of three-phase WAG injection: prediction of relative permeabilities and trapping for different displacement cycles." *SPE/DOE 95594*.

Taylor, T. P., Rathfelder, K. M., Pennell, K. D., and Abriola, L. M. (2004). "Effects of ethanol addition on micellar solubilization and plume migration during surfactant enhanced recovery of tetrachloroethene." *J. Contam. Hydro.*, 69(1-2), 73-99.

Thulasidas, T. C., Abraham, M. A., and Cerro, R. L. (1995). "Bubble-train flow in capillaries of circular and square cross-section." *Chemical Engineering Science*, 50(2), 183-199.

Torza, S., and Mason, S. G. (1970). "Three-phase interactions in shear and electrical fields." *J. Colloid Interface Sci.*, 33(1), 67-83.

Trantham, H. H. and Durnford, D. S. "DNAPL source zone characterization using a stochastic aggregation model." *Hazardous Waste Research*, 191-198.

Tung, V. X., and Dhir, V. K. (1988). "A hydrodynamic model for two-phase flow through porous media." *Int. J. Multiphase Flow*, 14, 47-65.

Vassenden, F., and Holt, T. (April 1998). "Experimental foundation for relative permeability modeling of foam." *SPE Reserv. Eval. & Eng.,* 73-83.

Vikingstad, A. K., Skauge, A., Hoiland, H., and Aarra, M. (2005). "Foam-oil interactions analyzed by static foam tests." *Colloid Surf. A: Physicochem. Eng. Aspects*, 260, 189-198.

Wang, C. Y. (1997). "An alternative description of viscous coupling in two-phase flow through porous media." *Transport in Porous Media*, 28, 205-219.

Wang, S., and Mulligan, C. N. (2004). "An evaluation of surfactant foam technology in remediation of contaminated soil." *Chemosphere*, 57, 1079-1089.

White, M. D., and Oostrom, M. (December1998). "Modeling surfactant-enhanced nonaqueous-phase liquid remediation of porous media." *Soil Science*, 163(12), 931-940.

Willson, C. S., Hall, J. L., Miller, C. T., and Imhoff, P. T. (1999). "Factors affecting bank formulation during surfactant-enhanced mobilization of residual NAPL." *Environ. Sci. Technol.*, 33, 2440-2446.

Yan, W., Miller, C. A., and Hirasaki, G. J. (2006). "Foam sweep in fractures for enhanced oil recovery." *Colloids Surf. A: Physicochem. Eng. Aspects,* 282, 348-359.

Zhong, L., Mayer, A., and Glass, R. J. (March 2001). "Visualization of surfactant-enhanced nonaqueous phase liquid mobilization and solubilization in a two-dimensional micromodel." *Water Resour. Res*, 37(3), 523-537.

Zhong, L., Mayer, A. S., and Pope, G. A. (2003). "The effect of surfactant formulation on nonequilibrim NAPL solubilization." *J. Contam. Hydrol.*, 60, 55-75.

Zhou, D., Dillard, L. A., and Blunt, M. J. (2000). "A physically based model of dissolution of nonaqueous phase liquids in the saturated zone." *Transport in Porous Media*, 39, 227-255.

.

VITA

Name: SUN HEE YOON

Address: Department of Civil Engineering, Texas A&M University, 3136 TAMU, College Station, Texas 77843-3136, USA

Email Address: sunnydreams@gmail.com

Education: Ph.D. Civil Engineering, Texas A&M University, Texas, 2007
M.S. Environmental Science, Keimyung University, South Korea, 2002
B.S. Environmental Science, Keimyung University, South Korea, 1999

Experience: Research Assistant, Keimyung University, Korea (2002-2003), Treatment of suspended substances and reductive dechlorination

Research Assistant, Keimyung University, Korea (1999-2000), removal of chlorinated-chemicals and adsorption modeling

Teaching Assistant, Keimyung University, Korea (1999), assisted in environmental microbiology class

Intellectual Contributions:

"Analysis of NAPL Blobs Displaced by Surfactant-Enhanced Air Sparging in Porous Media", Sun Hee Yoon and M. Yavuz Corapcioglu (2007), NGWA, Houston, TX

"Mobilization of DNAPL Residuals in Porous Media", Sun Hee Yoon and M. Yavuz Corapcioglu (2006), presented at the 232nd ACS National Meeting, San Francisco, CA.

"Development of Physical Model for Displacement of NAPL Ganglia Trapped in Porous Media", Sun Hee Yoon and M. Yavuz Corapcioglu (2006), presented at Korean-American Scientists and Engineers Association (KSEA), Teaneck, NJ.

"Pore-scale Analysis of Residual NAPL Blob Mobilization and Solubilization in Porous Media", Sun Hee Yoon and M. Yavuz Corapcioglu (2005), presented at AGU Fall Meeting, San Francisco, CA.